Progress in Materials Science 76 (2016) 319–380

Contents lists available at ScienceDirect

Progress in Materials Science

journal homepage: www.elsevier.com/locate/pmatsci

# Recent advances in electrospun carbon nanofibers and their application in electrochemical energy storage

Biao Zhang [a,b], Feiyu Kang [c], Jean-Marie Tarascon [b], Jang-Kyo Kim [a,*]

[a] Department of Mechanical and Aerospace Engineering, The Hong Kong University of Science and Technology, Hong Kong, China
[b] FRE 3677 "Chimie du Solide et Energie", College de France, 11 Place Marcelin Berthelot, 75231 Paris Cedex 05, France
[c] Key Laboratory of Thermal Management Engineering and Materials, Graduate School at Shenzhen, Tsinghua University, Shenzhen, Guangdong 518055, PR China

ARTICLE INFO

*Article history:*
Received 20 January 2015
Received in revised form 7 August 2015
Accepted 12 August 2015
Available online 1 October 2015

*Keywords:*
Electrospinning
Carbon nanofiber
Battery
Energy storage

ABSTRACT

Carbon nanofibers (CNFs) have been widely used in electrochemical energy storage devices because of their excellent conductivities, extremely large surface areas and structural stability. In energy storage devices like rechargeable batteries and supercapacitors, CNFs play multi-functional roles as active electrode materials, conductive additives and substrates for supporting active metal (oxides). Electrospinning offers a low cost and scalable technique to fabricate CNFs and their hybrids with tunable nanostructures. This paper summarizes various design strategies for producing random, aligned and core/shell structured fibers, and elucidates the influences of polymer precursors, processing parameters, conductive additives and catalysts on functional, morphological and structural characteristics of CNFs. The current start-of-the-art developments for applications in Li-ion batteries, supercapacitors, Na-ion batteries, Li–$O_2$ batteries and Li–S batteries are reviewed. Key issues that affect the electrochemical performance of the electrodes, such as the chemical and atomic structures, electrical conductivities, surface areas and pore size distribution of CNFs, and the particle size, shape and dispersion of metal (oxides) encapsulated in CNFs, are discussed and their solutions suggested. Future prospects on further optimization of the structure and performance, and challenges encountered in large-scale applications of electrospun CNFs are proposed.
© 2015 Elsevier Ltd. All rights reserved.

* Corresponding author. Tel.: +852 2358 7207; fax: +852 2358 1543.
*E-mail address:* mejkkim@ust.hk (J.-K. Kim).

http://dx.doi.org/10.1016/j.pmatsci.2015.08.002
0079-6425/© 2015 Elsevier Ltd. All rights reserved.

**Nomenclature**

*Acronyms*

| | |
|---|---|
| CNF | carbon nanofiber |
| CNT | carbon nanotube |
| CVD | chemical vapor deposition |
| DMAc | N,N-dimethylacetamide |
| DMF | dimethylformamide |
| EDLC | electric double-layer capacitance |
| EV | electric vehicle |
| LABs | Li–air batteries |
| LFP | $LiFePO_4$ |
| LIBs | Li-ion batteries |
| LSBs | Li–sulfur batteries |
| LTO | $Li_4Ti_5O_{12}$ |
| MP | mesophase pitch |
| NIBs | Na-ion batteries |
| ODA | oxydianiline |
| ORR | oxygen reduction reaction |
| PAA | polyamic acid |
| PAN | polyacrylonitrile |
| PANI | polyaniline |
| PBI | polybenzimidazole |
| PC | pseudocapacitance |
| PEO | poly(ethylene oxide) |
| PI | polyimide |
| PLA | poly(L-lactide) |
| PMDA | pyromellitic dianhydride |
| PMHS | polymethylhydrosiloxane |
| PMMA | poly(methyl methacrylate) |
| PPy | polypyrrole |
| PS | polystyrene |
| PVA | polyvinyl alcohol |
| PVDF | poly(vinylidene fluoride) |
| PVP | polyvinylpyrrolidone |
| SAN | styrene-co-acrylonitrile |
| SCs | supercapacitors |
| SEM | scanning electron microscope |
| TEM | transmission electron microscope |
| TEOS | tetraethyl orthosilicate |
| THF | tetrahydrofuran |
| TMO | transition metal oxide |
| VGCF | vapor grown carbon fiber |
| 1D | one dimensional |

*Symbols*

| | |
|---|---|
| $d_j$ | jet diameter |
| $d_f$ | fiber diameter |
| $d_n$ | diameter of nozzle |
| $E_{critical}$ | critical voltage for stretching the precursor solution |
| $I$ | current of jets |
| $l$ | length of initial jet |
| $M$ | molecular weight of polymer |
| $Q$ | solution flow rate |

| | |
|---|---|
| $\varepsilon$ | dielectric constant |
| $\eta$ | viscosity of solution |
| $\gamma$ | surface tension |

**Contents**


1. Introduction . . . 321
   1.1. Carbon materials for energy storage . . . 321
   1.2. Carbon nanofibers . . . 323
2. Electrospinning . . . 325
   2.1. Set-ups for producing fibers with different structures . . . 325
      2.1.1. Random fibers . . . 326
      2.1.2. Aligned fibers . . . 326
      2.1.3. Core/shell structured fibers . . . 330
   2.2. Precursors for electrospinning . . . 331
   2.3. Processing parameters . . . 335
3. Optimization of structure and morphology of CNFs . . . 338
   3.1. Diameter . . . 338
   3.2. Structure . . . 339
   3.3. Electrical conductivity . . . 339
   3.4. Surface area and pore size distribution . . . 344
   3.5. Particle size, dispersion and morphology of metal oxides in CNFs . . . 353
4. Application of CNFs in Li ion batteries . . . 354
   4.1. Anodes . . . 355
      4.1.1. Neat CNFs . . . 355
      4.1.2. Ti/CNF electrodes . . . 355
      4.1.3. Transition metal oxide/CNF anodes . . . 357
      4.1.4. Metal alloy/CNFs . . . 357
   4.2. Cathodes . . . 358
   4.3. Discussion on electrospinning for Li ion batteries . . . 359
      4.3.1. Comparison between porous and nonporous CNFs . . . 359
      4.3.2. Comparison between neat metal oxide fiber and metal oxide/CNF composites . . . 361
      4.3.3. Comparison between in-situ deposition and ex-situ growth . . . 362
5. Application of CNFs in supercapacitors . . . 362
   5.1. Neat CNFs . . . 365
   5.2. CNFs containing metal oxides and/or conducting polymers . . . 365
6. Other electrochemical energy storage devices . . . 366
   6.1. Na ion batteries . . . 366
   6.2. Li–$O_2$ or Li–air batteries . . . 366
   6.3. Li–sulfur batteries . . . 369
7. Issues facing practical application . . . 369
8. Conclusions and perspectives . . . 372
   Acknowledgements . . . 372
   References . . . 372


## 1. Introduction

### *1.1. Carbon materials for energy storage*

The combined effects of rapid population growth and global energy needs, as well as geopolitical and global warming issues necessitate a policy change to renewable energy sources. The development of high performance energy storage devices has been in increasingly high demand to enable efficient

use of clean and renewable energy sources, such as wind and solar energies. In particular, the widespread application of electric vehicles (EVs) requires finding alternative power sources with high power/energy densities, long cyclic life and enhanced safety. Among many advanced electrochemical energy storage devices, rechargeable Li-ion batteries (LIBs), Li–air batteries (LABs), Li–sulfur batteries (LSBs), Na-ion batteries (NIBs) and supercapacitors (SCs) are of particular interest due to their high energy/power densities [1,2]. The characteristics of electrode materials are the most critical factors that govern the performance of these energy storage devices. Carbon materials have been widely utilized in the electrodes because of their excellent electrical conductivities, large surface areas and chemical stability [3]. Moreover, they can play multi-functional roles as (i) electrode materials [4–6], (ii) conductive additives [7,8] and (iii) substrates for supporting metal (oxides) in the electrochemical energy storage devices [9–11].

Various forms and allotropes of carbon in different dimensions have been explored for application in energy storage systems. One dimensional (1D) carbon nanofibers (CNFs) and carbon nanotubes (CNTs) have several advantages over other forms of carbon allotropes. Firstly, the high aspect ratio of over a few hundreds enables the formation of conductive network at an extremely low percolation [12,13]. Theoretical and experimental studies of polymer-based composites show that a percolation threshold below 0.1 vol.% was not difficult to achieve if they were well dispersed [14]. Secondly, the large surface area can accommodate deposition and encapsulation of metals and metal oxides in high concentrations when employed as substrates or supports [15]. A great number of active metals and metal oxides, such as Sn [16], $MnO_2$ [17] and Ru [18], have been deposited on CNTs/CNFs for LIBs, LABs and SCs. Last but not the least, CNFs/CNTs possess excellent mechanical strengths and flexibility, useful attributes for potential applications in bendable, thin film-based energy storage devices [19,20], where CNFs/CNTs act either as current collectors to replace metal foils [21] or as integrated electrodes with embedded active materials [22]. CNFs and CNTs are also used directly as electrode materials in energy storage systems, where CNFs can be more attractive than CNTs because of the flexibility of creating various morphological features, like core/shell structure and hierarchical pores, which can serve as active sites for reactions. Generally speaking, CNFs have lower crystallinity than CNTs, and can contain numerous defects and functional groups that are active for charge storage and useful in enhancing the energy density [3,23]. The important properties, such as specific gravity, electrical and thermal conductivities, and applications of various forms of carbon, including carbon black, CNTs, CNFs, graphite and graphene, are compared in Table 1 [24–30]. Although CNFs in general possess slightly lower electrical conductivities and smaller surface areas than CNTs, they have unique advantages like easy dispersion and low fabrication cost. They have been widely used for reinforcement of polymer-based nanocomposites [31] and energy storage [32,33]. This paper reviews the current state-of-the art devel-

**Table 1**
Properties of carbon materials and their applications in energy storage devices.

| Carbon | Properties | | | | Application |
|---|---|---|---|---|---|
| | Specific gravity ($g\ cm^{-3}$) | Electrical conductivity (S/cm) | Thermal conductivity (W/(m K)) | Surface area ($m^2/g$) | |
| Carbon black [24] | 0.13–2 | 5–30 | ~0.4 | 10–1443 | Conductive additives; electrodes in LABs |
| CNTs [25,26] | 0.8–1.8 | $10^2$–$10^6$ | 2000–6000 | 50–1315 | Conductive additive; electrode materials; substrates for supporting active metal (oxide) |
| CNFs [27,28] | 1.5–2.0 | $10^{-7}$–$10^3$ | 5–1600 (graphitic CNFs) | 20–2500 | Conductive additives; electrode materials; substrates for supporting active metal (oxide) |
| Graphite [25] | 1.9–2.3 | 4000 (in plane), 3.3 (*c*-axis) | $298^p$, $2.2^c$ | 1–20 | Anodes in LIB |
| Graphene [29,30] | 2.3 | $10^6$ | 600–5000 | 500–2630 | Conductive additives; electrode materials; substrates for supporting active metal (oxide) |

opments and recent advances of electrospun CNFs and their hybrids for electrochemical energy storage, and discusses the strategies for the improvement of their electrochemical performance, as well as future prospects of these interesting materials.

### 1.2. Carbon nanofibers

Unlike CNTs that commonly consist of graphene layers rolled up into a seamless cylinder with the plane parallel to the longitudinal axis, CNFs have various forms depending on the stacking manner of graphene layers, as shown in Fig. 1. The graphene layers can be perpendicular, inclined or even coiled along the fiber axis [34]. Amorphous CNFs without graphene layers can also be prepared by spinning of a polymer precursor, followed by carbonization at a low temperature [35]. Due to excellent mechanical properties, superior thermal and electrical conductivities and high chemical stability, CNFs have shown great potential for large-scale applications in many areas, such as energy storage, nanocomposites, sensors, tissue engineering and biomedicine [36–38]. Two main approaches have been developed for the fabrication of CNFs, namely chemical vapor deposition (CVD) and spinning of carbon precursor.

*Chemical vapor deposition (CVD).* The production of CNFs through CVD process can be traced back to 1889 when carbon filaments were grown from hydrocarbon gas on metal crucibles. The CNFs produced by CVD are also called vapor grown carbon fibers (VGCFs) [39]. Extensive studies were conducted in the 1980s and various hydrocarbons, including methane, ethyne, ethane and carbon monoxide, have been employed as carbon precursors. The hydrocarbon molecules decompose on the metal catalyst in the temperature range 700–1200 K and the diffusion of carbon atoms allows the formation of fiber structures with embedded graphene layers. The most commonly used catalysts are iron, cobalt and nickel, which play an important role in determining the structure of as-prepared CNFs. Martin-Gullon et al. investigated the different properties of CNFs produced using Fe and Ni catalysts, and found that thick CNFs with a multi-walled CNT core were produced when Fe was employed as the catalyst. In comparison, stacked-cup-type CNFs were produced with Ni as the catalyst [34]. VGCFs possessed excellent electrical conductivities arising from the high graphitization temperature. Therefore, they have been considered as potential conductive additives to replace carbon black in LIBs because they greatly improved the electrochemical performance with lower contents [40]. However, the production cost was relatively high, which inhibited their widespread applications. Moreover, VGCFs has a hydrophobic surface, making it difficult to uniformly attach metal (oxides) for energy storage application.

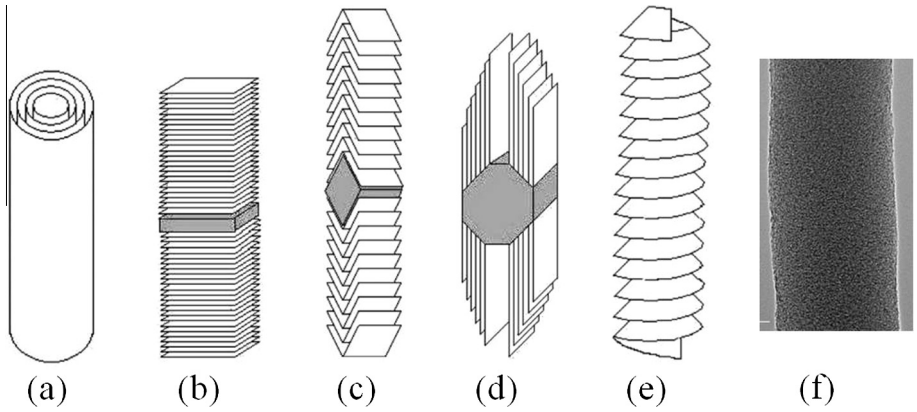


**Fig. 1.** Structure of (a) multi-walled CNTs; (b) graphene platelets, (c) graphene fishbones, (d) graphene ribbons and (e) stacked-cup CNFs [34]; and (f) amorphous CNF without graphene layers. (Reprinted with permission from [34]. Copyright 2006 Elsevier.)

*Spinning*. Production of carbon fibers from polymer precursors has a long history of more than 60 years. Precursor polymers are extruded to form multiple continuous filaments using a spinneret based on several spinning techniques, such as wet, gel, melt and dry spinning [41–43]. A typical wet spinning apparatus is shown in Fig. 2 [44,45]. Polymer is dissolved in a solvent to produce the precursor solution, which is then ejected out through the spinneret in a coagulation bath. The polymer fibers are precipitated after drawing into the bath and solidified to form a one-dimension structure after washing and evaporation of solvent. If the polymer solution is ejected into air instead of the coagulation bath, and is solidified by gas flow, this technique is called "dry spinning" [46]. To obtain high strength fibers, in some cases the polymer precursor solution is made into a gel to keep polymer chains partly entangled. The spinning technique using the gel precursor is named as "gel spinning" [47]. Apart from dissolution of polymer into a solvent, the precursor can also be prepared by melting a polymer at an elevated temperature between 250 and 400 °C in the absence of a solvent. The spinning process using the polymer melt is called "melt spinning" [41]. The diameter of the spun fibers can be tailored by adjusting the spinneret size and drawing speed. The polymer fibers can also be stabilized and graphitized under tension to form into strong/stiff carbon fibers in a continuous multistep thermal treatment. Polyacrylonitrile (PAN) and mesophase pitch (MP) are the two major precursors for the production of carbon fibers through wet-spinning or melt-spinning. PAN-based carbon fibers have a high strength while MP-based fibers possess a high modulus [48]. Due to their excellent mechanical properties (up to 900 GPa in modulus) and thermal stability, they have been extensively applied to reinforce polymer-based composites for a number of structural applications, including aerospace, automobile, sporting goods and construction industries.

However, carbon fibers produced by these spinning techniques typically have diameters of more than 5 μm. It should be noted that the so-called "CNFs" normally refer to carbon fibers whose diameter is less than 1 μm. The large diameter makes electrons and ions difficult to diffuse into the core part of carbon fibers when used in energy storage systems. In addition, the large diameter means a

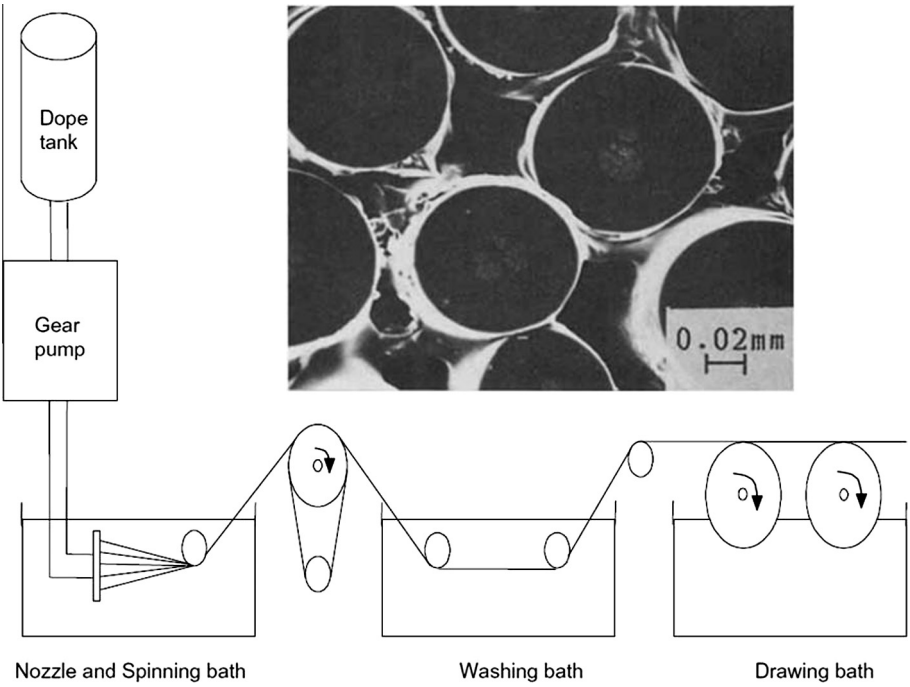


**Fig. 2.** Schematic of wet spinning apparatus [44], the inset shows typical morphology of fibers produced by wet spinning [45]. (Reprinted with permission from [44,45]. Copyright 2007 Elsevier, 1989 Wiley.)

**Table 2**
Comparison of various techniques for producing CNFs.

| | Diameter | Electrical conductivity | Cost |
|---|---|---|---|
| CVD | <1 μm | High | >US$50/kg |
| Traditional spinning | >5 μm | Vary[a] | ~US$20/kg |
| Electrospinning | 10 nm–10 μm | Vary[a] | – |

[a] Depending on thermal annealing process.

drastically reduced aspect ratio, requiring much higher contents to establish percolation to form conductive networks. Therefore, the aforementioned microsized carbon fibers are seldom used for energy storage. One of their potential applications is the current collector to replace traditional copper or aluminum foil in view of their high conductivities, low densities and excellent mechanical properties [49].

In contrast to mechanically-driven spinning, in electrospinning a high voltage is applied to the polymer solution which is ejected in a fiber form making use of the interaction between the charged polymer and external electrical field. Among all of these spinning techniques, electrospinning is the most effective way to produce CNFs with diameters ranging from tens of nanometers to several hundred nanometers which have been widely used in electrochemical storage devices with multifunctionalities [50]. Moreover, the electrospinning technique can be easily scaled up, thus showing promising future for industrial production [51]. The qualities of CNFs produced by three major techniques, including CVD, traditional spinning and electrospinning, are compared in Table 2 in terms of diameter, electrical conductivity and cost. It is apparent that electrospinning is much more effective in producing CNFs with small diameters and high electrical conductivities than the traditional spinning technique. The cost of electrospun CNFs is expected to be much lower than that produced by CVD methods because of more simple processes. Moreover, electrospinning offers facile approaches to fabricate metal (oxides)/CNF hybrids as will be discussed later.

## 2. Electrospinning

### 2.1. Set-ups for producing fibers with different structures

The fundamental ideal of electrospinning can be traced back to 100 years ago when an electric force was applied to stretch fluids [52,53]. Although significant improvement has been made since then, the basic device with its operating principle is similar, as illustrated in Fig. 3. The spinning device

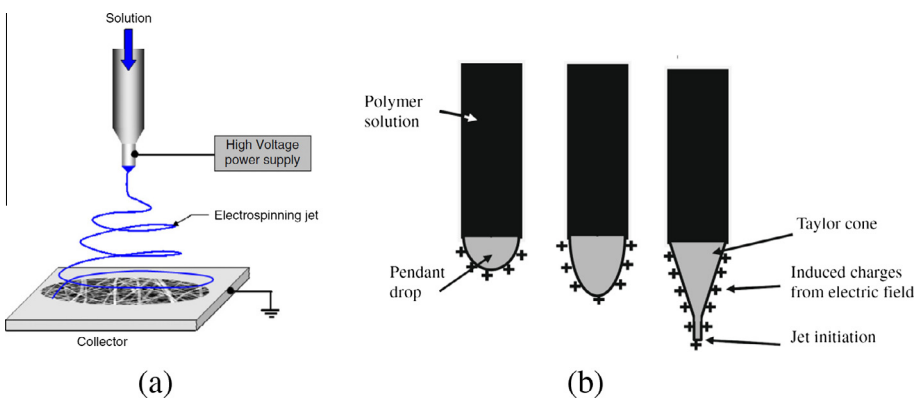


**Fig. 3.** Schematic drawings of (a) electrospinning device [54] and (b) formation of Taylor cone under increasing voltage (from left to right) [55]. (Reprinted with permission from [54,55]. Copyright 2006 IOPscience, 2010 Elsevier.)

typically comprises of a syringe pump to control the flow rate of polymer solution, a spinneret for ejecting fibers, a collector for collecting fibers and a high voltage supply to apply an electric current between the spinneret and the collector [54]. The polymer solution is charged under a high voltage, resulting in the generation of an electrostatic force. The balance between the electrostatic force and surface tension makes the hemispherical surface contour of the solution into a conical shape, the so-called "Taylor cone", as shown in Fig. 3b [55]. The electrostatic force overcomes the surface tension when the electric field is high enough so that a jet will be ejected from the spinneret. The initial jet near the "Taylor cone" is straight. After the ejection, the electrostatic repulsion force between the charged jets becomes stronger because of the evaporation of solvent, leading to splitting of the jet into a number of tiny jets. The process at this stage is unstable causing the jet to spiral, resulting in the whipping region. When the jets arrive at the collector, they become solidified into fibers due to further evaporation of solvents.

The real mechanisms behind the electrospinning process are quite complex. Several theoretical models have been established in order to give in-depth insights into the process, especially on whipping instability. The first model was developed by Taylor in the 1960s, which is called the "leaky dielectric model". This model is applicable when the electrical conductivity of fluids is finite and has been successful in predicting the jet initiation [56]. Following this, various models have appeared to predict the behaviors of jet thinning in the whipping stage [57] and jet solidification to form nanofibers [58]. While they were used to predict part of the electrospinning process under certain conditions, none of them were able to estimate quantitatively the final diameters and orientations of fibers [59,60]. Optimized models based on in-depth understanding of the dynamics and chaos phenomenon during electrospinning should be further developed.

In order to best utilize the advantages of fiber structure, a large number of modifications have been incorporated into the basic design for fabricating interesting nanostructures with different fiber orientations and configurations. Most of the modifications are based on engineering advances of spinnerets and collectors for preparing fibers with random, aligned, twisted and core/shell structures.

#### *2.1.1. Random fibers*

Due to the whipping occurring when the spun fibers arrive at the collector, the collected products are likely to be randomly-oriented and entangled polymer fibers in the form of a thin film. The set-up for producing randomly-oriented fiber webs is simple: a single nozzle with a metal plate or graphite paper collector is used, as shown in Table 3 [61–63]. The collector can be placed either vertically or horizontally, and the positive and negative electrodes are connected to the spinneret and collector, respectively. Multiple nozzles are sometimes employed to speed up the spinning process. In order to produce a fiber film with a uniform thickness, a relatively low rotation speed, say less than 500 rpm, can be adopted for the drum collector together with a transverse movement of the spinneret [35,54].

After a thermal treatment, the polymer fiber film is transformed to CNFs, and the film structure can be maintained to make freestanding CNF films. The freestanding films with fibers of random orientation are the major form of CNFs that have thus far been popularly employed in electrochemical energy storage. Recently, many studies are directed toward production of aligned or core/shell structured fibers capable of offering additional benefits that the fibers with random orientations are lacking.

#### *2.1.2. Aligned fibers*

Aligned fibers deliver many advantages compared to their random counterparts in the application of many fields, such as carbon fiber-reinforced nanocomposites and neural tissue engineering [55,64,65]. Electrospun fibers have a high orientation of polymer macromolecular chains along the fiber axis due to the elongation strains and shear forces in the jet, making them much stronger than traditional fibers [55]. Apart from the molecular orientation, the alignment of electrospun fibers can have a great potential in the production of high strength/high toughness fiber reinforced composites. To produce aligned fibers, several new set-ups are necessary with modifications, especially on collectors.

One of the most popular ways to produce aligned fibers is to use a drum collector that rotates at a very high speed, as shown in Table 3. Matthews et al. first observed the alignment of collagen fibers

**Table 3**
Different set-ups for producing various fiber structures. (Reprinted with permission from [35,54,55,61,63,68,70–72,74,76,77]. Copyright 2003, 2004, 2006, 2014 Wiley, 2006 IOPscience, 2009, 2010 Elsevier, 2003, 2004, 2005 ACS.)

| Fibers | Set-up | Morphology | Advantages | Disadvantages | Refs. |
|---|---|---|---|---|---|
| Randomly oriented | 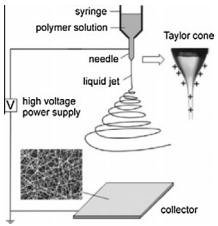 A plate collector | 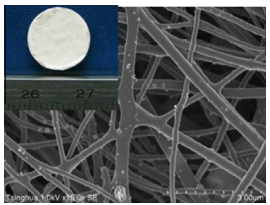 | Simple | Non-uniform film thickness | Li et al. [61,62]<br>Zou et al.[63] |
| | 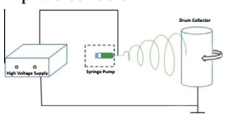 Drum collector, rotating at a low speed | 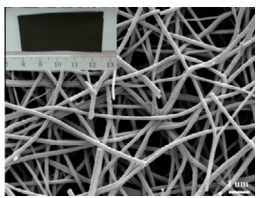 | Uniform thickness | A motor is required to keep the collector rotating | Zhang et al. [35] |
| Aligned | 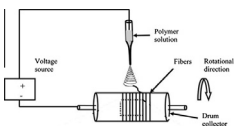 Drum collector, rotating at a high speed | 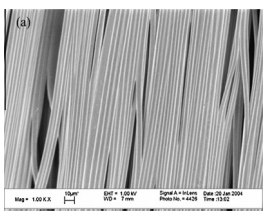 | Long aligned fibers are possible | High rotating speed; difficult to obtain thick films | Baji et al. [55]<br>Chew et al. [68] |

(*continued on next page*)

**Table 3** (*continued*)

| Fibers | Set-up | Morphology | Advantages | Disadvantages | Refs. |
|---|---|---|---|---|---|
| | 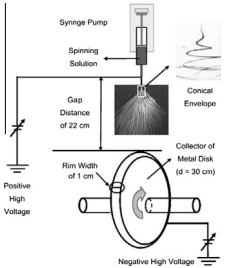 Disk collector, rotating at a high speed | 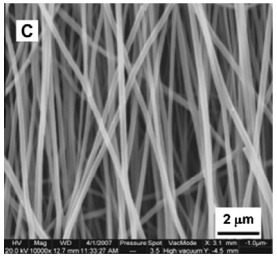 | Long aligned fibers are possible | Small area and difficult to obtain thick films | Zhou et al. [70] |
| | 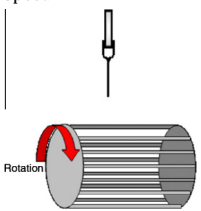 Wire drum collector, rotating at a low speed | 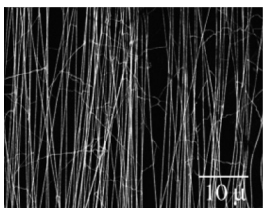 | Do not need a high rotating speed | Difficult to obtain thick films | Teo et al. [54]<br>Katta et al. [71] |
| | 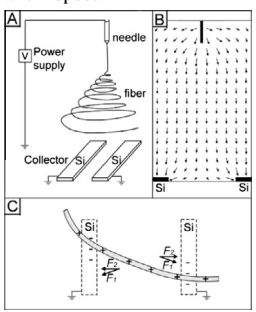 Two parallel plate collector | 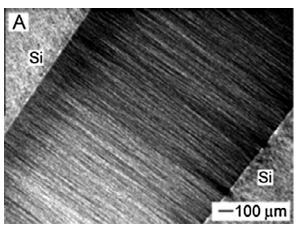 | Simple approach | Length of fiber is restricted by the gap distance; difficult to obtain thick films | Li et al. [72] |

| | | | | | |
|---|---|---|---|---|---|
| Core/shell structure | 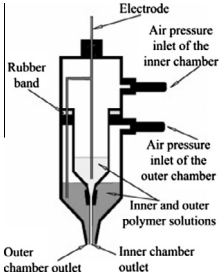 <br>Dual nozzle spinning with two different polymer solution | 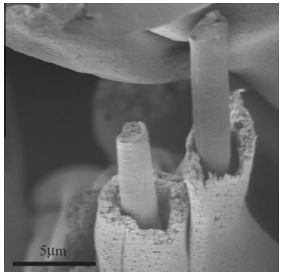 | Core–shell structured fiber | Outer and inner solutions may diffuse and mix together | Sun et al. [74]<br>Zussman et al. [76] |
| | 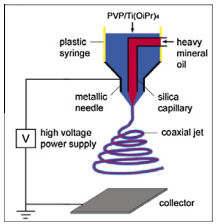 <br>Coaxial spinning with mineral oil inside and polymer solution outside | 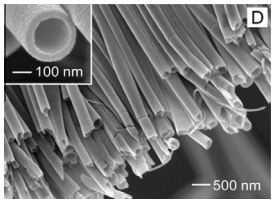 | Diffusion of inside solution can be avoided | Require additional process to remove oil | Li et al. [77,78] |

when a rotation speed of 1.4 m/s was used: at speeds lower than this value, the fibers were found to be randomly-oriented [66]. In another study using electrospun PAN fibers, partial alignment was observed when the rotation speed was 3.5 m/s, and the degree of orientation increased with increasing rotation speed [67,68]. During electrospinning, one end of the fibers is electrostatically attached to the surface of the rotating collector, which will continuously stretch the fibers generated by the unstable whipping jet. The drawing force increases with increasing rotation speed, leading to better alignment. Similar alignment can be produced using a disk collector to replace the drum collector, which also rotates at a high speed [69,70]. It should be noted, however, that too high a rotation speed may break the fibers. Currently, no studies have proposed threshold rotation speeds required to achieve fiber alignment using different kinds of polymers. A theoretical model is needed to predict the optimized rotation speed, taking into account the processing parameters, polymer properties and jet velocity. One major drawback of the technique based on a high collector speed is that it is difficult to obtain perfectly aligned fibers. The residual charges on the previously collected fibers may interfere with the new fibers, resulting in their disorientation. In order to improve the alignment quality, a wire drum collector was designed (Table 3) where a high rotation speed was unnecessary for the collector. The electrospun fibers moved from one wire to another of the collector trailing the shortest distance between the wires under electrostatic forces, thus making them aligned. Highly aligned nylon-6 fibers were obtained in less than 40 min of electrospinning. However, when spinning was continued for two and a half hour along with a thickness increase, the alignment was disrupted possibly due to the accumulation of charges [71].

An alternative alignment approach is to use two stripes of parallel conductors as collectors, as illustrated in Table 3 [72]. The applied electric field splits into two fractions pointing the two stripes and generates a force marked as F1, which pulls the ends of fibers to the stripes. The other force designated as F2 is related to the force between the charged fibers and surface charges of the collector, placing the fibers across the gap perpendicular to the stripes. A major disadvantage of this technique is that the length of fibers is limited by the gap distance between the two stripes, which may also affects the orientation of fibers. A gap distance of 3 cm produced the best alignment for PAN fibers [73].

### *2.1.3. Core/shell structured fibers*

Core/shell structures have been widely studied for various applications because of their unique features that can ameliorate the desired properties. In general, the core plays the major role in enhancing the required functional characteristics while the shell serves as a protective layer or a support/substrate to hold the core materials for sustainable function of the core. A well-developed core/shell structured fibers have many advantages over mono-structured fibers, including the feasibility to tune, modify, reconstruct, dope and functionalize the core materials which are otherwise simply dispersed within the mono-structured matrix fiber. Fibers with a core/shell structure have attracted much attention as electrode materials for electrochemical energy storage devices. Electrospinning employing dual nozzles provides a facile way to produce continuous, core/shell structured fibers on a large scale. A typical set-up for the process is shown in Table 3 where two separate precursor solutions are filled into the outer and inner nozzles [74,75]. Co-electrospinning of the two different polymer solutions using a co-axial nozzle was first reported in 2003 [74], when poly(ethylene oxide) (PEO) in chloroform and poly(L-lactide) (PLA) in dichloromethane were used as the outer and inner solutions, respectively. Following this work, Zussman et al. investigated the poly(methyl methacrylate) (PMMA)/PAN core–shell systems [76]. They found that a critical issue to obtain a fine core/shell structure was to use two immiscible polymer solutions; otherwise, the two solutions blended together without creating the desired core/shell structure. Therefore, a blended solvent of acetone and dimethylformamide (DMF) was used to dissolve PMMA for the inner solution, where acetone separated the core and shell by precipitating PAN.

Co-electrospinning is also used to fabricate hollow fibers using the same principle and set-up. One approach is to produce core/shell polymer fibers in which the inner polymer is removed as a sacrificial phase. For example, the inner PMMA fibers were decomposed at an elevated temperature whereas the shell PAN fibers were carbonized to produce hollow CNFs [76]. Another approach proposed later was to adopt heavy mineral oil as the core solution. The oil was extracted out by immersing the fibers in octane after electrospinning, leaving only the shell fiber with a hollow structure [77,78].

The core/shell structure has great potential for producing new types of CNFs that consist of a carbon shell and a metal or metal oxide core. The electrodes made from the core/shell structure can accommodate large volumetric strains of metal (oxides) generated during the electrochemical cyclic reactions of energy storage devices. Si and Sn nanoparticles were successfully encapsulated in the hollow CNFs for application as anodes in LIBs [79,80]. The advantages of maintaining the structure integrity and delivering excellent electrochemical performance arising from the unique core–shell structure will be discussed in Section 3.

### 2.2. Precursors for electrospinning

The optimal processing conditions that can successfully produce fibers in electrospinning is strongly dependent on precursors that also affect the final fiber structure, such as diameter and length. The precursors for use in energy storage devices are mainly polymers which are dissolved in a solvent. Table 4 summarizes the precursors widely employed for energy storage applications. Depending on the functions that the precursors should play, they can be divided into two groups, namely the host precursor and the guest precursor. The host precursors, such as PAN and polyimide (PI), function as the scaffold for fiber structure, and are normally carbonized to form CNFs after thermal treatment (s) in an inert atmosphere. The guest precursors, such as PMMA and polystyrene (PS), are a sacrificial phase and removed after heat treatment(s) to create special features in the finished CNFs. One of the most popular purposes of using guest precursors is to produce void space for accommodating various metal (oxides), which will be discussed later.

*Polyacrylonitrile (PAN)*. PAN is the most popular host polymer precursor for producing electrospun CNFs. It has a high carbon yield of more than 50% and the CNFs made therefrom show excellent mechanical properties. Pristine PAN fiber films are also investigated as separators [81]. To convert the spun polymer fibers into CNFs, a two-step heat treatment is required, namely stabilization and carbonization. Stabilization aims at maintaining fiber structure during the high temperature carbonization, and is normally carried out at a temperature between 200 and 280 °C in air to form a ladder structure consisting of a series of connected C–N aromatic rings by the dehydrogenation and cyclization process, as shown in Fig. 4a [82]. Double bonds are formed during the dehydrogenation process through oxidation and elimination of water. Nitrile groups react with adjacent groups to form a ladder structure so that PAN fibers become thermally stable in the following carbonization process. The carbonization process is carried out in an inert atmosphere, where the heteroatoms like nitrogen are eliminated and the aromatic structure grows, as shown in Fig. 4b [83,84]. Essentially the same two-step processes are applied for the conversion of polymer fibers produced using other precursors into CNFs although the exact processing conditions may differ. Similarly to the procedure required for the production of high modulus carbon fibers, another process named 'graphitization' is sometimes added to further remove heteroatoms and increase the orientation of basal planes. A high temperature up to 3000 °C is employed for graphitization, after which CNFs contain more than 99% of carbon atoms and graphitic layers, resulting in an excellent electrical conductivity [83]. Nevertheless, the graphitization process is rarely conducted for PAN-based CNFs intended for energy storage, because it may bring about deteriorating effects arising from the high temperature treatment. The O and N containing functional groups that actively participate in Li/Na storage as well as pseudocapacitance in SCs are mostly eliminated after annealing at high temperatures [35]. Moreover, a high temperature treatment could lead to rapid growth and separation of metal oxides that are embedded in CNFs [63].

*Pitch*. Pitch is another important precursor for the production of CNFs. Due to its high carbon yield (~60% at 1000 °C) and low cost, it has been widely used by traditional spinning techniques, such as melt spinning of carbon fibers. A high concentration pitch solution is required to achieve sufficient viscosity for electrospinning [85]. Tetrahydrofuran (THF) has been proven to be a proper solvent for preparing pitch solution, and a 40 wt.% of pitch is needed to obtain fibers of uniform thickness and properties by electrospinning. The molecular structure of pitch significantly affects the spinnability [86,87]: pitch with a high molecular weight has shown a high solubility and viscosity, resulting in better spinnability. A blend of pitch and PAN has also been used as a precursor for electrospinning: the addition of PAN increases the spinnability and decreases the diameter of the as-prepared fibers [86].

**Table 4**
Polymer precursors used in electrospinning.

| Precursors | Chemical structure | Electrospinning condition | Functionalities | Advantages | Disadvantages |
|---|---|---|---|---|---|
| PAN | 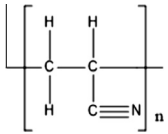 | 4–10 wt.% in DMF, 10–30 kV | Carbon source for CNFs and their hybrids | High carbon yield (>50%) and spinnability | Typically only DMF is used as solvent |
| Pitch | – | 30–40 wt.% THF/DMF, 18–25 kV | Carbon source for CNFs | High carbon yield (60% at 1000 °C) | Low spinnability |
| Lignin | – | 20–35 wt.% in DMF/water, 6–26 kV | Carbon source for CNFs | Large surface area | Large diameter; low carbon yield of 20–40% |
| PI | 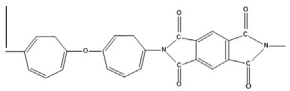 PMDA/ODA type | 10–20 wt.% in N-methyl, pyrrolidone/THF/methanol/DMAc, 8–25 kV | Carbon source for CNFs, separator for LIB | High conductivity of as-prepared CNFs | Complex fabrication process |
| PVDF | 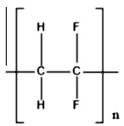 | 7–25 wt.% in DMAc/DMF/acetone, 15–20 kV | Separator and gel electrolyte for LIB | High mechanical properties | Require dehydrofluorination for carbonization |
| PVP | 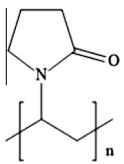 | 4–10 wt.% in ethanol/DMF, 10–25 kV | Carbon source for metal oxide/CNF composites and template for neat metal oxide fibers | Soluble in various solvent | Low carbon yield of ~15% |
| PVA | 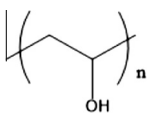 | 10 wt.% in water, 8–35 kV | Carbon source for metal oxide/CNF composites | Water soluble | Low carbon yield of 3–10% |

| | | | | | |
|---|---|---|---|---|---|
| PMMA | 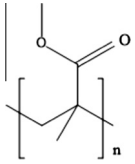 | 8–10 wt.% in DMF, 10–20 kV | Scaffold for neat metal oxide fibers and sacrificial phase for voids | Compatible with other host polymer, such as PAN | Difficult to be fully removed, requiring 1000 °C |
| PS | 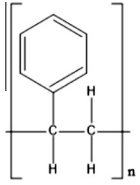 | 5–35 wt.% in DMF/THF/chloroform, 15–25 kV | Scaffold for neat metal oxide fibers and sacrificial phase for voids | Easy to be decomposed at ~450 °C | Poor compatibility with host polymer, beads are easy to form |

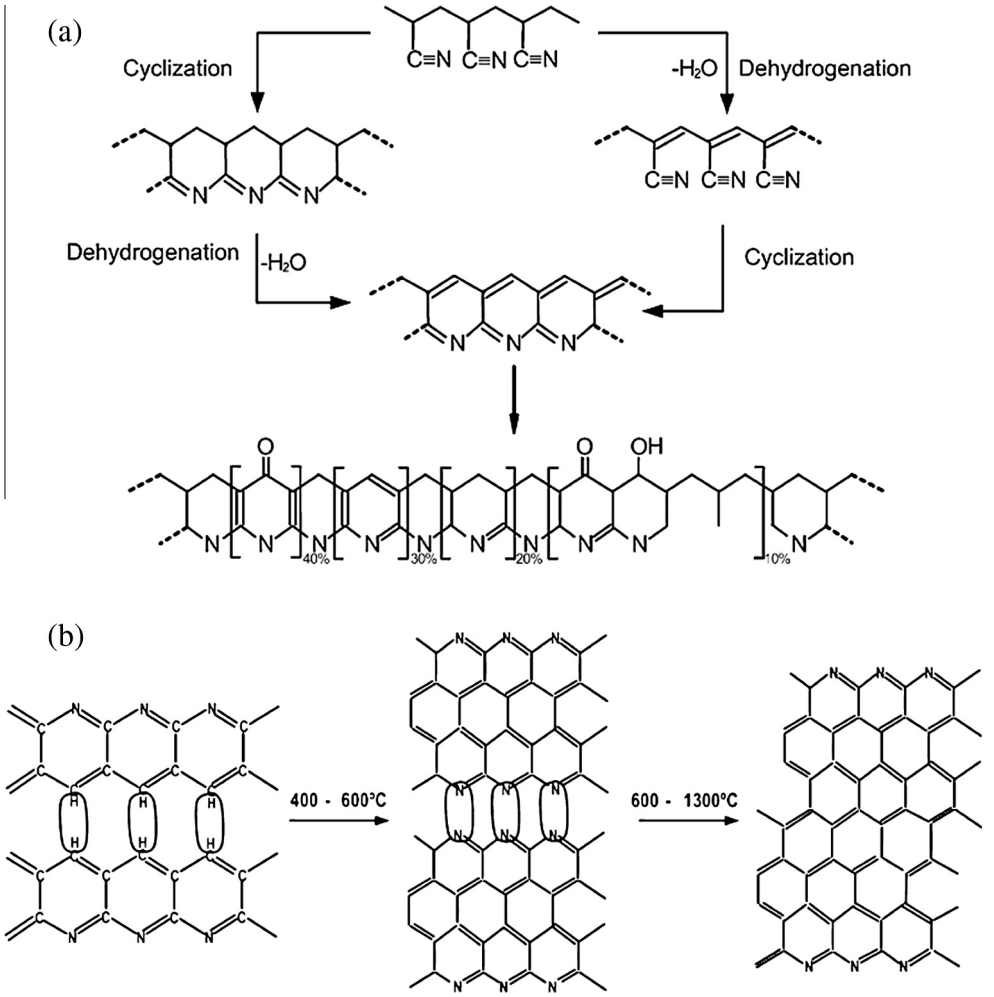


**Fig. 4.** Structural changes of PAN during (a) stabilization [82] and (b) carbonization [83]. (Reprinted with permission from [82,83]. Copyright 2002, 2007 Elsevier.)

*Lignin*. Being the second abundant polymer in nature and possessing a number of aromatic components, lignin has great potential as the carbon source for electrospun CNFs. Two kinds of lignin are employed for electrospinning: one is Alcell lignin with a small amount of impurities, and the other is alkali lignin which contains large amounts of ashes and salts [88]. In order to avoid the fusion of fibers at high temperatures, lignin-based fibers are stabilized at 180–220 °C for several hours in air before carbonization at 600–1000 °C [89,90]. One of the main features of lignin-based CNFs is the large specific surface area, attributed to the activation by high content oxygen which is generated during the stabilization process. A remarkable surface area of 1195 $m^2/g$ for Alcell lignin-based CNFs carbonized at 900 °C was reported [91]. One drawback of lignin is the low carbon yield of only around 20–40% depending on the carbonization temperature [92].

*Polyimide (PI)*. Membranes made from electrospun PI fibers have attracted much attention as separators in LIBs due to the high stability of PI at temperatures up to 500 °C [93]. Moreover, PI-based CNF mats delivered a high electrical conductivity of 16 S/cm when carbonized at 1000 °C, proving to be an excellent candidate for freestanding electrode in energy storage devices [94]. Most of PI-based electrospun CNFs uses a pyromellitic dianhydride (PMDA)–oxydianiline (ODA) type PI precursor. Poly(amic

acid) (PAA) is synthesized through polymerization of PMDA and ODA, which is then dissolved in N,N-dimethylacetamide (DMAc) prior to electrospinning into PAA fibers. PI fibers are obtained by inidization of PAA fibers, followed by carbonization for conversion into CNFs [95]. Similar to PAN-based CNFs, the thermal treatment of PI fibers also includes the elimination of heteroatoms at a low temperature ranging 350–800 °C, aromatic growth at 800–1600 °C, followed by graphitization at 1600–3000 °C [96]. PI has a similar carbon yield to PAN: e.g. 53% yield was reported after carbonization at 1000 °C [97].

*Poly(vinylidene fluoride) (PVDF).* PVDF membranes consisting of electrospun PVDF fibers have been widely studied as a gel electrolyte for LIBs [98]. The membranes possess excellent mechanical properties with a tensile modulus of 153.4 MPa, a tensile strength of 15.9 MPa and an elongation of 10–20%, making them a potential candidate for replacing the commercial polypropylene-based Celgard separator. Furthermore, the PVDF membranes have a porosity of 80–89% being able to uptake a high content of electrolyte solution of 320–350%, an important attribute for a promising gel electrolyte [99,100]. Modifications were made by incorporating $SiO_2$ nanoparticles and PEO into the electrospun PVDF membranes for improved wettability and ionic conductivity. An ionic conductivity of $4.9 \times 10^{-3}$ S/cm at room temperature was achieved by the PEO/PVDF membrane [101,102]. Before carbonization of PVDF fibers, chemical dehydrofluorination was required to stabilize the fibers. Highly porous PVDF-based CNFs with a surface area of more than 380 $m^2/g$ were obtained after carbonization at 1000 °C, showing potential application in supercapacitors [103].

*Polyvinyl alcohol (PVA) and polyvinylpyrrolidone (PVP).* PVA is often used to produce freestanding CNF films and their hybrids with metal oxides. Although it has a low carbon yield of only 3–10% due to decomposition at high temperatures, PVA is easy to handle because of the excellent solubility in water [63]. The carbon yield of PVA can be improved to 40–50% after an iodination treatment [104]. PVP also has a low carbon yield of around 15% [105], making it difficult to mass produce PVP-based CNF films. Thus, PVP is mainly employed as a scaffold to produce neat metal oxide fibers after removing PVP using a thermal treatment in air [106]. One of the major advantages making PVP attractive for electrospinning is its solubility in various solvents, including water, ethanol, DMF and dichloromethane. PVP can also be carbonized in an inert gas to produce carbon-coated metal oxide fibers [107].

*Poly(methyl_methacrylate) (PMMA) and polystyrene (PS).* PMMA and PS are the most popular sacrificial polymers employed in electrospinning. They can function as (i) scaffold for producing neat metal oxide fibers and (ii) sacrificial phase to create void space after decomposition by carbonization. PMMA was the first sacrificial phase employed in electrospun PAN fibers using a dual nozzle and was later employed to create randomly-dispersed pores along the CNFs by blending with PAN using in single nozzle [108]. PS decomposes at ~400 °C in an inert environment. The electrospun $TiO_2$/PS fibers yielded only 0.47 wt.% of carbon after a thermal treatment at 450 °C for 1 h in Ar gas [109]. PMMA was almost fully decomposed at 1000 °C with less than 0.2 wt.% residue [110].

In summary, the advantages and disadvantages of various polymer precursors are included in Table 4. The following several points should be considered when selecting polymer precursors for electrospun CNFs and their hybrids: namely (i) carbon yields; (ii) compatibility with other precursors; (iii) properties of metal (oxide) precursors. For producing neat CNF films and metal/CNF composite films, precursors with high carbon yields should be chosen, such as PAN, pitch and PI. Otherwise, it is difficult to maintain a freestanding film. When the carbon matrix does not much contribute to the capacity/capacitance of the electrodes, then a low carbon yield may be preferred where PVP is frequently used. When several different precursors have to be blended together into a solution, such as metal oxide precursors and polymers, it is necessary to consider their chemical/physical compatibility with the solvent and additional stabilization and carbonization treatments after electrospinning. The properties of as-prepared CNFs, including their diameters, surface areas, electrical conductivities and compositions, are strongly dependent on the properties of the individual precursors employed. All of these properties have significant influences on the performance of the final CNFs.

### 2.3. Processing parameters

One of the major objectives of electrospinning is to produce fibers with uniformly small diameters. However, "beads" of much larger sizes than the fiber diameter are often formed if the processing and

material parameters are not optimized. When the viscosity of the precursor material is insufficient to resist the electrostatic field, the polymer jets tend to break up to form droplets in the shape of ellipsoid or sphere due to the polymer surface tension. The viscosity and surface tension of the precursor solution as well as the electrostatic forces govern the quality of the fibers formed. The electrostatic forces are applied to stretch the polymer jets into a fiber shape. In contrast, a high surface tension tends to maintain the jets in a spherical shape to decrease the surface energy. Meanwhile, quick changes of jet shapes are inhibited by the viscoelastic force. All materials and processing parameters that affect the above three forces influence the quality of the final products. There are several parameters which have been widely investigated, including the molecular weights of polymer precursors; concentrations, electrical conductivities and viscosities of precursor solution; applied voltage, flow rate and distance between the nozzle and collector, the so-called "collecting distance". The principles and importance of these factors are further discussed in the following.

*Viscosity of precursor solution*. The viscosity, $\eta$, of the precursor solution is among the most important factors that influence the bead formation and the diameter of fibers. It is determined by both the concentration and molecular weight ($M$) of polymers. For a linear polymer, the Mark–Houwink–Sakur ada equation gives:

$$\eta = k_1 M^a \tag{1}$$

where the constants $k_1$ and $a$ are determined by the applied temperature, and the types of polymer and solvent. They can be obtained empirically by logarithmic fitting of experimental data [111]. A sufficiently high viscosity is required to prepare bead-free fibers, while a high molecular weight increases the viscosity. The viscosity of a PS/DMF solution was shown to increase almost linearly with its concentration [112]. The morphologies of PEO fibers produced using solutions of different viscosities were studied, finding an optimal viscosity of PEO/water solution of 1250 cP for uniform fiber diameters. Beads were formed at viscosities lower than the optimal value and the number of beads per area increased with a decrease in viscosity [113]. A similar conclusion was also drawn for a PAN/DMF solution: the beads are more easy to form in a low concentration of 5 wt.% compared to that of 7 wt.% which has a high viscosity, as shown in Fig. 5a [114]. The viscosity also had a strong effect on fiber diameter. Generally speaking, the fiber diameter, $d_f$, increases with an increase in viscosity, according to the equation:

$$d_f = k_2 \eta^n \tag{2}$$

where $k_2$ is a constant and $n$ depends on the type of polymer precursor: $n$ was found to be 0.41 and 0.72 for PS and PMMA, respectively [111,115]. The relationship between the fiber diameter and viscosity of PMMA solutions with different molecular weights is shown in Fig. 5b.

*Surface tension of precursor solution*. The surface tension of polymer solution should be kept low to reduce the required applied voltage. A low surface tension also favors smooth fibers by avoiding the formation of beads [113]. The surface tension is determined not only by the inherent surface tension of polymer, but also by the type of solvent used. For example, the PEO/water solution had a much higher surface tension than the PEO/water/ethanol solution. However, the concentration of the solution did not have much impact on surface tension [113,115]. These findings have a significant implication when choosing appropriate polymer precursors and solvents. Solvents with a high surface tension, such as water, may decrease the spinnability because it is more likely to form beads.

*Electric field and collecting distance*. The electric field controls the electrostatic force acting on the polymer jet in the Taylor cone. Both the applied voltage and collecting distance affect the electric field established between the nozzle and collector. It is surprising to note that the applied voltage had a negligible effect on fiber diameter for a range of polymer concentration between 6 and 12 wt.%, as shown in Fig. 5c [116]. However, there is a critical voltage required for effectively stretching the polymer jet into fibers, which is governed by both the surface tension and viscosity of solution. For instance, the relation between the critical voltage and molecular weight of PAA is given by:

$$E^2_{\text{critical}} \approx 563\left[1 - \left(\frac{57,178}{M}\right)^{1.8}\right] \tag{3}$$

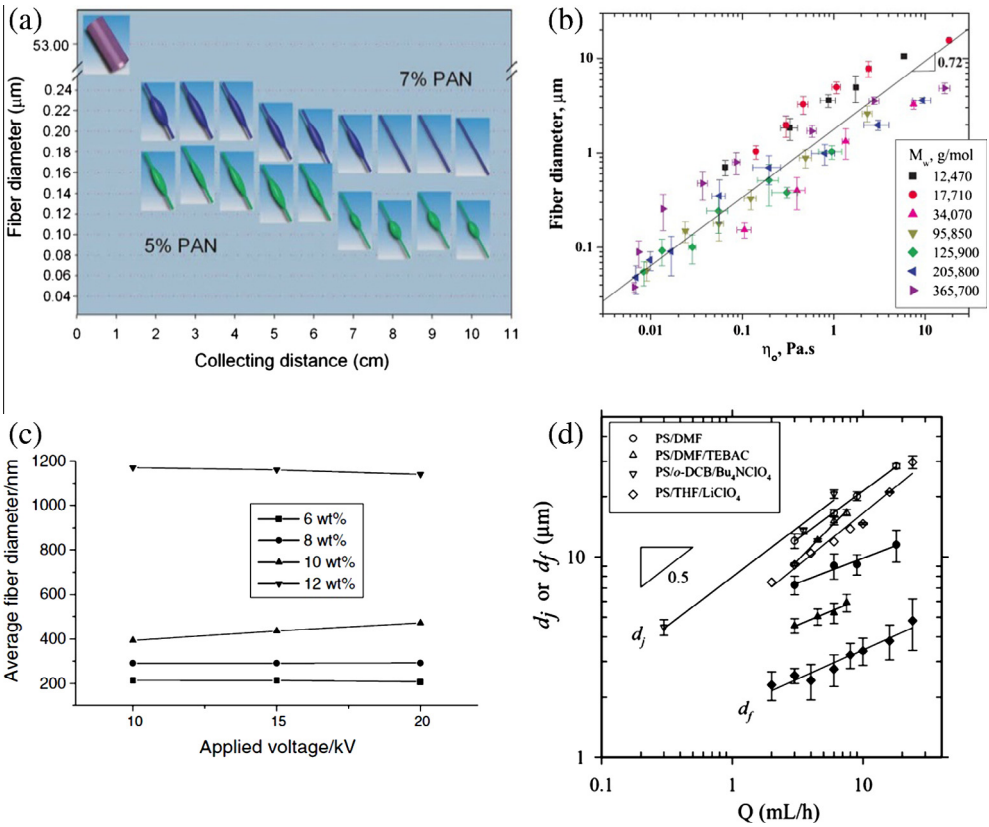


**Fig. 5.** (a) Bead formation in PAN/DMF solution with different concentrations and fiber diameters as a function of collecting distance [114]; (b) relationship between PMMA fiber diameter and viscosity of precursor solution, where $d_f \sim \eta^{0.72}$ [111]; (c) PAN fiber diameter as a function of applied voltage [116]; and (d) diameters of jet ($d_j$) and fiber ($d_f$) as a function of flow rate ($Q$) in different polymer/solvent systems [115]. (Reprinted with permission from [111,114–116]. Copyright 2005 Elsevier, 2010 Wiley, 2006 ACS.)

where $E_{\text{critical}}$ is the critical voltage and $M$ the molecular weight of PAA. The higher the molecular weight, the higher the critical voltage required for polymer stretching because a higher molecular weight increases the viscosity [94]. The influence of collecting distance is similar to that of applied voltage: it should be large enough to avoid the formation of beads, as shown in Fig. 5a. When the distance was shorter than about 8 cm, beads were formed for 7% PAN solution because the spinning solution was not fully stretched [114]. Nevertheless, the fiber diameter did not change much even with a longer collecting distance.

*Flow rate of solution.* The flow rate of polymer solution is important because it determines the fiber structure as well as the electrospinning efficiency. A study on PS solution indicates that increasing the flow rate greatly increases both the diameters of jet and final fibers, as shown in Fig. 5d. In addition, the flow rate of solution needs to be taken into account when deciding the applied voltage. A high voltage is normally required to obtain a stable cone-jet mode when the flow rate is high [115]. Maintaining a smooth fiber structure and suitable fiber diameter at a high flow rate is desired for mass production of electrospun CNFs for energy storage so as to improve the production efficiency.

Apart from the above, other parameters, such as the electrical conductivity of solution, solvent volatility and humidity, also affect the structure and quality of fibers. A high electrical conductivity favors small-diameter fibers. However, the Taylor cone did not form when the conductivity of solution was too high, resulting in the failure to produce fibers [117]. A suitable solvent volatility is also

required to avoid the self-dissolution of fibers in the collector. Nevertheless, if the solvent evaporates too fast, the precursor solution may solidify on the nozzle tip and block it. Humidity can affect both the processability and morphology of fibers. In general, the humidity should be kept at a low level to avoid possible reactions between the polymer fibers and moisture. Polymer systems, like PVP/ethanol, are difficult to spin when the humidity is too high because PVP is highly hygroscopic. There is a study making use of water to create a porous fiber structure by spinning in a high humidity environment [118]. In-depth and quantitative studies are required on the effect of humidity to assess the best humidity condition for producing fibers.

## 3. Optimization of structure and morphology of CNFs

The structure and morphology of electrospun CNFs can vary significantly due to different processing conditions, such as thermal treatment, functionalization and grafting of second phases, which in turn greatly influence their performance in electrochemical devices. Considerable and meaningful progress has been made to tailor both the structure and morphology of CNFs, which is discussed in the following.

### *3.1. Diameter*

One of the major advantages of 1D fiber structure for electrochemical energy storage is the small diameter, which offers a high active area for electrochemical reactions and shortens the charge diffusion length. The diameter of electrospun fibers can vary from 10 nm to 10 μm. The carbon fibers used in electrochemical devices typically have a diameter less than 1 μm. In some core/shell structured fibers, the diameter can become larger with over 1 μm, which are also called 'ultrafine' fibers in some reports. Nevertheless, nanofibers with small diameters are desired in most cases. Many studies have been conducted in tailoring the diameters of electrospun fibers by both experiments and theoretical calculation [111,119].

The final diameter of CNFs is determined mainly by the polymer fiber diameter which in turn is influenced by both the properties of precursor solution and processing parameters. As discussed in Section 2.3, the diameter of fibers increases with an increase in viscosity according to a power law (Fig. 5b) [111]. Therefore, all the factors that influence the viscosity, such as the molecular weight of polymer and the concentration of precursor solution, affect the diameters. A solution with a low polymer concentration and a polymer with a small molecular weight result in smaller fiber diameters. Among various processing parameters, many studies indicate that neither the collecting distance nor the applied voltage has large influences on fiber diameter while they should be kept in an optimized range to produce smooth fibers. One possible reason is that these parameters employed in practical electrospinning do not vary much, making their effects negligible compared to other processing parameters. Instead, the flow rate significantly affects the fiber diameter, as shown in Fig. 5d [115]. The jet and fiber diameters significantly increase with increasing the flow rate because the fiber diameter is affected by the volume charge density, $I/Q$ (where $I$ is the current of jets and $Q$ is the flow rate), which has been proven by the below theoretical calculation. If the influences of jet thinning and solvent evaporation on fiber diameter are not taken into account, the fiber diameter can be predicted by the equation:

$$d_f = \left( \gamma \varepsilon \frac{Q^2}{I^2} \frac{2}{\pi \left( 2 \ln \left( \frac{l}{d_n} - 3 \right) \right)} \right)^{1/3} \tag{4}$$

where $\gamma$ is the surface tension, $\varepsilon$ is the dielectric constant, $l$ is the length of initial jet and $d_n$ is the nozzle diameter [55,119]. It is shown that the fiber diameters decrease with an increase in volume charge density which is the cumulative charge carried by the jets and presents the combined effects of precursor solution conductivity, ion mobility, electric field and flow rate. It should be noted that Eq. (4) is not comprehensive in view of the complexity of the electrospinning process with a large number of parameters to optimize. Although the model assumes that the surface tension should have a large effect on fiber diameter, several other works presented only a minor influence by surface tension [120]. However, a high surface tension should be avoided to limit the formation of beads. The diameter

usually has a large variation along the fiber length, which is also aggravated by the fluctuation in Taylor cone volume. The volume of Taylor cone is dependent mainly on the applied voltage and flow rate that need to be optimized to match with each other for maintaining a stable jet and thus producing fibers with a uniform diameter [121].

Thermal treatments are required to convert polymer fibers to CNFs, during which the diameter decreases because of the removal of heteroatoms and the evaporation of remaining solvents. Studies based on carbonization of PAN fibers confirms a continuous reduction of fiber diameter with increasing the temperature from 400 to 2600 °C. The most significant reduction took place at around 1000 °C. The diameter could be decreased by 30–50% upon high temperature carbonization [122], and a similar phenomena should happen during carbonization of other types of polymer fibers.

### 3.2. Structure

The atomic structure of CNFs, such as defects and the degree of graphitization, can affect both Li and Na ion storage, as well as the charge transfer coefficients. Thermal treatments are conveniently used to remove the defects and heteroatoms while the carbon atoms are re-arranged to transform into graphitic structure. Comprehensive studies have been conducted on the structural evolution of PAN during thermal treatments, as discussed in Section 2.2 and Fig. 4. Fig. 6a–d shows that at a low carbonization temperature of 550 °C, the almost entire CNFs still maintain an disordered structure. Once the temperature is increased to 950 °C, partial graphitization is observed. Full graphitization of PAN-based CNFs takes place at a temperature higher than 2000 °C, and a similar phenomenon was also observed in PI-based CNFs [96]. A high graphitization temperature can lead to both growth of graphitic layers and improvement of stacking order. Similar in-depth studies are required for other precursors, such as pitch and lignin.

Doping of heteroatoms and functionalization are among the most popular means to tailor the structure of carbon materials. N-doping of carbon has been widely studied, and the corresponding electrochemical performance depends both on doping amount and site. For instance, the polysulfide shuttle effect in LSBs was partly suppressed through encapsulation of sulfur into N-doped mesoporous carbon cathodes [123]. In addition, pyridinic N-doping was shown to help facilitate the first-electron transfer during the oxygen reduction reaction (ORR) in LABs [124]. N-doping in electrospun CNFs can be achieved either by *in-situ* doping or treatments of electrospun fibers by N-containing chemicals. PAN, in its chemical formula of $(C_3H_3N)_n$, contains a large amount of N atoms. These atoms can be maintained after transformation of PAN fibers into CNFs using a low carbonization temperature process. It is found that the N content decreases with increasing carbonization temperature. A high N content of 15.2 at.% was obtained in the CNFs carbonized at 550 °C, compared to a very low 3.6 at.% when carbonized at 950 °C. Growth of the C–C domain was noted during the carbonization process, accompanied by elimination of heteroatoms, as shown in Fig. 6e [35].

Chemical methods have also been used to dope CNFs spun from other polymers or to increase the N content in PAN-based CNFs. A high N content of 13.2 at.% was achieved by immersing lignin-based CNF mats in an urea aqueous solution and thermal annealing, which in turn gave rise to a capacity increase by ~30% [89]. Other N-containing chemicals, such as 1-ethyl-3-methylimidazolium dicyanamide [125], and other heteroatoms, like P using $H_3PO_4$ as a P source [126], were also studied to improve the electrochemical performance of CNFs. Functionalization of CNFs improved both the capacities of LIBs and the capacitances of SCs. The $HNO_3$ treatment of CNFs resulted in the attachment of oxygenated groups that were accessible to Li ions and thus contributed to a higher capacity [127]. Other functional groups, like Si–O, were attached onto the CNFs by adding Tetraethyl orthosilicate (TEOS) in the PAN solution, resulting in an improved capacitance due to a Faradic reaction between the functional groups and the electrolyte [128].

### 3.3. Electrical conductivity

A high electrical conductivity is a prerequisite for an electrode material to achieve high electrochemical performance especially at high current densities. Many metal oxides that inherently possess high capacities/capacitances do not have high electrical conductivities required for fast charge trans-

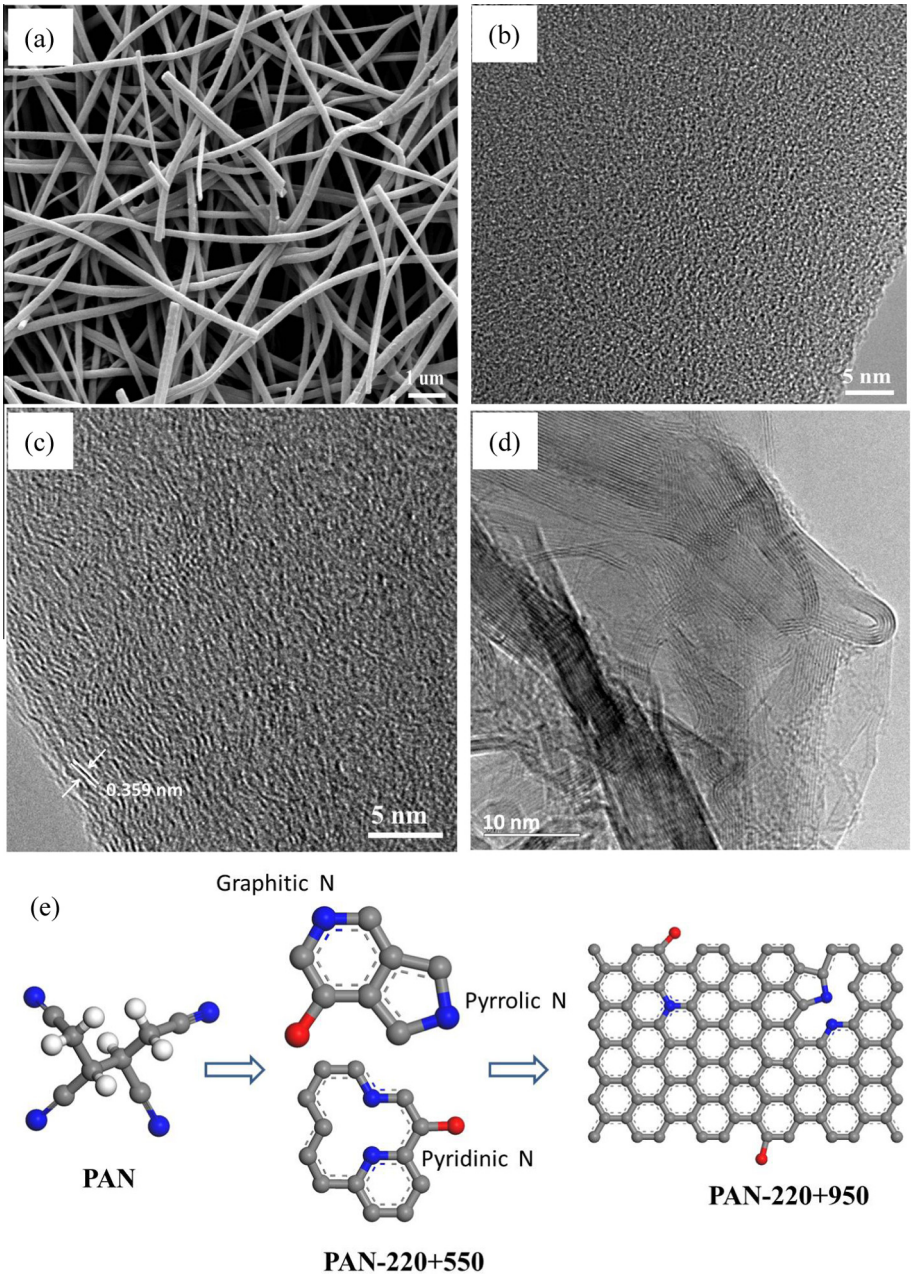


**Fig. 6.** SEM (a) and TEM (b) images of PAN-based electrospun CNFs carbonized at 550 °C; TEM images after carbonization at (c) 950 °C and (d) 2800 °C (unpublished work); and (e) schematic of structural evolution of PAN during thermal treatment (white = hydrogen (H) atoms; gray = carbon (C) atoms; blue = nitrogen (N) atoms; and red = oxygen (O) atoms) [35]. (Reprinted with permission from [35]. Copyright 2014 Wiley.)

fer. This means that CNFs should have a sufficiently high conductivity to establish conductive networks. A summary of various approaches used to improve the conductivity of CNFs and the discussions on their advantages and disadvantages are presented in Table 5.

**Table 5**
Approaches used to improve electrical conductivities of CNFs. (Reprinted with permission from [35,127,131,132,134,135,138,140,141]. Copyright 2014 Wiley, 2008, 2010, 2013, 2014 Elsevier, 2009, 2012, 2013, 2014 RSC.)

| Approaches | | Process | Morphology | Conductivity | Advantages | Disadvantages |
|---|---|---|---|---|---|---|
| Carbonization at high temperatures [35] | | 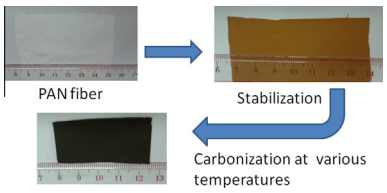 | 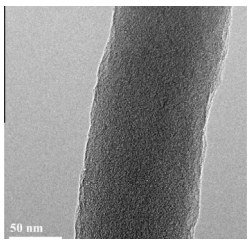 | From $7.35 \times 10^{-8}$ to 1.41 S/cm | Simple process | Detrimental to electrochemical performance |
| Use of catalysts | Fe [127] | 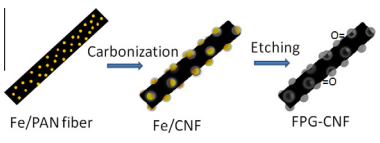 | 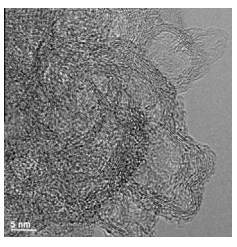 | From $8.30 \times 10^{-5}$ to 0.21 S/cm | Low temperature | Need etching to remove catalyst particles |

(*continued on next page*)

**Table 5** (*continued*)

| Approaches | | Process | Morphology | Conductivity | Advantages | Disadvantages |
|---|---|---|---|---|---|---|
| | Ni [131] | 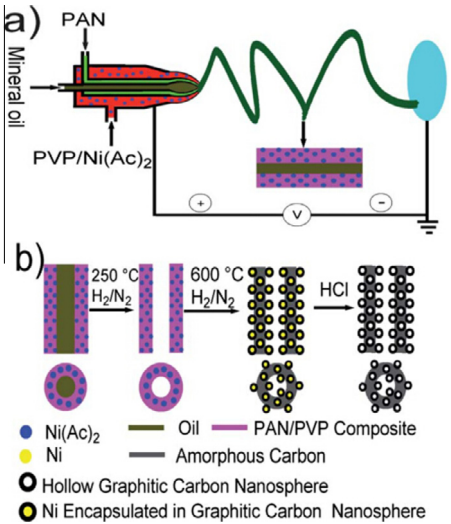 | 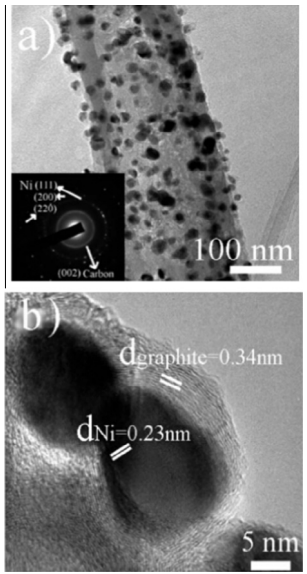 | | | |
| Incorporation of CNTs | Incorporation in polymer solution [132,134] | 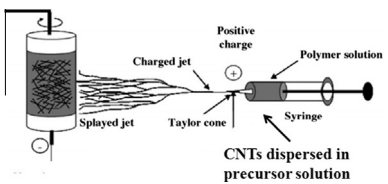 | 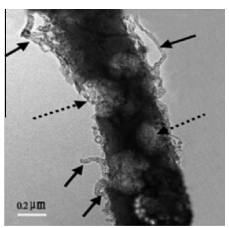 | From 0.86 to 5.32 S/cm | Simple process, and CNTs are easily embedded in CNFs | CNTs tend to aggregate |

| | | | | | | |
|---|---|---|---|---|---|---|
| | CVD growth on CNFs [135] | 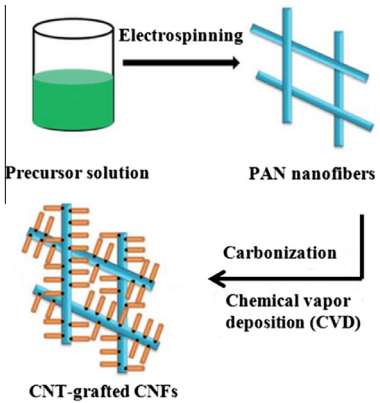 | 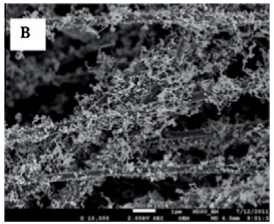 | – | Excellent contact between CNTs and CNFs | Complex process |
| Incorporation of graphene, rGO | In polymer solution [137,138,140] | 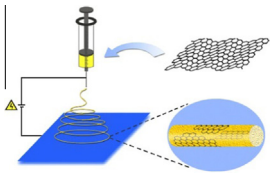 | 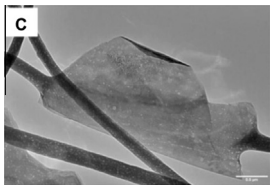 | From 1.11 to 2.0 S/cm [137] | Simple process | Beads may form with high graphene contents |
| | Mixing CNFs and graphene [141] | 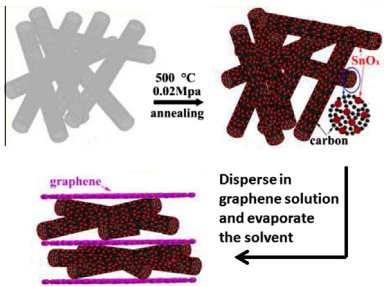 | 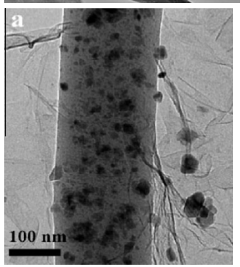 | – | Large amount of graphene can be incorporated | Two step process, and graphene dispersion in CNFs may be a problem |

Generally speaking, the electrical conductivity of CNFs increases with an increase in carbonization temperature and thus the degree of graphitization. For instance, the electrical conductivity of PAN-based CNFs increases by eight orders of magnitude when the carbonization temperature is increased from 550 to 950 °C [35]. However, too high a carbonization temperature may be detrimental to electrochemical performance of both neat CNFs and metal oxide/CNF composite electrodes. This is because a very high temperature completely destroys the functional groups and disordered structure that may be beneficial to energy storage, while a high temperature can also cause the metal oxide particles to aggregate and separate from the CNF matrix [129,130]. In order to obtain a sufficiently high conductivity at a relatively low carbonization temperature, several strategies were adopted, including: (i) the use of catalysts for graphitization; (ii) the incorporation of CNTs as conductive additive; and (iii) the incorporation of graphene. Fe and Ni are effective catalysts for promoting graphitization of carbon materials. The electrical conductivity of CNFs improved from $8.30 \times 10^{-5}$ to 0.21 S/cm when Fe was used as the catalyst for graphitization [127,131]. A drawback of this approach is that the catalysts need to be removed using an acid after the carbonization process. Therefore, CNTs have been added into CNFs for electrodes of both LIBs and SCs [132,133]. Two different strategies have been employed to fabricate CNT/CNF hybrids. A simple way is to disperse CNTs into the polymer solution before electrospinning after functionalization or surfactant treatment of CNTs [134]. The other interesting approach is to grow CNTs on CNFs by CVD. Ni was first deposited onto the CNFs during electrospinning, which was later used as catalyst for the growth of CNTs [135,136]. Due to the excellent electrical conductivity and high aspect ratio, graphene has also been considered an ideal conductive additive. Many studies reported the use of graphene to improve the conductivity of neat CNFs [137,138] and metal (oxide)/CNF composites, such as Si/graphene/CNFs [139]. Graphene can be incorporated either before [140] or after electrospinning of CNFs, the latter being possible by solution mixing [141].

### *3.4. Surface area and pore size distribution*

CNFs possessing a large surface area and a suitable pore size distribution can give rise to high electrochemical performance due to several distinct benefits, including a large number of reaction sites, capability to accommodate a high loading of active metal oxides, buffering large volume changes, an improved electric double-layer capacitance (EDLC) in SCs, entrapping of polysulfides in LSBs and facilitating the $O_2$ diffusion in LABs. Because neat CNFs electrospun from most polymer precursors seldom have large surface areas, a great deal of studies have been directed toward enhancing the surface areas of CNFs. The specific details are discussed in the following, and typical morphologies and surface areas as well as pore sizes of CNFs produced by various approaches are summarized in Table 6. Two typical approach including using sacrificial phases and activation are used (see Table 7).

The incorporation of inorganic particles, such as $SiO_2$ [142], is an effective way to produce nanoscale pores and the size of pores can be tailored by controlling the original particle size. However, the removal of these particles to create pores requires corrosive acid etching. Unlike the above inorganic sacrificial phases, sacrificial polymers, like PLA [143], PMMA [108], styrene-co-acrylonitrile (SAN) [144] and Nafion [145], do not need an additional etching process to remove them [146]. They can be removed by *in-situ* decomposition during carbonization, leaving behind pores in CNFs. A totally new approach has been developed by employing ice as soft template, which is a very simple, low cost and environmentally friendly process for producing porous CNFs [147].

Both the physical and chemical activation processes have been used to produce porous CNFs. Activation can produce porous CNFs with a much larger surface area than using sacrificial phases because the majority of pores produced by activation has sizes less than 2 nm, i.e. micropores. In the physical activation, an oxidation atmosphere is supplied to remove part of carbon by oxidation for producing pores. $H_2O$ steam in a carrier of $N_2$ has been widely used for this purpose [148]. The chemical activation process involves activation agents, such as KOH and $ZnCl_2$, which can etch carbon to generate pores [149,150]. One of the benefits of chemical activation is that it can be conducted at a relatively low temperature [151]. However, it requires an additional treatment to remove the activation agents. Evaporation of gas has also been utilized to produce pores. Incorporation of chemical compounds, such

**Table 6**
Approaches used to enlarge the surface area and produce nanosized pores. (Reprinted with permission from [108,127,128,131,142–145,147–150]. Copyright 2009, 2012, 2013 ACS, 2011, 2013, 2014 Elsevier, 2012 RSC, 2009 IOPscience, 2003 AIP Publishing LLC, 2007 Wiley.)

| Approaches | | Morphology | Surface area ($m^2/g$) | Pore size | Application |
|---|---|---|---|---|---|
| Inorganic sacrificial phases | 24 wt.% $Fe_3C$ [127] | 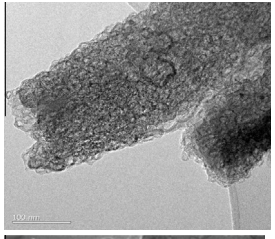 | 198 | Average 4.9 nm | LIBs, LSBs, LABs |
| | 17.1% Ni in CNFs [131] | 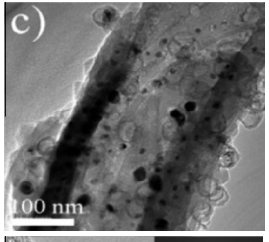  | – | Average 15 nm | LIBs, LSBs, LABs |
| | $SiO_2$ in CNFs [142] | 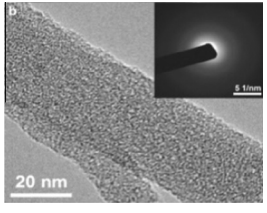  | 950 | Centered at 0.5 and 1.2 nm | LIBs, SCs |

(*continued on next page*)

**Table 6** (*continued*)

| Approaches | | Morphology | Surface area ($m^2/g$) | Pore size | Application |
|---|---|---|---|---|---|
| Polymer sacrificial phases | PLA:PAN = 1:9 [143] | 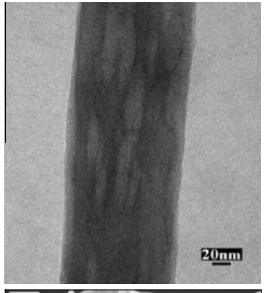  | 235 | 75% micropores | LIBs, NIBs, LSBs |
| | PMMA:PAN = 1:1 [108] | 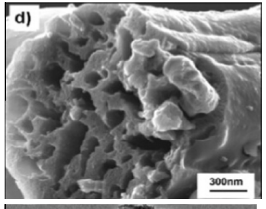  | – | ~150 nm | LIBs, LSBs |
| | SAN:PAN = 1:3 [144] | 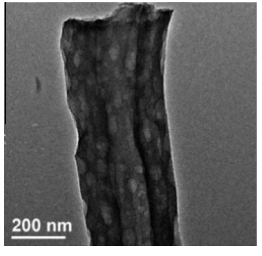  | 13 | Average 12 nm | LIBs, NIBs, LSBs |

| | | | | | |
|---|---|---|---|---|---|
| | Nafion:PAN = 6:4 [145] | 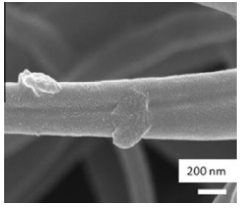  | 1614 | Average 1.35 nm, 78% micropores | SCs |
| Soft template | Ice in PVA fiber [147] | 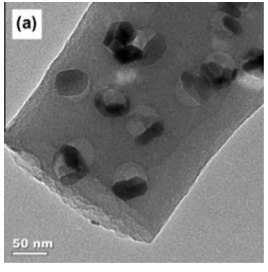  | 352 | Broad size range: both micropores and macropores exist | LIBs |
| Activation | 30 vol.% $H_2O$ [148] | 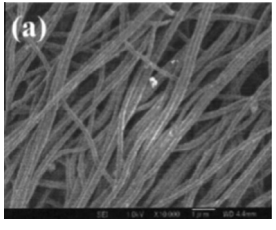  | 1230 | Average 3.1 nm, 64% micropores and 36% mesopores | SCs, LSBs |

(*continued on next page*)

**Table 6** (*continued*)

| Approaches | | Morphology | Surface area ($m^2/g$) | Pore size | Application |
|---|---|---|---|---|---|
| | KOH:CNF = 5:1, combined with Ni and PMMA sacrificial phases [149] | 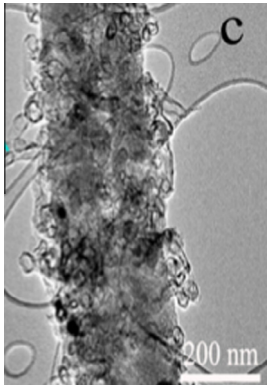  | 1840 | Broad pore size range | LIBs, LSBs |
| | 5 wt.% $ZnCl_2$ [150] | 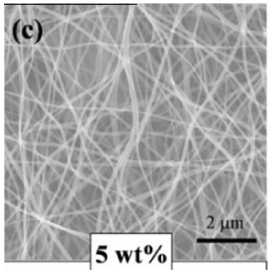  | 550 | Average 0.59 nm, 76% micropore and 24% mesopore | SCs, LSBs |
| Gas evaporation | TEOS:PAN = 1:4, combined with activation by $H_2O$ [128] | 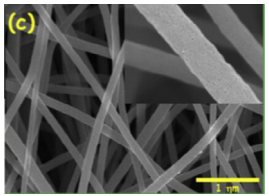  | 1387 | Average 2.1 nm, 61% micropore and 39% mesopore | SCs |
| | PMHS:PAN = 5:100 [152] | – | 303 | Average 1.6 nm | SCs |

**Table 7**
Techniques used for dispersion of metal oxides in CNFs. (Reprinted with permission from [79,80,129,157–162]. Copyright 2009, 2013, 2014 Wiley, 2012 ACS, 2012, 2014 RSC, 2011, 2013, 2014 Elsevier.)

| Structure | Process | Morphology | Advantages |
|---|---|---|---|
| Uniform distribution of Si [157] | 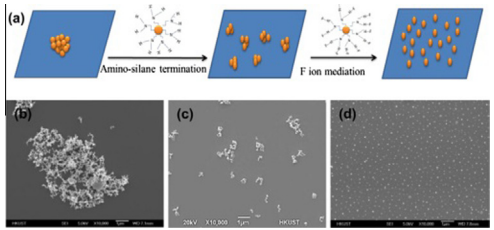  | 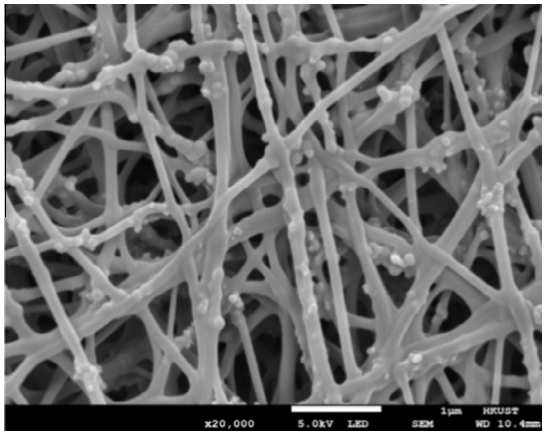  | Free space between particles can accommodate volume changes |
| Hollow $Co_3O_4$ particles [158] | 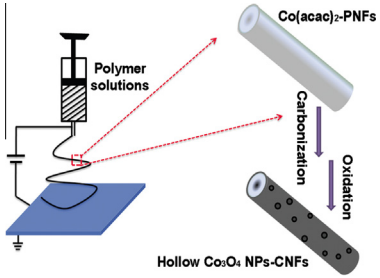  | 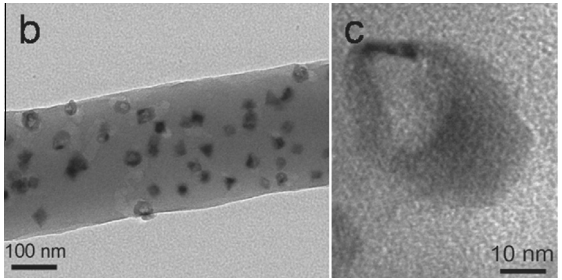  | Increased active sites and free space for volume change |

(*continued on next page*)

**Table 7** (*continued*)

| Structure | Process | Morphology | Advantages |
|---|---|---|---|
| Single-layer $MoS_2$ nanoplates [159] | 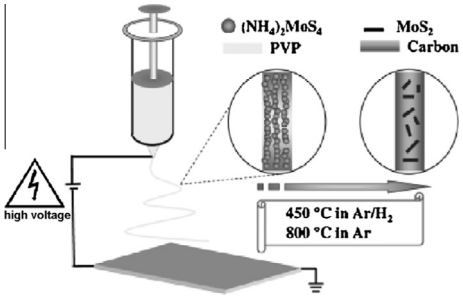  | 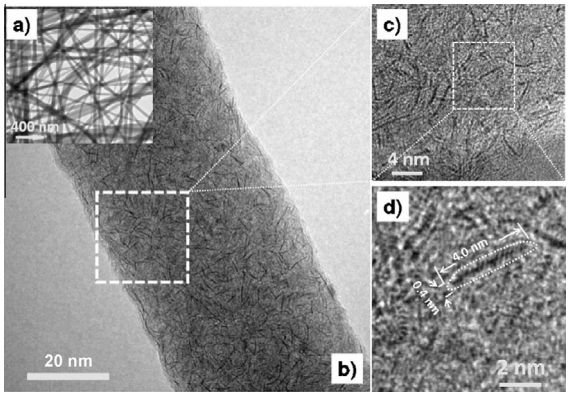  | Short charge transfer length for high rate performance and increased reaction sites |
| Thin $MnO_2$ sheets [160] | 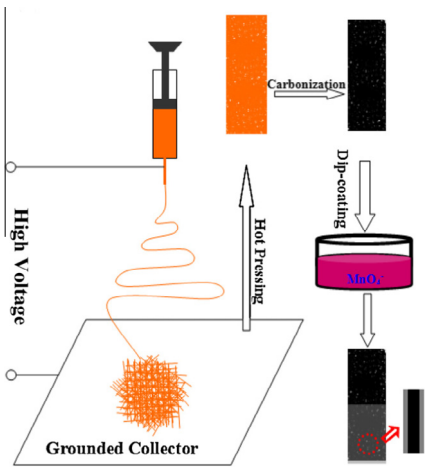  | 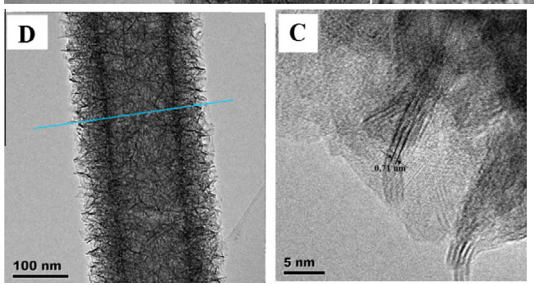  | Short charge transfer length for high rate performance and increased reaction area |

| | | | |
|---|---|---|---|
| Amorphous, sub-nanosized $SnO_x$ [129] | 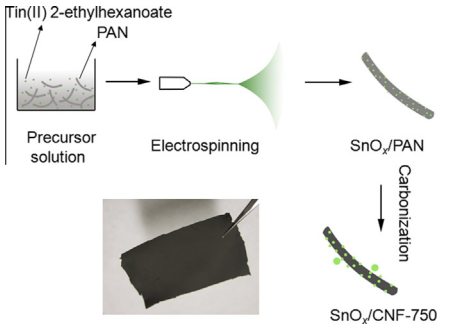 | 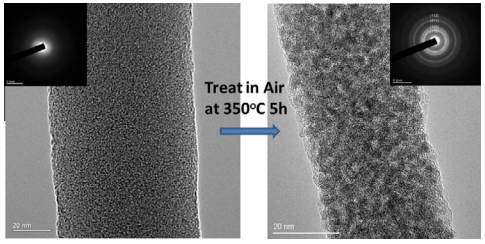 | Short charge transfer length and enhanced reversibility |
| Si@C@CNFs [161] | 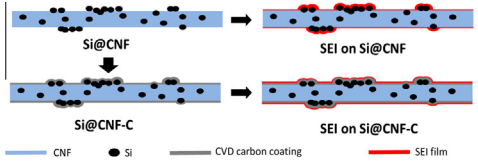 | 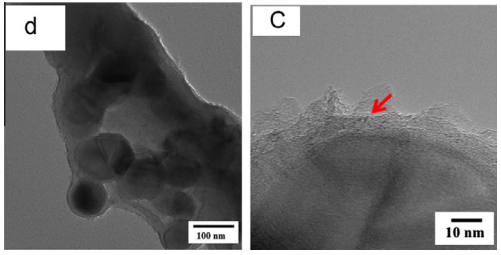 | Detachment of metal oxides is avoided during cycles |
| $Fe_2O_3$@graphitic carbon@CNFs [162] | 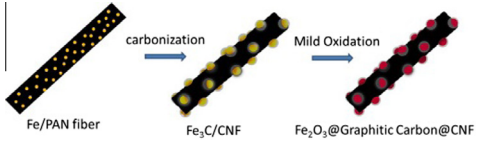 | 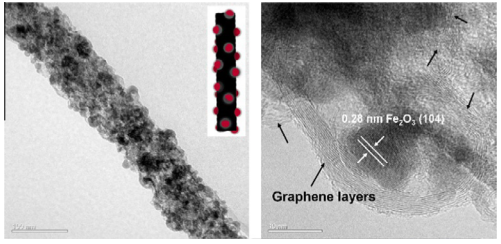 | Detachment of metal oxides is avoided during cycles |

(*continued on next page*)

**Table 7** (*continued*)

| Structure | Process | Morphology | Advantages |
|---|---|---|---|
| Sn encapsulated into hollow CNFs [79] | 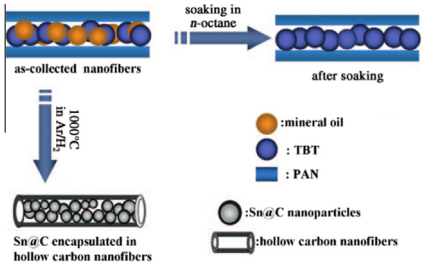  | 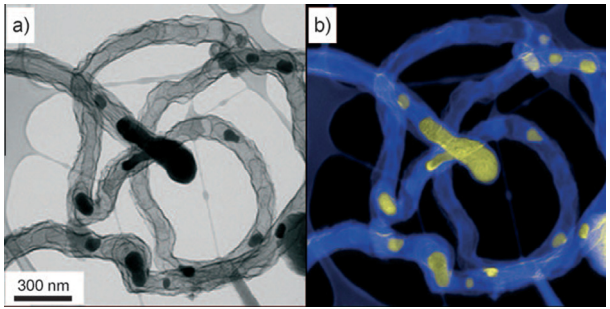  | Intimate contact between metal (oxides) and CNFs, and separation of particles is avoided |
| Si encapsulated in the core of CNFs [80] | 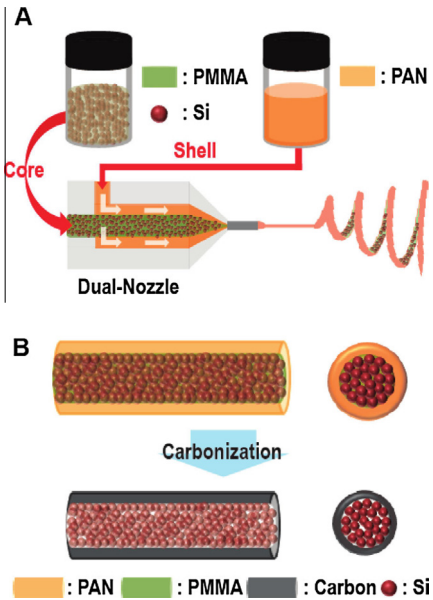  | 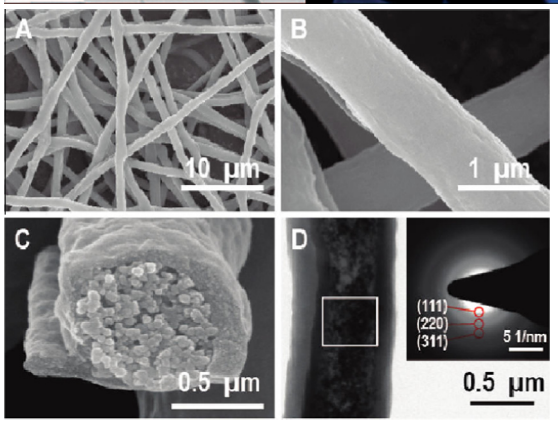  | Stable structure for long cycles |

as TEOS and polymethylhydrosiloxane (PMHS), in the polymer precursor results in the release of gases, leaving behind pores, during the thermal treatment because of pyrolysis and chemical reactions [128,152].

The selection of appropriate methods to produce porous CNFs should be based on the desired effects because the optimized surface area and pore size largely differ depending on the roles that they play in different electrochemical devices. A large surface area is generally beneficial to the enhancement of EDLC in SCs. CNFs used in LSBs also favor a large surface area to accommodate a high sulfur content. However, too large a surface area may not be always useful in LIBs because a large contact area between the electrode and electrolyte often results the formation of thick SEI films, increasing the irreversible capacity in the first several cycles.

The pore size also plays an important role in determining the electrochemical performance. Pores can be divided into three types depending on their sizes, i.e., macropore (>50 nm), mesopore (between 2 and 50 nm) and micropore (<2 nm). The three types of pores have their own effects on charge storage and transfer. Generally speaking, macropores are useful for permeation of electrolyte, while mesopores can facilitate the charge transfer and serve as active sites for charge storage for both Li and Na ions [3]. However, the effect of micropores is quite complex and is not straightforward. Although some studies indicate that they were helpful in obtaining a high capacity/capacitance, the charge mobility in micropores somehow decreased giving rise to a low power density [153]. In addition, sub-nanometer size pores may not be accessible when the pore size is smaller than the size of solvated electrolyte ions. Therefore, the optimized pore size is also dependent on the electrolyte: it is reported that the pore size that leads to maximum capacitance in SCs was close to the ion size in electrolyte [154]. Further studies are necessary to establish better understanding of the charge storage and transfer in pores of different sizes [155,156].

### 3.5. Particle size, dispersion and morphology of metal oxides in CNFs

Metal (oxides) possessing inherently high theoretical capacities/capacitances are widely used to incorporate into electrospun CNFs to obtain high energy densities. Dispersion quality and morphology of metal oxides in CNFs are critical to achieving high electrochemical performance of metal oxide/CNF composite electrodes. Well-dispersed metal particles are obtained in CNFs when a soluble metal precursor is added into the polymer for electrospinning. However, some active metals, such as Si, are very difficult to directly obtain from a Si-containing precursor. Therefore, nanosized Si particles need to be directly added into the polymer precursor, making it difficult to disperse in the polymer solution. Aggregation of Si was observed in most of the previous studies, resulting in poor cyclic performance. Therefore, the Si surface was functionalized sequentially by amino-silane and F ions to achieve uniform and stable dispersion of Si nanoparticles in water, which was electrospun together with the PVA matrix to produce Si/CNF composites [157]. The space between the Si particles within the CNFs should be ample enough to accommodate the large volume change of Si, a prerequisite for improved cyclic performance. The morphology of metal oxides was further optimized using various approaches, such as making hollow particles, increase in reaction sites and the accommodation of volume changes. For example, $Co_3O_4$ hollow particles were prepared by oxidizing Co nanoparticles in air making use of the diffusion speed difference in the outward and inward particles during phase transformation, so called the "Kirkendall effect" [158].

Metal oxides in the form of one to several layers of thin films can greatly shorten the ion diffusion lengths, which can contribute to high rate performance. For example, CNFs containing single layer $MoS_2$ nanoplates delivered an extremely high capacity of 661 mA h/g at 10 A/g for up to 1000 cycles in LIBs. Similarly, the anodes made from the same material showed excellent performance in NIBs due to the fast charge transfer [159]. The layer-structured $MnO_2$ sheets in CNFs also showed a similar high-rate performance because of the large surface area [160]. A further reduction of particle size into a sub-nanometer level brought about additional benefits. The study on sub-nanometer, amorphous $SnO_x$/CNF composites as anodes in LIBs revealed that the reaction $Li + SnO_x \leftrightarrow Sn + Li_2O$ became partly reversible, which was previously thought irreversible. Thus, the reversible reactions imparted extremely high capacities at high current densities [129].

Coating another layer of carbon is used to further enhanced the performance of metal (oxide)/CNF composites. Although metal oxides can be *in-situ* deposited in a polymer solution, most of the particles are exposed on the surface of CNFs because they tend to move to the surface during the evaporation of solvent after forming the fibers. These metal oxides may even drop off from the CNFs when they grow large and aggregate. To avoid this problem, a carbon coating needs to be applied to keep them within the CNFs. A few different methods have been devised for this purpose, including (i) the growth of carbon by a CVD method, (ii) addition of catalysts to grow graphitic carbon on the surface of metal oxide particles and (iii) designing a core/shell structure. A CVD carbon coating was applied on top of the Si/CNF composites to prevent detachment of Si during cycles [161]. Fe, Ni or Co oxides were also added to make use of their catalytic effects so as to form graphitic carbon layers during carbonization [162,163]. One of the most effective and systematic approaches to prevent the detachment of particles is to design a core/shell structure consisting of a metal (oxide) core and a CNF shell. The core/shell structure was produced using a dual nozzle in electrospinning, where the metal precursors were placed in the inner part and the neat polymer solution in the outer part. Sn and Si encapsulated CNFs were successfully synthesized and delivered remarkable cyclic stability even at high current densities [79,80]. Apart from preventing the detachment of metal particles, the carbon shell effectively buffered the large volume changes of Sn and Si, and provided conductive paths for electron and Li ion transfer.

## 4. Application of CNFs in Li ion batteries

LIBs have been widely used in our daily life to power portable electronic devices, such as mobile phones and notebooks. They possess much higher energy densities than traditional Pb–acid or Ni–Cd batteries [164]. The current LIB typically consists of a graphite anode and a $LiCoO_2$ cathode, which are separated by a polymer membrane and immersed in the electrolyte. The electrospinning technique has been widely used to fabricate all important components of LIBs, namely the anode materials, cathode materials and separator. Separator membranes containing electrospun polymer fibers have been extensively investigated. The polymer fibers can also be used as gel electrolyte after adsorbing the electrolyte solution thanks to their high porosity [99]. The application of electrospun fibers as separator is beyond the scope of this paper, thus will not be further discussed.

Graphite has been demonstrated as an excellent anode material for LIBs to power portable electronics due to its relatively low cost and long cyclic life. However, critical challenges have been encountered when the LIBs with a graphite anode are used in electric vehicles: the challenges include the safety issue arising from the deposition of metallic Li on the anode surface and its low theoretical capacity of 372 mA h/g. Other forms of carbon materials, such as CNTs, CNFs and graphene, possess much higher capacities than graphite. In addition, several metal and metal oxides, such as Si, $SnO_2$ and $Fe_2O_3$, have also been investigated as potential replacements due to their extremely high capacities [165]. Encapsulation of these metal oxides into the nanocarbon material is an efficient way to obtain anode materials with both high energy and power densities as well as long cyclic life. Electrospinning offers one of the most facile and convenient means to produce CNFs and their hybrids containing various metal and metal oxides.

Lithium metal oxides (LMOs, where M represents Co, Fe, Mn, etc.) including layered oxides and polyanions are widely used as cathode materials. They have relatively high capacities and maintain structural stability during the Li ion intercalation and extraction. One major drawback of them is their low electrical conductivities: for instance, $LiFePO_4$ (LFP) has a very low electrical conductivity of $10^{-9}$ S/cm. In order to facilitate charge transfer during cycles, several strategies have been adopted, including: (i) fabrication of nanostructured cathode materials consisting of nanosized particles, effectively reducing the charge transfer distance [166]; (ii) doping with heteroatoms to improve the intrinsic conductivities of LMOs [167]; and (iii) incorporation of nanocarbon materials to establish conductive networks surrounding the active particles [168]. Electrospinning is a useful technique to form 1D LMO fibers comprising nanosized particles, or to *in-situ* incorporate LMO particles into the CNF matrix for enhanced electrical conductivities and structural integrity with better cyclic performance.

### 4.1. Anodes

#### 4.1.1. Neat CNFs

CNFs can deliver a much higher capacity than traditional graphite because Li ions can be intercalated into the pores and defects present in the CNFs. Another distinct advantage of electrospun CNF films is that they can be used as freestanding, binder-free and additive-free electrodes without extra processing steps or materials. As such, PAN-based CNFs have been extensively studied as anodes in LIBs. The PAN-based CNFs carbonized at 1000 °C delivered a capacity of 450 mA h/g, which is much higher than 372 mA h/g of graphite [169]. The capacity is greatly influenced by the atomic structure that can be tailored by controlling the stabilization/carbonization temperatures. It was also demonstrated that a low carbonization temperature of 550 °C maintained a high N content of 15.3 at.% in electrospun PAN-based CNF films, giving rise to a high capacity of 550 mA h/g because the defects created by nitrogen atoms provided extra reaction sites for Li ions [35]. A similar phenomenon was also observed in electrospun lignin-derived CNF mats where the capacity of CNFs increased from 445 to 576 mA h/g after annealing in the presence of urea that also created nitrogen functional groups in the fibers [89].

A high electrical conductivity of CNFs is essential for a high rate capability of the electrodes. While high carbonization and graphitization temperatures can generate a more graphitic carbon structure with sufficiently high conductivities, CNFs annealed at too high a temperature may fail to deliver a high capacity because of the elimination of defects. Instead of applying a very high temperature, Ni and Fe have been employed as catalysts to promote graphitization of amorphous CNFs at a relatively low carbonization temperature so as to achieve a high conductivity: 650 °C was sufficient to induce graphitic carbon around the Fe particles. Moreover, the N heteroatoms partially remained with a N-content of 6.7 at.% due to incomplete graphitization, thereby maintaining part of the defect sites for Li storage [127]. The study on the Ni–PAN system also presented a similar finding [131]. In addition, nanoscale pores generated by etching the Ni and Fe particles had ameliorating effects of offering extra electrochemical reaction sites. Remarkable capacities of 983 and 969 mA h/g were obtained for the electrodes made from porous CNFs with Fe and Ni sacrificial catalysts, respectively [127,131].

Creation of nanoscale pores in electrospun CNF electrodes is of great importance in achieving a high capacity. Besides using Fe and Ni, other sacrificial materials are also considered. Kang et al. reported the use of $SiO_2$ as sacrificial particles for producing PI-based porous CNFs where $SiO_2$ particles were removed by etching using HF solution after carbonization [142]. Compared to metal and metal oxide sacrificial phases, polymer sacrifices do not require additional treatments or toxic etchants to create pores. Instead, the sacrificial polymers are decomposed while the host polymer is carbonized. PLA, SAN and PMMA have been used as sacrificial polymers in producing PAN-based porous CNFs [142,143,170]. The surface area of porous CNFs produced from the mixture of PAN and PLA sacrifice was 235 $m^2/g$, six times larger than 34 $m^2/g$ of the non-porous, control CNFs. The pores gave rise to a high capacity of 435 mA h/g to the electrode, which is 40% higher than the non-porous CNF counterpart [143]. Hollow CNFs with a porous shell structure were fabricated using a dual nozzle (shown in Table 3) with SAN/DMF as the core solution and PAN/SAN/DMF as the shell solution. The decomposition of SAN during carbonization resulted in the formation of hollow core and porous shell [144].

Activation is also used to increase the surface area of CNFs for achieving a high capacity. PAN-based CNFs were activated by 15 wt.% $ZnCl_2$, leading to a drastic rise in surface area to 438 $m^2/g$ from the low 31.6 $m^2/g$ measured before activation [171]. KOH was also successfully used to activate CNFs where the activation process was conducted along with Ni and PMMA sacrificial phases. A remarkable BET surface area of 1840 $m^2/g$ and a pore volume of 1.21 $m^3/g$ were achieved for the activated CNF electrodes which also delivered an excellent capacity of 1150 mA h/g when discharged at 0.1 A/g [149].

#### 4.1.2. Ti/CNF electrodes

Ti-based anodes, most notably $TiO_2$ and $Li_4Ti_5O_{12}$ (LTO), are considered among the most promising electrode materials for EVs. Although they do not have very high theoretic capacities, i.e. 335 mA h/g for $TiO_2$ and 175 mA h/g for LTO, Ti-based anodes possess a very stable cyclic performance with low volumetric strains occurring during the Li ion insertion/extraction. In addition, the deposition of metallic Li on the surface of electrodes can be avoided due to the high discharge/charge plateau of

~1.5 V vs. $Li/Li^+$, which in turn guarantees the safety of LIBs during charging at high current densities [172]. One drawback that limits the practical application of Ti-based anodes is their low electrical conductivities. Doping and incorporation of carbon are among the most popular methods to improve the electrical conductivities [173,174]. The incorporation of Ti-based particles into the electrospun CNFs has shown much enhanced electrochemical performance due to the formation of conductive networks throughout the CNF matrix.

Two major techniques have been adopted to produce $TiO_2$/CNF composite electrodes, including (i) *in-situ* deposition and (ii) *ex-situ* growth. For *in-situ* deposition, Ti precursors, such as titanium butoxide, were mixed with the polymer precursor, like PVP and PAN, to prepare the electrospinning solution [125] and CNFs with embedded $TiO_2$ nanoparticles were produced as the final product. *Ex-situ* growth involved a two-step process where neat CNF films were fabricated in the first step, followed by deposition of $TiO_2$ by a hydrothermal process in the following step, as shown in Fig. 7a and b [175]. A new technique was devised to form a well-connected 3D porous $TiO_2$ nanotube/CNF composite architecture [176]. The synthesis process involved electrospinning of CNFs, on which rutile $TiO_2$ nanoparticles were *ex-situ* deposited followed by hydrothermal reaction in NaOH solution. The CNFs with a tailored $TiO_2$ structure delivered a very stable cyclic performance of over 110 mA h/g for 1000 cycles at a remarkably high current density of 5 A/g.

In order to further improve the performance of $TiO_2$/CNF composite electrodes, several other strategies have been employed, namely (i) doping with nitrogen, (ii) incorporation of conductive additives and (iii) generation of pores. N-doping of $TiO_2$/CNF composites was shown to have several synergies, including enhanced crystallinity of $TiO_2$, formation of a mesoporous structure, and significantly reduced charge transfer resistance [125]. Different conductive additives, notably CNTs and graphene, have been incorporated into the $TiO_2$/CNF composites to enhance the electrical conductivities of the electrodes, especially for better high rate capabilities [109,177]. The capacity of $TiO_2$ fiber was increased from 98 to 131 mA h/g after discharging at 150 mA/g for 300 cycles by incorporating conductive graphene sheets. To create pores that can facilitate electrolyte permeation for fast charge transfer, a mixture containing PAN and PMMA was used as the electrospinning precursor [178].

LTO electrodes have a reputation of "zero strain" during Li ion intercalation, giving rise to an excellent cyclic stability. However, the low electrical conductivities of LTO electrodes led to major research efforts toward improving their conductivities. Nanosized LTO particles were *in-situ* embedded into

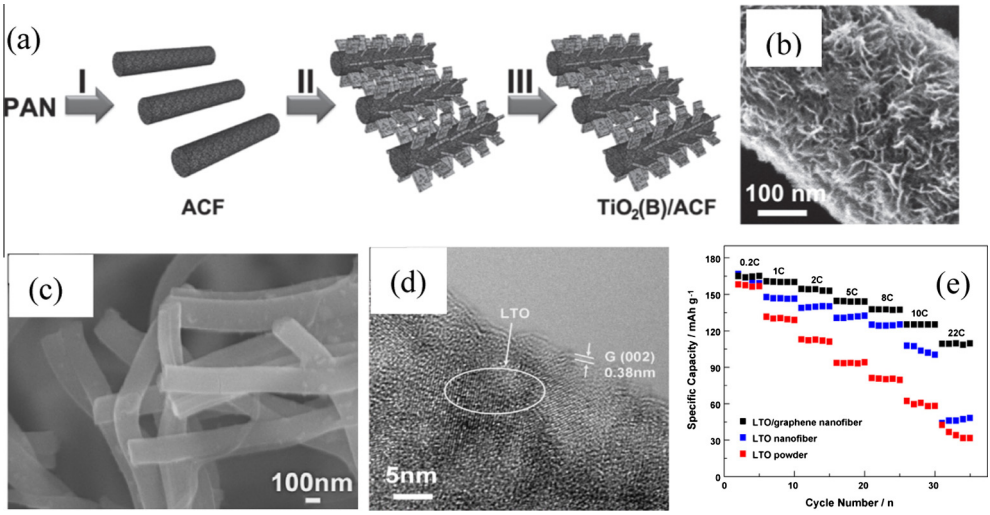


**Fig. 7.** (a) Ex-situ growth of $TiO_2$ on PAN-derived CNF films and (b) representative SEM images [175]; (c) SEM, (d) TEM images of the fibers of LTO/graphene/CNF composites and (e) their electrochemical performance [140]. (Reprinted with permission from [140,175]. Copyright 2010 Elsevier, 2013 Wiley.)

CNFs via electrospinning, and the electrodes made therefrom delivered a high rate capability and capacity retention after more than 1000 cycles. Graphene sheets were also incorporated for further improvement in conductivity and thus the performance at high rates. The SEM and TEM morphologies of the composite electrodes and the comparison of the rate performance between different electrodes are shown in Fig. 7c–e [140]. Doping has also been used to improve the intrinsic conductivity of LTO in $Li_4Ti_{4.95}Nb_{0.05}O_{12}$/CNF composites as a high performance anode [179]. It should be noted that LTO is usually discharged/charged at a cut-off voltage range of 1–3 V, where carbon does not show a high capacity and the CNF mainly plays a role of conductive network in the composite. As such, the carbon content should be maintained low, normally less than 10%, making low-carbon yield polymers, such as PVP, most popular for this purpose. In some studies, the polymer was completely burnt out, instead of carbonization, by thermal treatment in air [180].

#### *4.1.3. Transition metal oxide/CNF anodes*

Transition metal oxides (TMOs) (where M represents Mn, Fe, Co, Ni and Cu) are another type of intensively-studied anodes. Unlike graphite and Ti-based anodes with a Li ion intercalation mechanism, TMOs store Li ions based on a conversion reaction, as shown below:

$$MO_x + Li^+ \leftrightarrow Li_2O + M \tag{5}$$

The new mechanism offers the TMOs capacities several times higher than the anodes made from graphite, $TiO_2$ and LTO [181]. However, they suffer from poor cyclic and rate performance due to their volumetric changes and sluggish kinetics during the charge/discharge processes. To address the issues on structural instability and poor charge transfer kinetics, carbon materials have been incorporated in various ways [182].

Electrospinning has been widely adopted to produce CNFs containing nanosized TMO particles. Typically, polymer solutions mixed with Fe, Co, Ni and Mn precursors are electrospun to *in-situ* produce composite fibers, followed by thermal treatment to obtain well-dispersed TMO in CNFs. For instance, Chen et al. reported the synthesis of $Fe_3O_4$/CNF composites from ferric(II) acetylacetonate and PAN precursors. Nano-sized $Fe_3O_4$ particles of 8.5–52 nm in diameter were uniformly distributed in the CNFs, imparting a reversible capacity of 1007 mA h/g after discharging at 200 mA/g for 80 cycles [183]. Similar strategies have also been employed to produce CNFs containing MnO [184,185] and $Co_3O_4$ [186] nanoparticles, both of which showed much improved cyclic performance than the neat TMO electrodes. *Ex-situ* growth of TMOs on CNFs by a hydrothermal method was also investigated [187]. However, the TMOs produced in this approach always had particle sizes of tens of nanometers and were attached on the surface of CNFs. As a result, the corresponding electrochemical performance was slightly poorer than the electrodes obtained directly from the *in-situ* deposition that produced smaller TMO particles encapsulated within the CNF matrix.

Graphene has been extensively studied as conductive additive in the TMO/CNF composites: for example, the addition of graphene into a flexible CoO/CNF composite mat not only increased the electrical conductivity, but also the mechanical properties of the LIB anodes [188]. Another promising strategy to improve the conductivity of TMO/CNF composites is to make use of the catalytic effect of Fe, Ni and Co on graphitization [189]. It was demonstrated that graphitic layers were *in-situ* formed around the $Fe_2O_3$ and $Co_3O_4$ particles within the CNFs after a carbonization process [162,163]. The graphitic carbon layers had an ameliorating effect of improving both the conductivity and cyclic performance by maintaining the $Fe_2O_3$ and $Co_3O_4$ particles within the carbon core.

#### *4.1.4. Metal alloy/CNFs*

Alloy anodes are well known for their excellent capacities and characteristics of safety arising from the medium plateau. $SnO_x$ and Si are among the most attractive alloy anodes that have received much attention because of their high theoretical capacities of 994 and 4200 mA h/g for Sn and Si, respectively. Li ions are stored through the formation of $Li_{4.4}Sn$ and $Li_{4.4}Si$ alloys. One of the most critical issues that need to be addressed for these metal alloy anodes is the large volume change (of up to ~300%) during charge and discharge, resulting in poor cyclic performance [190–192]. Dispersion of nano-sized $SnO_x$ and Si particles into the CNF matrix is effective in improving the cyclic performance,

where the CNFs function as both the buffer to adsorb the volume change and the conducting network for efficient charge transfer.

Various polymer precursors have been used as precursors for electrospun $SnO_x$/CNF composites, among which PVA and PAN are the most common. The crystallinity and size of $SnO_x$ particles in CNFs were affected by the type and the amount of Sn precursors added. With PAN as precursor, it was found that the $SnO_x$ particle size varied from sub-nanometer to ~2 nm and even up to 40 nm when tin(II) 2-ethylhexanoate, tin(II) acetate and tin(IV) chloride were used, respectively [129,130,193]. The electrochemical performance of $SnO_x$ electrodes was substantially affected by the particle size, where smaller particles had better cyclic performance than larger ones by preventing aggregation into large Sn clusters during the cyclic tests [194]. It was demonstrated that amorphous, sub-nanosized $SnO_x$/CNF composites significantly outperformed the composites containing nanosized counterparts [129], as confirmed later by the report in that ultra-uniform, amorphous $SnO_x$ particles showed excellent cyclic reversibility [195]. The carbonization temperature is another important factor that influences the crystallinity and particle size. It has been widely reported that too high a carbonization temperature may cause the $SnO_x$ particles to drop off from the CNF matrix. An optimized carbonization temperature and suitable precursors should be chosen to prepare high performance $SnO_x$/CNF composites.

Uniform dispersion of Si particles in electrospun CNFs is not trivial, because it is difficult to obtain Si particles directly from the soluble precursors containing the Si elements. Instead, almost all the studies reported so far involved direct addition of Si powder in the polymer solution before electrospinning. The Si/CNF composites synthesized in this way often found agglomerated Si particles that were attached on the CNF surface [196]. The Si particle dispersion in the polymer solution was significantly improved after functionalization with amino-silane and F ions [157]. An interesting observation was made during the preparation of Si/CNF composites where an amorphous $SiO_2$ layer was coated on the Si particles to form a core/shell structure after carbonization. The $SiO_2$ layer was proven to be beneficial to construct a stable SEI layer and thus improve the cyclic performance [197–199].

Nano-sized pores were introduced into the CNFs to accommodate the volumetric changes of the Sn and Si particles. Similarly to the ways how porous CNFs were produced, sacrificial polymers, such as PLA and PMMA, have been incorporated into the mixture of PAN and the active metal particles for electrospinning [108,200]. After carbonization of PAN at 1000 °C, PMMA was decomposed, resulting in the encapsulation of Sn nanoparticles in the porous CNFs, as shown in Fig. 8a. The as-prepared composites delivered a high capacity of 648 mA h/g after discharging at 100 mA/g for 140 cycles (Fig. 8b) [108]. Inorganic particles, such as $Fe_3C$, were also used as the sacrificial phase to prepare Si encapsulated porous CNFs [201]. Another attractive method to produce porous Sn/CNF composites without adding the sacrificial phase is to make use of phase separation between the active material and the solvent [147]. The solvent consisting of $SnCl_2$ and $H_2O$ in PVA fibers was frozen in an ice box and the rapid evaporation of ice in the form of steam during carbonization generated numerous nanoscale pores in CNFs, as shown in Fig. 8c. Among many different approaches, the core/shell structure with either Sn or Si nanoparticles encapsulated by the CNF shell has delivered the best electrochemical performance to date. A dual nozzle described in Section 2.1 was employed for the synthesis of Sn/CNF or Si/CNF composites with a core/shell structure [79,80]. The carbon shell effectively buffered the large volume changes of Sn and Si, and guaranteed intimate contacts between the conductive carbon and active particles. Thus, stable cyclic performance was obtained for the core/shell Si/CNF electrodes with a remarkable specific capacity of 721 mA h/g after charging/discharging at 2.75 A/g for 300 cycles [80].

### 4.2. Cathodes

CNFs contribute little to the capacities when employed as the cathodes of LIBs. Instead, the main purpose of using CNFs in cathodes is to offer a high electrical conductivity and structural stability. Therefore, the content of CNFs in the LMO/CNF composites should not be very high to maintain a sufficiently high energy density of the cathode. In addition, some cathode materials, such as $LiCoO_2$, $Li(NiCoMn)_{1/3}O_2$ and $LiMn_2O_4$, are required to be calcined in air, making it very difficult to carbonize as-spun polymer fibers into CNFs. As a result, only a few studies have so far been reported on LMO/CNF cathodes, most of which were focused on LFP.

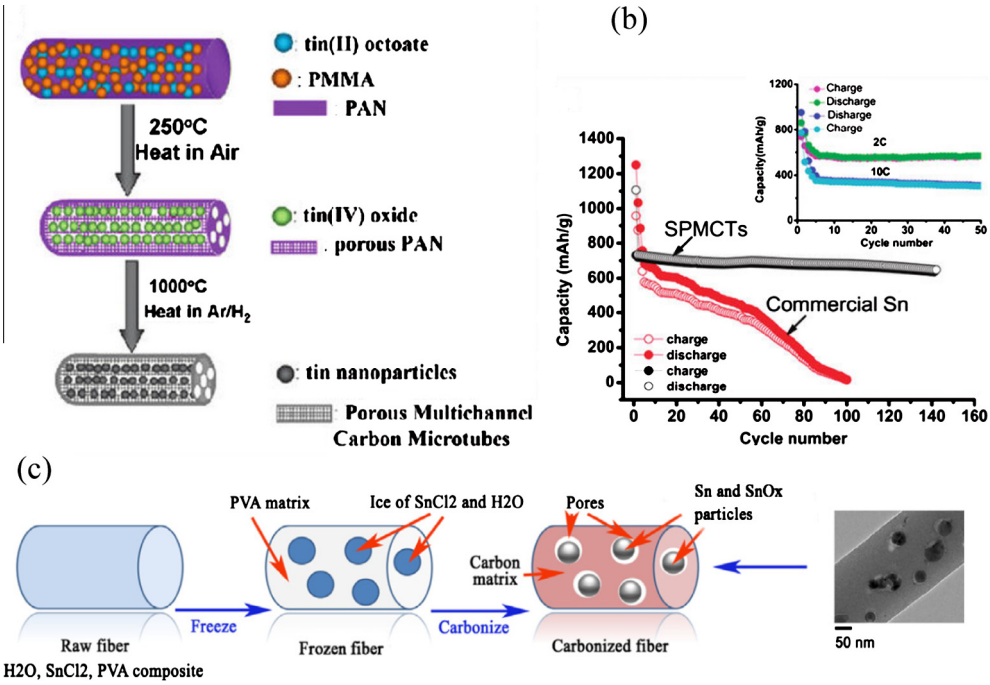


**Fig. 8.** (a) Synthesis of porous Sn/CNF composites by co-electrospinning of PAN–PMMA–Tin octoate blend and (b) the corresponding electrochemical performance of as-prepared composites [108]; (c) creation of pores making use of phase separation between PVA matrix and ice of $SnCl_2$ and $H_2O$ [147]. (Reprinted with permission from [108,147]. Copyright 2009 ACS, 2011 Elsevier.)

The influences of precursor composition and stabilization/carbonization temperatures of LFP/CNF composites were studied [202]. An optimized processing condition was established when 8.0 wt.% LFP precursor and 4.0 wt.% PAN were added in DMF to prepare the electrospinning solution, and the electrodes delivered the best performance after the fibers were stabilized at 280 °C followed by carbonization at 700 °C. PEO was also used as the carbon source to produce carbon-coated single-crystalline LFP so as to achieve stable cyclic performance for up to 100 cycles [203]. The electrochemical performance of the LFP/CNF electrodes was optimized by improving their conductivities using other conductive additives, such as CNTs [204], VGCFs [205] and Ag [206], and doping of cations using Mn ions [207]. Similar approaches have been adopted to produce $Li_3V_2(PO_4)_3$/CNF [107] and $Li_2Mn_{0.8}Fe_{0.2}SiO_4$/CNF [208] composite cathodes with enhanced electrochemical performance.

### *4.3. Discussion on electrospinning for Li ion batteries*

Differing processing parameters have been employed to produce CNFs and their hybrids with metal (oxides) in various structures and morphologies. While the majority of these structural/morphological features may contribute to improving the capacities while some may bring detrimental effects on certain properties of the electrodes. Critical discussion is made on the effects of several factors, like pores, form of hybrids and deposition method, in the following, along with clarification of several important issues of electrospun CNFs for LIBs.

#### *4.3.1. Comparison between porous and nonporous CNFs*

The storage of Li ions in nanopores of carbon materials has been widely reported. A number of strategies have been employed to produce porous CNFs to improve the capacities. Table 8 summarizes

**Table 8**
Electrospun CNFs for LIBs.

| Materials | Process parameters | | | Electrochemical performance | | | Irreversible capacity (mA h/g) |
|---|---|---|---|---|---|---|---|
| | Precursor | Electrospinning voltage (kV)/distance (cm)/flow rate (ml/h) | Chemical and thermal treatments | Capacity (mA h/g) | Current density (mA/g) | Cyclic number | |
| CNF films [169] | 10 wt.% PAN/DMF | 25/–/– | 280 °C 1 h in air + 1000 °C in Ar | 450 | 30 | – | 500 |
| CNF films [35] | 5 wt.% PAN/DMF | 18/15/1 | 220 °C 3 h in air + 550 °C 1 h in $N_2$ | 550 | 100 | 105 | 268 |
| Porous CNF films; $S_{BET}$ = 473 $m^2$/g [89] | (~20 wt.% lignin + ~2 wt.% PEO)/DMF | 6.5–7.0/–/1 | 200 °C 2 h in air + 900 °C 2 h in Ar | 445 | 30 | 50 | 207 |
| Porous CNF powder; $S_{BET}$ = 198 $m^2$/g [127] | (5 wt.% PAN + 7.5% Fe)/DMF | 18/15/1 | 220 °C 3 h in air + 650 °C 1 h in $N_2$, $HNO_3$ etch | 983 | 100 | 80 | 371 |
| Porous CNF powder [131] | (6 wt.% PAN + ~8 wt.% Ni)/DMF | 17/20/~0.4 | 250 °C 2 h in air + 600 °C 3 h in $H_2$(5%)/$N_2$, HCl etch | 969 | 50 | 100 | 705 |
| Porous CNF powder; $S_{BET}$ = 950 $m^2$/g [142] | (15 wt.% PAA + TEOS)/DMAc | –/–/– | 700 °C 1 h, HF etch | 445 | 50 | 50 | 800 |
| Porous CNF films; $S_{BET}$ = 235 $m^2$/g [143] | (8 wt.% PAN + 0.9 wt.% PLA)/DMF | 17/15/0.5 | 250 °C 5.5 h in air + 800 °C 1 h | 435 | 50 | 50 | 292 |
| Porous CNF powder; $S_{BET}$ = 13 $m^2$/g [144] | 30% SAN/DMF (core), (20% PAN + 6.7 wt.% SAN)/DMF (shell) | 18/15 cm/0.5 ml/h (core), 1 ml/h (shell) | 270–300 °C 1 h in air + 1000 °C 1 h in $N_2$ | 501 | 50 | 10 | 383 |
| Porous CNF films; $S_{BET}$ = 438 $m^2$/g [171] | (7 wt.% PAN + 15 wt.% $ZnCl_2$)/DMF | 14/15/0.5 | 280 °C 2.5 h in air + 700 °C 1 h in $N_2$, HCl wash | 450 | 50 | 10 | 455 |
| Porous CNF powder; $S_{BET}$ = 1840 $m^2$/g [149] | 5 wt.% PMMA/DMF (core), (5 wt.% PAN + 5 wt.% $Ni(Ac)_2$)/DMF (shell) + KOH activation | 21/20/0.8 | 250 °C 2 h in air + 700 °C 6 h in $H_2$(5%)/$N_2$ + 750 °C 1 h in the presence of KOH, $HNO_3$ etch | 1150 | 100 | 70 | 928 |

the processing parameters employed and the corresponding electrochemical performance of the CNFs with and without nanoscalepores. In general, porous CNFs deliver much higher capacities than non-porous counterparts. A high capacity of more than 1000 mA h/g was reported for the porous CNFs with an extremely large surface area of 1840 $m^2$/g. However, the large surface area also led to a large irreversible capacity of 928 mA h/g [149], due probably to the formation of thick SEI films stemming from the large contact area between the electrode and electrolyte. This means that it is necessary to strike a balance between the large surface area of porous CNFs and their large irreversible capacities. However, there are few studies focusing mainly on the effect of different pore sizes on Li ion transfer and storage, which is the key issue for designing porous CNFs. Another detrimental effect induced by the generation of pores is the decrease in mechanical properties of CNFs. The presence of pores normally makes the CNF films more brittle. One can see from Table 8 that many of the porous CNFs are characterized in powder form instead of a thin film. Moreover, there are few studies focusing mainly on the effects of different pore sizes on electrical conductivity and Li ion transfer/storage, which are the key issues for designing porous CNFs. It is postulated that the porosity should have a negligible, negative influence on electrical conductivity because the conductivity of carbon depends mainly on the crystallinity and atomic structure, instead of nano-/microscopic morphological features, like pores. In fact, isolating the effect of porosity may not be trivial because the creation of pores always results in simultaneous modification of carbon structures surrounding the pores due to the incorporation of catalysts, application of high annealing temperatures, etc. Further investigations are needed to clarify this challenging issue.

#### *4.3.2. Comparison between neat metal oxide fiber and metal oxide/CNF composites*

A number of previous studies employed fibers containing only the neat metal oxides, such as $SnO_2$ [209] and $Fe_2O_3$ [106], directly as the electrode materials. The polymer precursor was used only for preparing a spinnable solution that had a sufficiently high viscosity for electrospinning. The polymer precursor was completely decomposed after calcination in air, leaving only the neat metal oxide fibers. There are some important benefits of using neat metal oxide fibers, such as high capacities, high volumetric energy densities and reduced first cycle irreversible capacity. TMO and alloy anodes have much higher capacities than carbon materials, and as such the capacities of the fibers consisting of only the metal oxides should be higher than those containing a large amount of carbon in CNFs. Metal (oxides) normally have much higher densities than carbon materials, thus eliminating carbon is also helpful in obtaining a high volumetric energy density. In addition, the large surface area of carbon means a large solid/electrolyte interface area, resulting in a high irreversible capacity in the first several cycles.

Nevertheless, the complete removal of carbon from the electrospun fibers also brings about several problems in terms of both structure and performance. The issues include easy collapse of the fiber structure, excessive growth of particle size, reduced electrical conductivity and thus poor cyclic stability [106]. Carbon functions as a scaffold to establish a 1D structure. Complete removal of carbon often leads to the collapse of fiber into particles, reducing the aspect ratios of fibers due to the shortened fiber lengths. Therefore, the neat metal oxide fibers without carbon are difficult to maintain the free-standing nature of CNF films, which cannot be used as electrodes without adding binders. In addition, metal oxide particles are easy to grow into large sizes in the absence of carbon confinement. A large particle size increases the Li ion transfer length, thus inevitably leading to a slower kinetic process. Although other conductive additives, such as carbon black, can be added when preparing the electrodes, the contact of metal oxides with the conductive additives is not as intimate as that expected from the metal oxide/CNF composites where the metal oxides are fully encapsulated by the CNF matrix. Apart from enhancing the electrical conductivities, the CNF matrix functions as stress buffer to accommodate the volume change of metal oxides. The absence of CNF means that there is no mechanism to alleviate the large volume change of metal oxides, leading to the formation of cracks and capacity degradation [209]. Therefore, full removal of carbon is not recommended to obtain high performance electrodes. Instead, an optimized carbon content should be included to sustain the structure integrity, high volumetric and gravimetric energy densities as well as long cyclic life of the electrodes. However, it should be noted that some cathode materials cannot be calcined for carbonization

in an inert atmosphere, thus fibers have to be produced using only neat metal oxides, like $LiCoO_2$ [210] and $LiMn_2O_4$ [211].

*4.3.3. Comparison between in-situ deposition and ex-situ growth*

Two major techniques have been developed to incorporate metal oxides in CNFs: namely, *in-situ* deposition and *ex-situ* growth. The vast majority of previous studies on CNF fabrication for LIBs involved *in-situ* deposition, which have an advantage of simple fabrication processes and uniform distribution of metal oxides. However, some metal oxides can be better encapsulated into the carbon matrix by *ex-situ* growth. The *ex-situ* growth involves the preparation of CNFs on which metal oxides are subsequently grown by a sol–gel or hydrothermal process. A major benefit of *ex-situ* growth is that the morphologies of grown metal oxides can be modified, especially through a hydrothermal process [176]. Another possible application of *ex-situ* growth is to deposit metal oxides that cannot be annealed at high temperatures. Therefore, both morphologies and properties of metal oxides should be taken into account for proper selection of deposition methods.

## 5. Application of CNFs in supercapacitors

SCs is another important electrochemical energy storage device that can deliver much higher power densities than LIBs, but with lower energy densities. It has a structural configuration similar to LIBs, where two electrodes separated by a membrane are immersed in the electrolyte, as shown

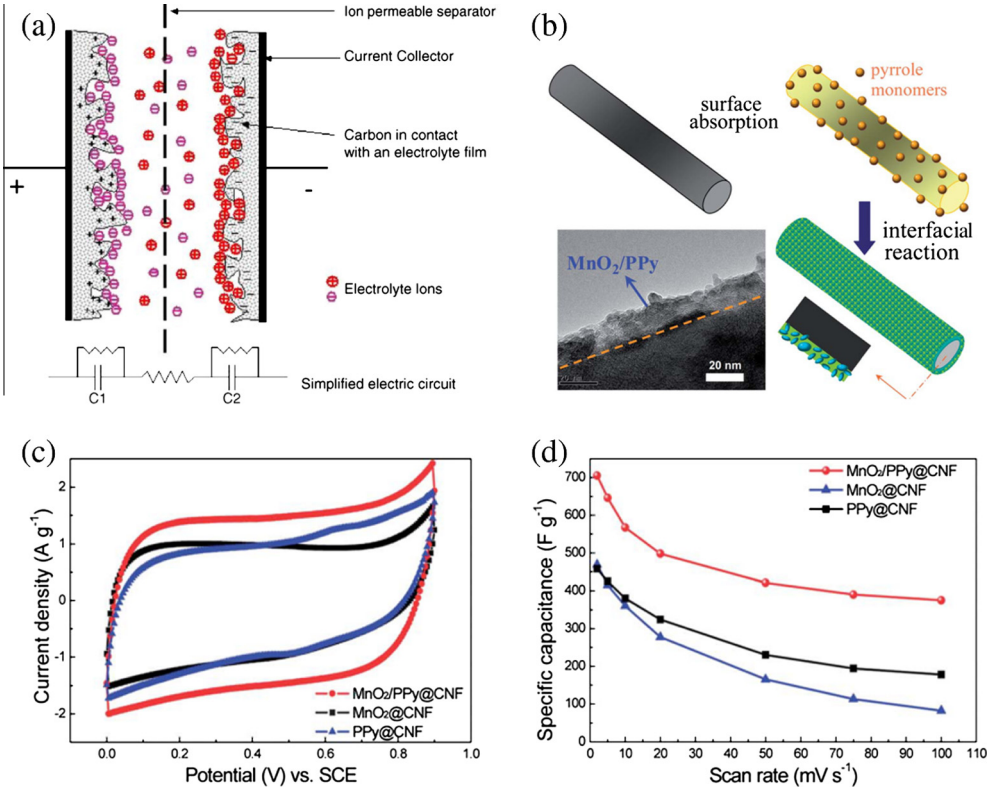


**Fig. 9.** (a) Representation of an electrochemical double layer capacitor (EDLC) [156]; (b) schematic illustration of the design and fabrication of $MnO_2$/PPy/CNF hybrid composites and their corresponding (c) CV curves and (d) capacitances at various scan rates [220]. (Reprinted with permission from [156,220]. Copyright 2006 Elsevier, 2012 RSC.)

**Table 9**
Electrospun CNFs and their hybrids with metal (oxides)/conducting polymer for supercapacitors.

| Materials | Process parameters | | | Electrochemical performance | | | Ref. |
|---|---|---|---|---|---|---|---|
| | Precursor | Electrospinning voltage (kV)/distance (cm)/flow rate (ml/h) | Thermal treatment | Capacitance (F/g) | Current density (mA/g) | Cycle number | |
| Porous CNFs, $S_{BET}$ = 1230 $m^2/g$ | 10 wt.% PAN in DMF | –/–/– | 280 °C 1 h in air + 700 °C 0.5 h in 30 vol.% steam/$N_2$ | 175 | 10 | – | [148] |
| Porous CNFs, $S_{BET}$ = 1453 $m^2/g$ | PAA/(THF + methanol) | 15/–/– | 1000 °C + 750 °C in 40 vol.% steam/$N_2$ | 175 | 20 | – | [95] |
| Porous CNFs, $S_{BET}$ = 1220 $m^2/g$ | 20 wt.% PBI/DMAc | –/–/– | 800 °C in 30 vol.% steam/$N_2$ | 178 | 5 | – | [214] |
| Porous CNFs, $S_{BET}$ = 550 $m^2/g$ | (5 wt.% $ZnCl_2$ + 10 wt.% PAN)/DMF | 25/–/– | 280 °C 1 h in air + 800 °C 1 h in Ar | 140 | 5 mV/s | – | [150] |
| Porous CNFs, $S_{BET}$ = 1614 $m^2/g$ | (12% Nafion + 8% PAN)/DMF | 8–10/12–15/0.5 | 280 °C in air + 700 °C 1 h + 800 °C 1 h in Ar | 190 | 1000 | – | [145] |
| Porous CNFs, $S_{BET}$ = 1387 $m^2/g$ | (8 wt.% PAN + 2 wt.% TEOS)/DMF | 20/25/– | 280 °C in air + 800 °C 1 h 20 vol.% steam/$N_2$ | 90 | 1 mA/$cm^2$ | – | [128] |
| Porous CNFs, $S_{BET}$ = 302 $m^2/g$ | (10 wt.% PAN + 0.5 wt.% PMHS)/DMF | –/–/– | 280 °C in air + 800 °C in Ar | 120 | 3 mA/$cm^2$ | – | [152] |
| Porous CNFs, $S_{BET}$ = 577 $m^2/g$ | ($B_2O_3$ + 10 wt.% PAN)/(DMF + THF) | –/–/– | 280 °C in air + 800 °C in Ar | 184 | 1 mA/$cm^2$ | | [215] |
| N,P co-doped CNFs, $S_{BET}$ = 64 $m^2/g$ | ($H_3PO_4$ + 8 wt.% PAN)/DMF | 16/18/0.4 | 280 °C 2 h in air + 800 °C 2 h in $N_2$ | 203 | 5 | 8000 | [126] |
| Porous CNTs/CNFs, $S_{BET}$ = 810 $m^2/g$ | (0.8 wt.% CNT + 7.2 wt.% PAN)/DMF | 30/30/– | 240 °C 2 h in air + 350 °C 1 h + 700 °C 0.5 h in Ar + 650 °C 0.33 h $H_2O_2/H_2O$/Ar | 278 | 600 | 1000 | [134] |
| Graphene/CNFs | (1 wt.% graphene + 10 wt.% PAN)/DMF | 20/25/1.0 | 215 °C 1 h in air + 800 °C 0.5 h in Ar + 400 °C 1 h in air | 114 | 2500 | 2000 | [136] |
| Graphene/CNFs, $S_{BET}$ = 463 $m^2/g$ | (0.3 wt.% graphene + 10 wt.% PAN)/DMF | 15/15/0.5 | 270 °C 0.5 h in air + 900 °C 2 h in Ar | 165 | 1250 | 1500 | [137] |
| $MnO_2$/CNF film | 10 wt.% PAN/DMF + dip-coating in $KMnO_4$ solution | 18/15/– | 280 °C 2 h in air + 1000 °C 2 h in $N_2$ for CNF | 200 | 100 mV/s | 1500 | [160] |
| $MnO_2$/CNF film | PAN/DMF + dip-coating in $KMnO_4$ solution | 18/15/1.0 | 280 °C 1 h in air + 850 °C in $N_2$ for CNF | 209 | 10,000 | 1000 | [216] |
| Hollow $Co_3O_4$/CNF films | (8 wt.% PAN + 2 wt.% cobalt acetylacetonate)/DMF | 10/15/0.3 | 220 °C 1.5 h in air + 350 °C 5 h + 800 °C 1 h in $N_2$ + 300 °C 0.33 h in air | 484 | 4000 | 2000 | [158] |
| $RuO_2$/CNF films | 10 wt.% PAN + 20 wt.% ruthenium(III) acetylacetonate | 20/18/1.0 | 280 °C 1 h in air + 800 °C 1 h in 30% steam/$N_2$ | 391 | 1 mA/$cm^2$ | 1000 | [217] |

(*continued on next page*)

**Table 9** (*continued*)

| Materials | Process parameters | | | Electrochemical performance | | | Ref. |
|---|---|---|---|---|---|---|---|
| | Precursor | Electrospinning voltage (kV)/distance (cm)/flow rate (ml/h) | Thermal treatment | Capacitance (F/g) | Current density (mA/g) | Cycle number | |
| CNT/CNF/polypyrrole films | 3 wt.% CNT + 10 wt.% APN/DMF + polymerization in $FeCl_3$/pyrrole chloroform solution | 20/15/1.0 | 280 °C 1 h in air + 800 °C 1 h in 30% steam/$N_2$ | 326 | 1 mA/cm$^2$ | 500 | [132] |
| CNT/CNF/PANI film | 10 wt.% (PAN + $Ni(AcAc)_2$)/DMF + polymerization in 0.03 M aniline/ammonium persulfate/$H_2SO_4$ solution | 18/20/– | 215 °C 1 h in air + 500 °C 1 h in $H_2$/Ar<br>CNTs in CVD: 900 °C 0.5 h in Ar + 650 °C 1 h in Ar/$C_2H_4$ | 332 | 15,000 | 1000 | [135] |
| $MnO_2$/PPy/CNF film | 10 wt.% PAN/DMF + polymerization in 0.1 M pyrrole/0.05 M $KMnO_4$ solution | –/–/– | 280 °C 2 h in air + 1000 °C 2 h in $N_2$ for CNF | ~400 | 12 mA/cm$^2$ | 2000 | [220] |

in Fig. 9a [156]. The capacitance of a SC is determined by two charge storage mechanisms: namely (i) EDLC arising from the electrostatic absorbance of ions and (ii) pseudocapacitance (PC) due to the Faradic electrochemical storage. Table 9 summarizes the performance of electrospun CNFs and their hybrids with metal (oxides)/conducting polymers for SCs, and the detailed discussions are made in the following sections.

### 5.1. Neat CNFs

The EDLC is normally proportional to the surface area of electrode materials. Carbon materials, such as CNTs and graphene, have been widely used as electrodes for SCs taking advantage of their large specific surface areas [212,213]. A number of studies employed electrospun CNFs prepared using different polymer precursors, like PAN and polybenzimidazole (PBI), as the electrodes for SCs. Neat CNFs prepared from a polymer alone seldom possess a large surface area, necessitating the creation of nanoscale pores. One exception is the CNFs produced by a lignin precursor, which can be activated by itself due to the presence of high-content oxygen [88,91].

One of the most popular ways to produce nano-sized pores in CNFs for application in SCs is by activation in either a physical or chemical way. Activation by $H_2O$ steam has shown to be effective in improving the surface area. A remarkably large surface area of 1230 $m^2/g$ was obtained by activation of PAN-based CNFs in 30 vol.% steam using a carrier gas $N_2$ at 700 °C for 30 min [148]. Similar strategies have also been successfully applied to produce porous CNFs prepared using PBI and PAA [95,214]. Chemical activation was carried out using $ZnCl_2$ to activate PAN-based CNFs: Zn is known to be an efficient etchant of carbon atoms. A large surface area of 550 $m^2/g$ was obtained with 5 wt.% of $ZnCl_2$, giving rise to a high capacitance of 140 F/g [150]. Besides the activation process, incorporation of sacrificial phases has also been employed to generate pores. CNFs produced by electrospinning a blend of PAN and sacrificial Nafion showed a surface area as large as 1614 $m^2/g$ [145].

Doping with heteroatoms is found to be especially beneficial to the performance of CNFs. They not only improve the EDLC by introducing nanoscale pores, but also contribute to the PC by attaching useful functional groups. Several studies reported the formation of Si–C–O and Si–O–Si groups in the Si-doped CNFs. TEOS [128] or PMHS [152] was used as the Si precursor which was decomposed to release volatile gases, such as $CO_2$, $H_2$ and $H_2O$. Escape of these gases left numerous pores on the surface of CNFs. $B_2O_3$ was also incorporated into the polymer precursor and open pores were created on the CNF surface because of the release of gases through the reaction between $B_2O_3$ and C. In addition, [O]BN functional groups were found to be active in KOH aqueous electrolyte, contributing to PC [215]. Pyrrol-like nitrogen groups in N/P co-doped CNFs were also accessible to ions for pseudocapacitive Faradic reactions. The doped CNFs delivered an exceptional capacitance of 203 F/g after 8000 cycles [126].

The incorporation of other carbon allotropes, such as CNTs and graphene, has been widely studied to produce CNT/CNF and graphene/CNF hybrids. The electrical conductivities of PAN films increased from 0.86 to 5.32 S/cm with the addition of 10 wt.% CNTs. As a result, the capacitance improved from 134 to 278 F/g at a current density of 600 mA/g due to the reduced charge transfer resistance [134]. Graphene was embedded into CNFs by adding graphene oxide sheets into the PAN/DMF solution [136,137]. Both the surface area and electrical conductivity of CNF films were greatly improved, i.e. from 277 to 463 $m^2/g$ and from 1.11 to 2.0 S/cm, respectively, with 3 wt.% graphene, giving rise to an enhanced capacitance by 24% to 197 F/g [137].

### 5.2. CNFs containing metal oxides and/or conducting polymers

Several metal oxides, such as $MnO_2$ and $Co_3O_4$, have high PCs, but with poor cyclic life and rate capability due to their low electronic conductivities. Deposition of these metal oxides onto the electrospun CNFs have been widely studied in order to obtain high capacitances at high current densities with long-term cyclic stability. Nanocables consisting of $MnO_2$-coated CNFs were fabricated by a simple dip coating method. Electrospun CNF films were immersed into the $KMnO_4$ solution, where $MnO_4^-$ was reduced by C, resulting in coating of $MnO_2$ nanosheets on CNFs with a capacitance higher than 500 F/g [160,216]. Metal oxide nanoparticles were also *in-situ* encapsulated into the CNFs during electrospinning. Cobalt acetylacetonate was mixed with PAN/DMF solution to produce hollow $Co_3O_4$ par-

ticles embedded in the CNF films after a carefully controlled annealing process [158]. A similar strategy was used for CNFs embedded with $RuO_2$ particles [217].

Conducting polymers, such as polypyrrole (PPy) and polyaniline (PANI), have attracted great attention as electrodes of SCs due to their low costs and high capacitances [218,219]. These polymers were grafted onto the electrospun CNFs, especially based on *in-situ* chemical polymerization, to fabricate freestanding film electrodes. In addition, CNTs were also added producing CNT/CNF/PPy and CNT/CNF/PANI composite electrodes with further enhanced electrical conductivities [132,135]. The CNT/CNF/PANI electrode delivered a capacitance as high as 503 F/g when discharged at 0.3 A/g [138]. Further, the CNFs were functionalized with oxygenated groups by $HNO_3$ treatment, followed by absorption of pyrrole monomers and oxidation by $KMnO_4$, simultaneously producing $MnO_2$/PPy coated CNF composites. A mixture of PPy and $MnO_2$ was coated onto the CNFs to produce triaxial $MnO_2$/PPy@CNF nano-cables with a remarkable capacitance of 705 F/g, as shown in Fig. 9b–d [220].

The synthesis processes and performance of CNFs containing metal (oxides) and/or conducting polymers are summarized in Table 9. It is noted that the CNF acts mainly as a conductive substrate in the composites. Porous CNFs can contribute to improving the EDLC because of the large surface area, as discussed in Section 5.1. It is envisaged that the high EDLCs of porous CNFs and high PCs in metal oxides/conducting polymers can be combined together to further increase the electrochemical performance. The porous CNFs may be more effective than non-porous CNFs in supporting the metal oxides/conducting polymers so that a higher metal oxide content can be encapsulated into the CNFs.

## 6. Other electrochemical energy storage devices

### 6.1. Na ion batteries

The ever increasing demand in lithium sources and their rising costs are becoming a critical issue that limits the application of lithium batteries for large-scale energy storage. NIBs are considered a potential candidate to replace LIBs owing to the low cost and abundance of Na-containing precursors. Similar to LIBs, Na ions also shuttle between the cathode and anode. However, the energy densities of NIBs are generally lower than those of LIBs because of the higher potential of $Na/Na^+$ (−2.71 V vs. SHE) than $Li/Li^+$ (−3.04 V) [221]. Finding a host material that can accommodate more Na ions is therefore essential to achieving a sufficiently high capacity. The electrode materials widely used for LIBs are not fully compatible with NIBs because of the much larger (~55%) diameter of Na ions than that of Li ions.

Although graphite is known to be one of the most suitable anode materials for LIBs, it fails to deliver a sustainable capacity in NIBs using traditional carbonate electrolytes. Instead, non-graphitic carbon materials are shown to present an acceptable capacity for long cycles, where Na ions can be stored in "nanocavities" and misaligned graphene layers [222]. Electrospun CNFs carbonized at a low temperature of 600 °C were used as anode, and a capacity of 233 mA h/g was obtained after 100 cycles at 50 mA/g [223]. Nanoscale pores were also introduced in the CNFs to achieve a long cyclic life of 1000 cycles at a discharge current density of 500 mA/g, as shown in Fig. 10a [224]. A high specific capacity was achieved by embedding nanosized Sb [225,226] and SnSb [227] particles in electrospun CNFs, which led to alloying reactions to form NaSb and NaSn alloys. To achieve a high electrical conductivity and maintain a stable structure by alleviating the volume change, Sb/CNF composite films with Sb particles of 20–50 nm in diameter were produced using $SbCl_3$ and PAN as the precursors. The composite electrodes maintained a stable structure during the charge/discharge cycles and delivered a high capacity of 350 mA h/g after 300 cycles at 100 mA/g, as shown in Fig. 10b and c [225]. CNFs can also be used as a support for cathode materials in NIBs, although very few studies are carried out. Nanosized $Na_3V_2(PO_4)_3$ particles were encapsulated into CNFs to shorten the Na ion transfer length while facilitating the electron transfer for high rate performance [228].

### 6.2. Li–$O_2$ or Li–air batteries

LABs are well known for their excellent energy densities that are at least 2–3 times higher than those of LIBs. A LAB typically consists of a Li metal and a porous cathode, both of which are immersed

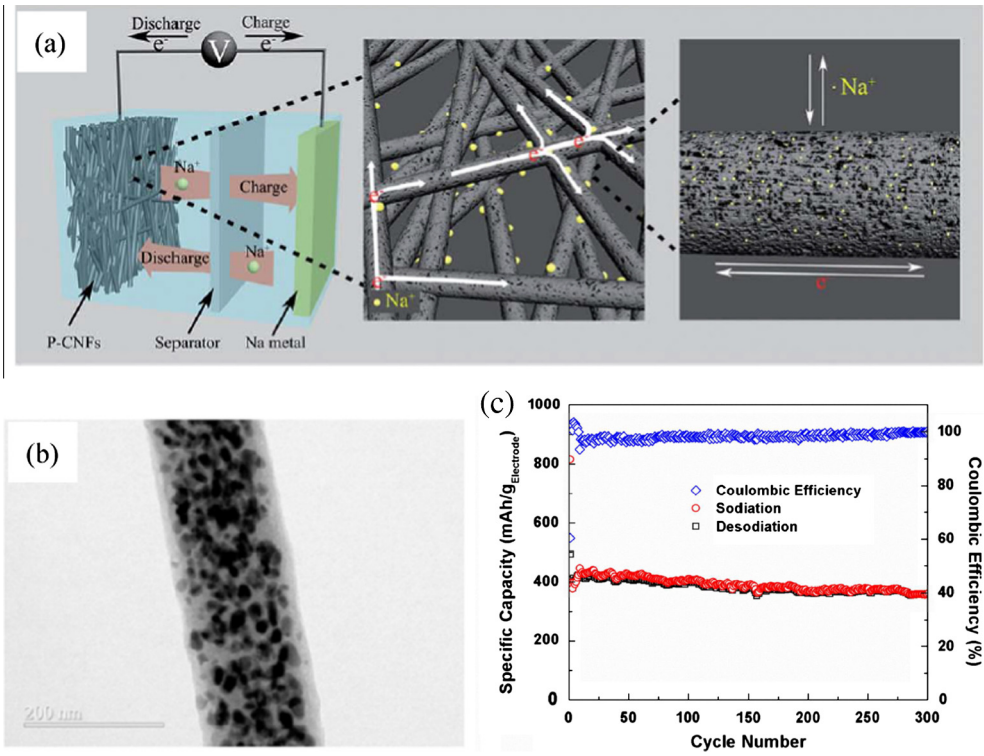


**Fig. 10.** (a) Schematic illustration of sodium storage in porous CNFs [224]; (b) Sb nanoparticles encapsulated in CNFs; and (c) cyclic performance of anode in NIBs at 0.1 A/g [225]. (Reprinted with permission from [224,225]. Copyright 2014 RSC, 2013 ACS.)

in electrolyte, as shown in Fig. 11a [229]. One of the most critical issues for LABs, however, is the poor reversibility related to the oxygen evolution reaction. Therefore, various catalysts have been developed to improve the reversibility, especially to decompose the reaction products, like $Li_2O_2$ and $Li_2O$, formed during the charging process [230]. Electrospun CNFs can be a promising substrate because of their high porosity and the potential to support and utilize the metallic catalysts so as to increase the active sites and establish conductive networks for fast electron transfer. In addition, carbon materials, such as carbon black [231] and graphene [232], have also shown catalytic effects. An extremely high capacity of 2799 mA h/g was obtained in the first discharge cycle of neat electrospun CNFs [233]. Incorporation of nanosized $Mn_3O_4$ [234], Fe [235], Fe/$Fe_3C$ [236] catalysts improved both the discharge capacities and cyclic performance of electrospun CNF electrodes. For example, the Fe/$Fe_3C$/CNF composite electrode delivered a capacity of 600 mA h/g after 40 cycles, which is considered a remarkable achievement for LABs, as shown in Fig. 11b [236]. Nevertheless, there was a recent report suggesting that carbon materials may not be stable when charging to above 3.5 V, where irreversible reaction products like $Li_2CO_3$ may form [237]. Therefore, neat metal oxides fibers, such as $La_{0.75}Sr_{0.25}MnO_3$ [229] and $Co_3O_4$ [238], were produced by electrospinning as cathode materials. It is also proposed that defect-free carbons with no or a few functional groups were more suitable for cathodes in LABs than those containing many functional groups [239]. This observation indicates that CNFs carbonized at high temperatures may perform better than the counterparts treated at low temperatures. Further analyses are necessary to identify the relationship between the chemical structure of CNFs and the corresponding catalytic effects.

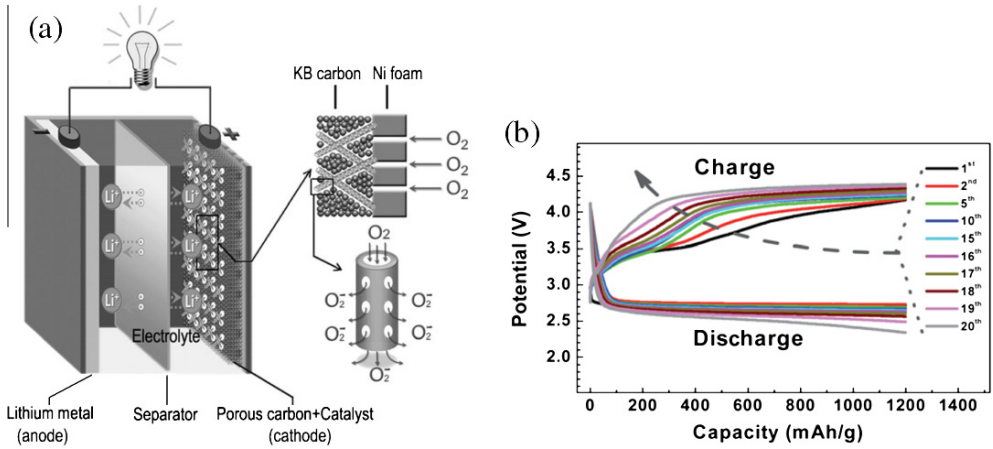


**Fig. 11.** (a) Illustration of a LAB [229]; (b) cyclic performance of Fe/$Fe_3C$–CNF electrode at 300 mA/g in LABs [236]. (Reprinted with permission from [229,236]. Copyright 2013 Wiley, 2014 RSC.)

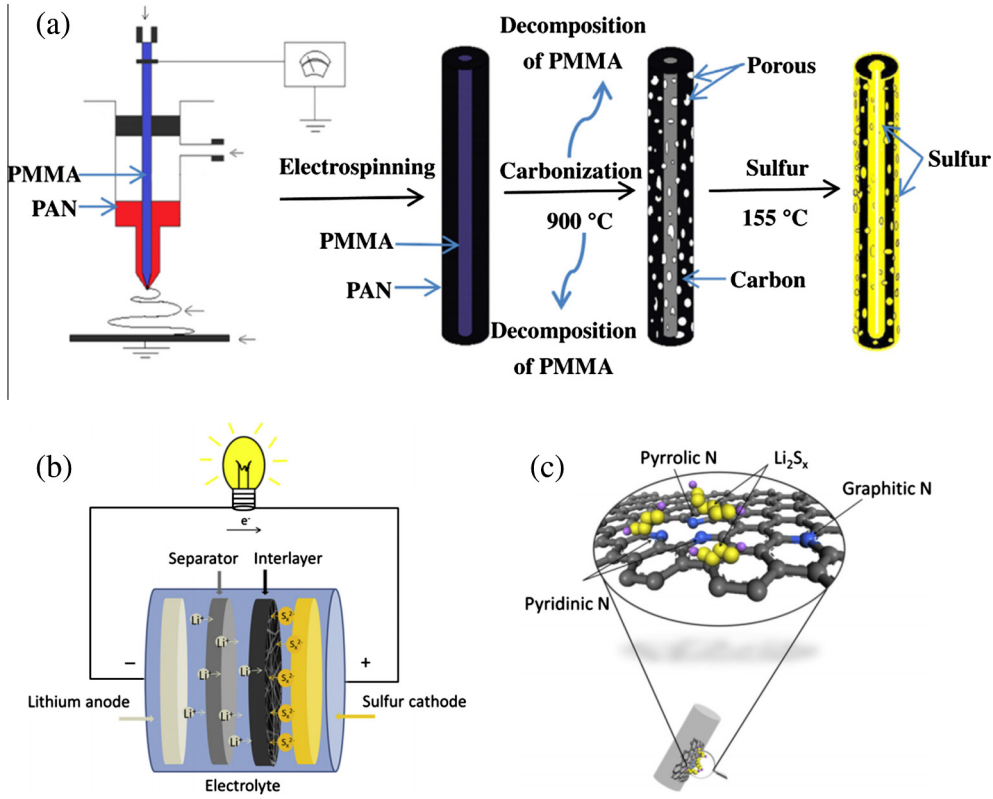


**Fig. 12.** (a) Illustration of encapsulation of sulfur in porous CNFs [242]; (b) schematic cell configuration with CNF interlayer in LSB and (c) the entrapment of polysulfides in the interlayer [248]. (Reprinted with permission from [242,248]. Copyright 2014, 2015 Elsevier.)

### 6.3. Li–sulfur batteries

LSBs have a theoretical energy density of 2567 kW/kg, making them very attractive for large-scale applications, such as EVs. However, their practical applications have been limited because of the following critical issues that need to be addressed: namely, (i) fast capacity degradation due to the "polysulfide shuttle" effect arising from dissolution of intermediate polysulfides; (ii) poor electronic conductivities of sulfur; and (iii) a large volumetric change ~80% of sulfur during cycles. Incorporation of sulfur into porous nanocarbon materials has been proven to be one of the most effective approaches to improve the cyclic performance [240]. Electrospun porous CNFs produced from a blend of PMMA/PAN [241,242] and PLA/PAN [243] have been employed to support sulfur. Sulfur particles were encapsulated into the porous CNFs through chemical deposition by dispersing porous CNFs in $Na_2S_x$ and HCOOH solution [241]. Another approach called the 'melt-diffusion' strategy was also used to entrap sulfur particles into the porous CNFs, where sulfur was heated together with CNFs at 155 °C in a sealed chamber, as shown in Fig. 12 [242,244]. An intimate contact between the conductive CNFs and sulfur allowed fast charge transfer, while the sulfur entrapped in the pores not only accommodated the volume changes but also partly prevented the polysulfide shuttling from taking place, thus improving the cyclic performance. Further research was proposed to use CNFs in LSBs after two major modification: namely, (i) incorporation of inorganic particles as polysulfide reservoirs; and (ii) interlayers made from CNFs. Both Ti–O and Si–O groups have been found to attract polysulfides by binding with positively charged surface [245,246]. Encapsulation of these particles into the porous CNFs with optimized pore sizes by the aforementioned *in-situ* deposition would further improve the cyclic performance. Meanwhile, insertion of a conductive interlayer between the cathode and separator was effective in inhibiting the transfer of polysulfides into the anode side [247]. Electrospinning provides a facile way to produce thin films consisting of CNFs as interlayers for LSBs with effective entrapment of polysulfides, as shown in Fig. 12b and c [248]. Functionalization of the CNFs could further increase the efficiency in entrapping the polysulfides for long-term cyclic stability.

## 7. Issues facing practical application

Even with the well-established understanding of electrospinning processes and the stellar performance of electrospun CNFs in electrochemical energy storage, there are still many fundamental issues that have not been fully explored and understood, which are discussed in the following:

(i) Accurate theoretical models are needed to predict the electrospinning process so as to reduce the time for process optimization. Existing models are still in the early stage of development and are not able to simulate all the parameters involved in the whole electrospinning process and predict the fiber diameter or bead formation.

(ii) While many studies have been devoted toward enlarging the surface area, a large surface area could also severely reduce the Columbic efficiently in the first several cycles. Thick and large-area SEI films may form due to the large area contact between the electrode and electrolyte [3]. Fig. 13a and b shows the first charge/discharge curves of PAN-based CNFs in LIBs and NIBs. A SEI film was formed at around 0.7 V, giving rise to a high irreversible capacity while the Columbic efficiency was only 76% and 60% in LIBs and NIBs, respectively. These values may further reduce if the surface areas of CNFs were increased by adding nanopores. Furthermore, the SEI film may continuously grow if a stable film could not be established. The nanostructure of electrode and the electrolyte composition need to be optimized to allow the formation of a stable SEI film on the large surface area of CNFs, which is critical for improving the cyclic reversibility. One potential solution has been proposed to improve the Coulombic efficiency in the first cycle by chemical pre-lithiation or pre-sodiation [249]. While few studies have so far been conducted to confirm the effectiveness of the above method in CNFs, a more efficient and facile approach needs to be established.

(iii) The influence of pore size in CNF electrodes on the performance of SCs has been extensively studied, and the presence of micropores is confirmed to be beneficial to improving the capaci-

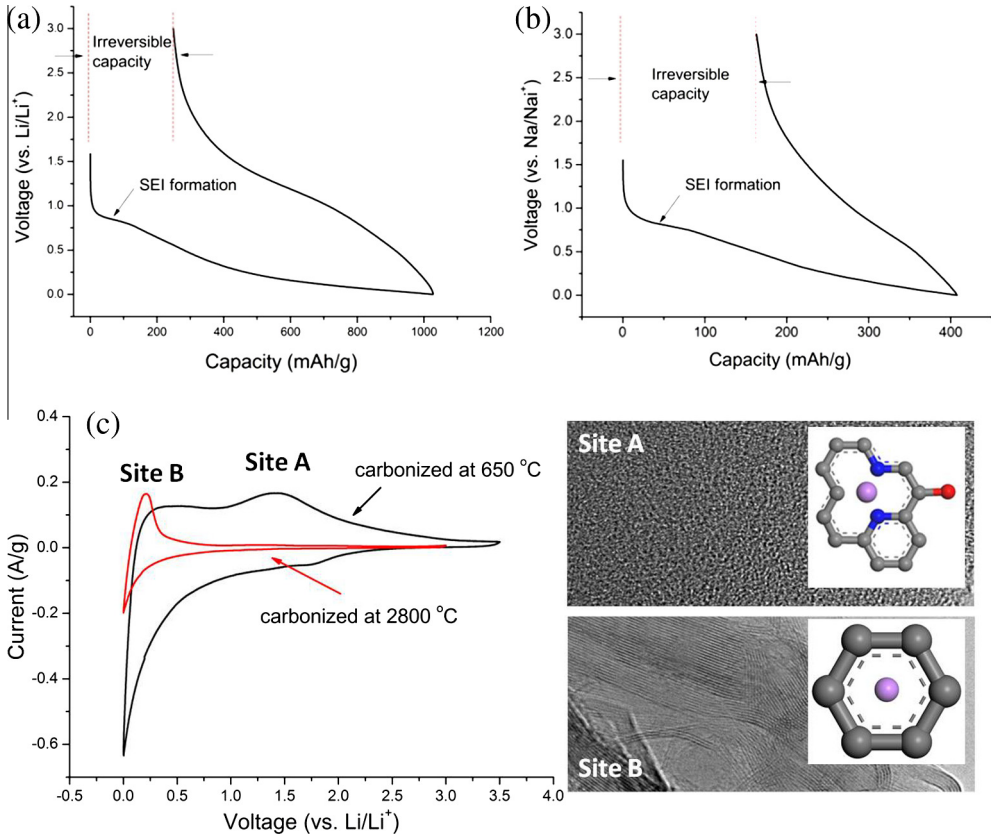


**Fig. 13.** Charge/discharge curves of PAN-based CNFs that carbonized at 650 °C in the first cycle in (a) LIBs and (b) NIBs. The electrolyte is 1 M $LiClO_4$ and $NaClO_4$ in ethyl carbonate/dimethyl carbonate (1:1 by volume) for LIBs and NIBs, respectively; (c) CV curves of CNFs carbonized at 650 and 2800 °C and the Li ion storage sites (A indicate Li ion stored in defect sites, B shows the intercalation of Li ions between graphene layers).

tance [250]. However, the effects of pore size in CNFs on Li/Na ion storage and transfer, $O_2$ diffusion in LABs and polysulfide entrapping in LSBs have rarely been systematically reported. Only disconnected and particle has thus far been established. For instance, it is found that mesopores were much more efficient in accommodating the reaction products than micropores in LABs [251]. Micropores were easily blocked by Li oxides during $O_2$ reduction, preventing further electrochemical reactions from taking place [231]. Mesopores of several nanometers in diameter were also found to be beneficial in entrapping polysulfides [240]. Full understanding of the effect of pores of different sizes in individual energy storage devices is necessary to optimize and balance the electrochemical performance of the devices for specific end applications.

(iv) The atomic and chemical structure of CNFs is important to determine their electrical conductivities and electrochemical reactions. The structural evolution during carbonization needs to be understood to optimize the annealing process. However, few studies have been reported on this topic so far, except for PAN-based CNFs. The effects of defects, surface reaction sites and the degree of graphitization on charge transfer and storage behaviors are still ill understood. Li and Na ion storage in non-graphitic carbon materials is quite complex where several mechanisms co-exist. In addition to intercalation of the metal ions between the graphene layers, they may also be stored in the isolated graphene layers or defect sites, as shown in Fig. 13c. PAN-based CNFs carbonized at 650 °C was amorphous and contains a number of defects because

of the high nitrogen content in the precursor polymer, PAN [35]. In contrast, an almost full graphitic structure was formed after carbonization at 2800 °C. The two samples showed entirely different Li ion storage mechanisms. The intercalation between graphene layers had a low potential at below 0.2 V (Site B), which is suitable for an anode with a high output voltage when matching with the cathode. In contrast, Li ions were stored at defect sites of CNFs at above 1 V (Site A). While this mechanism can offer an additional capacity to CNFs, it may be problematic when coupling with the cathode in full cells. Optimizing the structure of CNFs is of great importance in tailoring the plateau while keeping the high capacity by taking advantage of various charge storage mechanisms. Functional groups are expected to have similar effects on charge transfer and storage. CNTs and graphene are often functionalized to improve their performance. Many functional groups are proven to be beneficial to binding the metal oxides, storing the Li ions, facilitating the ORR in LABs and entrapping the polysulfides. However, few studies have been reported on functionalization of electrospun CNFs.

(v) Long-term cyclic stability is of great importance for practical applications of these energy storage devices in EVs where thousands of service cycles are required [252]. However, even after incorporating metal (oxide) particles having different nanostructures in CNFs, it is still difficult to achieve the desired stability. A strong bond between the metal oxides and CNFs may be required to guarantee long-term stability and electrical conduction between them. Meanwhile, CNFs should function to accommodate the volumetric strains during cycles. Although the core/shell structure with metal (oxides) encapsulated in the core of CNFs can avoid the detachment of the particles [253], the large strain arising from these metal (oxide) particles inside the shell may break the fibers. The transfer of ions and electrons among the particles in the core may become slowed, as indicated in Fig. 14a. A possible solution to this problem is to produce individual nanoscale pores with mono-dispersed metal (oxides) nanoparticles embedded in CNFs, as shown in Fig. 14b. The pore size can be optimized based on the volume change of the specific metal (oxides). Thus, the volume change can be fully accommodated and the intimate contact between the carbon matrix and the individual nanoparticles can guarantee fast charge transfer.

(vi) One of the major benefits arising from electrospun CNF films is the freestanding and flexible nature of the electrodes. Flexible energy storage devices have received considerable attention, where flexible electrodes play a key role in making the whole device flexible. Although the electrochemical performance of CNF- and graphene-based flexible electrodes have been extensively studied [254], the mechanical properties of electrospun CNF films and their electrochemical performance in bending or stretching under simulated service conditions have not been widely investigated.

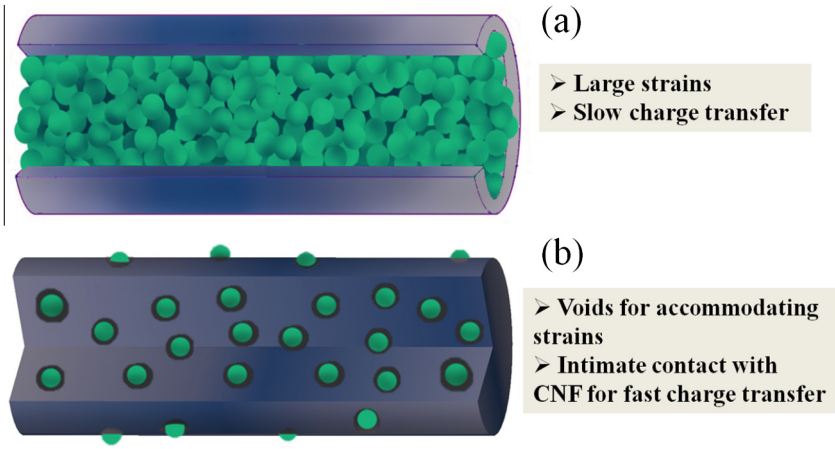


**Fig. 14.** Schematic of (a) core/shell structured CNFs with metal (oxides) encapsulated and (b) optimized metal (oxides)/CNF composites.

(vii) Another issue of electrospun CNF electrodes is the low production efficiency at this stage. Although the production capability of polymer fibers by electrospinning has reached a level of kg/h [51], the production rate of CNFs for energy storage is still very low because of the nanostructured fibers required for efficient charge transfer in electrochemical storage. The diameter of electrospun fibers tends to increase significantly when increasing the feeding rate of the precursor solution. Maintaining the nanostructure and geometric requirements of CNFs and their corresponding properties under a high production rate remains a big challenge to industrial-scale production.

## 8. Conclusions and perspectives

The excellent electrical conductivities, large surface areas and easy fabrication process offer electrospun CNFs huge potential for application in electrochemical energy storage devices, including LIBs, SCs, NIBs, LABs and LSBs. Among many different techniques to produce carbon fibers, electrospinning is the most efficient to produce CNFs with diameters down to tens of nanometers. In addition, the electrospinning process allows easy integration of metal (oxides) without complex chemical treatments. Compared to other types of carbon materials, such as CNTs and graphene, electrospun CNFs also enjoy advantages in both low fabrication cost and high performance. The intensive studies carried out in the past several years have established a good understanding and a technological basis needed to control the morphologies and structures of both metal (oxides) and CNFs. A large number of interesting micro- and nanostructures have been produced and many of them are proven to be effective in improving the electrochemical performance.

In this review, an overview is provided of the synthesis and properties of electrospun CNFs and their hybrids with metal (oxides) and other conductive additives. The effects of various set-ups and different polymer precursors, as well as processing parameters for producing CNFs are discussed. CNFs play many important roles, including the establishment of conductive networks, active materials for Li and Na ion storage, scaffold to support metal oxides and sulfur, and as catalyst in LABs. Several key factors are found to be of great importance in determining the electrochemical performance: namely, (i) fiber diameter; (ii) chemical structure; (iii) surface area and pore size distribution; (iv) electrical conductivity; and (v) particle size, dispersion and morphology of metal (oxides). Optimization of these parameters are summarized and discussed in this review.

In summary, owing to the intensive and extensive studies carried out in the past two decades, many progresses have been made to understand the formation of CNFs under electrostatic forces, and various design approaches have been established to produce CNFs with attractive nanostructures. Thanks to these efforts, electrospun CNFs are finding a number of useful applications, including biomedical scaffolds, tissue templates, gas sensors, smart clothing, filtration, environmental protection, liquid crystal devices, composites and energy conversion and storage. Considerable success has so far been achieved in exploring CNFs and their hybrids in electrochemical energy storage devices, where large scale, industrial production may become a reality in the near future. However, many challenges are still ahead: for example, fundamental understanding of the correlation between the atomic structure and electrochemical behavior of the devices needs to be further enhanced. Production efficiency is also required to be further improved while reducing the fabrication cost for industrial applications.

## Acknowledgements

This project was financially supported by the Research Grants Council (GRF Projects 613811 and 613612) and the Innovation and Technology Commission (ITS/318/14) of Hong Kong SAR. ZB was partly supported by the SENG PhD Fellowship from the School of Engineering at HKUST.

## References

[1] Bruce PG, Freunberger SA, Hardwick LJ, Tarascon JM. Li–$O_2$ and Li–S batteries with high energy storage. Nat Mater 2012;11:19–30.

[2] Goodenough JB. Electrochemical energy storage in a sustainable modern society. Energy Environ Sci 2014;7:14–8.
[3] Su DS, Schlögl R. Nanostructured carbon and carbon nanocomposites for electrochemical energy storage applications. ChemSusChem 2010;3:136–68.
[4] Frackowiak E, Béguin F. Carbon materials for the electrochemical storage of energy in capacitors. Carbon 2001;39:937–50.
[5] Yoo E, Kim J, Hosono E, Zhou H, Kudo T, Honma I. Large reversible Li storage of graphene nanosheet families for use in rechargeable lithium ion batteries. Nano Lett 2008;8:2277–82.
[6] Mitchell RR, Gallant BM, Thompson CV, Shao-Horn Y. All-carbon-nanofiber electrodes for high-energy rechargeable Li–$O_2$ batteries. Energy Environ Sci 2011;4:2952–8.
[7] Zhang B, Yu Y, Liu Y, Huang ZD, He Y, Kim JK. Percolation threshold of graphene nanosheets as conductive additives in $Li_4Ti_5O_{12}$ anodes of Li-ion batteries. Nanoscale 2013;5:2100–6.
[8] Li X, Kang F, Bai X, Shen W. A novel network composite cathode of $LiFePO_4$/multiwalled carbon nanotubes with high rate capability for lithium ion batteries. Electrochem Commun 2007;9:663–6.
[9] Wen Z, Wang Q, Zhang Q, Li J. In situ growth of mesoporous $SnO_2$ on multiwalled carbon nanotubes: a novel composite with porous-tube structure as anode for lithium batteries. Adv Funct Mater 2007;17:2772–8.
[10] Zheng G, Yang Y, Cha JJ, Hong SS, Cui Y. Hollow carbon nanofiber-encapsulated sulfur cathodes for high specific capacity rechargeable lithium batteries. Nano Lett 2011;11:4462–7.
[11] Paek S, Yoo E, Honma I. Enhanced cyclic performance and lithium storage capacity of $SnO_2$/graphene nanoporous electrodes with three-dimensionally delaminated flexible structure. Nano Lett 2009;9:2–5.
[12] Liu X-M, Huang ZD, Oh SW, Zhang B, Ma P-C, Yuen MMF, et al. Carbon nanotube (CNT)-based composites as electrode material for rechargeable Li-ion batteries: a review. Compos Sci Technol 2012;72:121–44.
[13] Lee J-H, Kim G-S, Choi Y-M, Park WII, Rogers Ja, Paik U. Comparison of multiwalled carbon nanotubes and carbon black as percolative paths in aqueous-based natural graphite negative electrodes with high-rate capability for lithium-ion batteries. J Power Sources 2008;184:308–11.
[14] Li J, Ma PC, Chow WS, To CK, Tang BZ, Kim J-K. Correlations between percolation threshold, dispersion state, and aspect ratio of carbon nanotubes. Adv Funct Mater 2007;17:3207–15.
[15] Gan L, Lv R, Du H, Li B, Kang F. High loading of Pt–Ru nanocatalysts by pentagon defects introduced in a bamboo-shaped carbon nanotube support for high performance anode of direct methanol fuel cells. Electrochem Commun 2009;11:355–8.
[16] Wang Y, Wu M, Jiao Z, Lee JY. Sn@CNT and Sn@C@CNT nanostructures for superior reversible lithium ion storage. Chem Mater 2009;21:3210–5.
[17] Chen LF, Huang Z-H, Liang HW, Guan QF, Yu SH. Bacterial-cellulose-derived carbon nanofiber@$MnO_2$ and nitrogen-doped carbon nanofiber electrode materials: an asymmetric supercapacitor with high energy and power density. Adv Mater 2013;25:4746–52.
[18] Li F, Chen Y, Tang D-M, Jian Z, Liu C, Golberg D, et al. Performance-improved Li–$O_2$ battery with Ru nanoparticles supported on binder-free multi-walled carbon nanotube paper as cathode. Energy Environ Sci 2014;7:1648–52.
[19] Zhang GQ, Zheng JP, Liang R, Zhang C, Wang B, Hendrickson M, et al. Lithium–air batteries using SWNT/CNF buckypapers as air electrodes. J Electrochem Soc 2010;157:A953–6.
[20] Yu C, Masarapu C, Rong J, Wei B, Jiang H. Stretchable supercapacitors based on buckled single-walled carbon-nanotube macrofilms. Adv Mater 2009;21:4793–7.
[21] Hu L, Wu H, La Mantia F, Yang Y, Cui Y. Thin, flexible secondary Li-ion paper batteries. ACS Nano 2010;4:5843–8.
[22] Zhang B, Zheng Q Bin, Huang ZD, Oh SW, Kim JK. $SnO_2$–graphene–carbon nanotube mixture for anode material with improved rate capacities. Carbon 2011;49:4524–34.
[23] Qie L, Chen W-M, Wang Z-H, Shao Q-G, Li X, Yuan L-X, et al. Nitrogen-doped porous carbon nanofiber webs as anodes for lithium ion batteries with a superhigh capacity and rate capability. Adv Mater 2012;24:2047–50.
[24] Donnet JB. Carbon black: science and technology. CRC Press; 1993.
[25] Ma PC, Siddiqui NA, Marom G, Kim JK. Dispersion and functionalization of carbon nanotubes for polymer-based nanocomposites: a review. Compos A: Appl Sci Manuf 2010;41:1345–67.
[26] Peigney A, Laurent C, Flahaut E, Bacsa RR, Rousset A. Specific surface area of carbon nanotubes and bundles of carbon nanotubes. Carbon 2001;39:507–14.
[27] Mahanta NK, Abramson AR, Lake ML, Burton DJ, Chang JC, Mayer HK, et al. Thermal conductivity of carbon nanofiber mats. Carbon 2010;48:4457–65.
[28] Mayhew E, Prakash V. Thermal conductivity of individual carbon nanofibers. Carbon 2013;62:493–500.
[29] Zhu Y, Murali S, Cai W, Li X, Suk JW, Potts JR, et al. Graphene and graphene oxide: synthesis, properties, and applications. Adv Mater 2010;22:3906–24.
[30] Geim aK, Novoselov KS. The rise of graphene. Nat Mater 2007;6:183–91.
[31] Tibbetts G, Lake M, Strong K, Rice B. A review of the fabrication and properties of vapor-grown carbon nanofiber/polymer composites. Compos Sci Technol 2007;67:1709–18.
[32] Inagaki M, Yang Y, Kang F. Carbon nanofibers prepared via electrospinning. Adv Mater 2012;24:2547–66.
[33] Dong Z, Kennedy SJ, Wu Y. Electrospinning materials for energy-related applications and devices. J Power Sources 2011;196:4886–904.
[34] Martin-Gullon I, Vera J, Conesa Ja, González JL, Merino C. Differences between carbon nanofibers produced using Fe and Ni catalysts in a floating catalyst reactor. Carbon 2006;44:1572–80.
[35] Zhang B, Yu Y, Xu Z-L, Abouali S, Akbari M, He YB, et al. Correlation between atomic structure and electrochemical performance of anodes made from electrospun carbon nanofiber films. Adv Energy Mater 2014;4:1301448.
[36] Thavasi V, Singh G, Ramakrishna S. Electrospun nanofibers in energy and environmental applications. Energy Environ Sci 2008;1:205–21.
[37] Ramakrishna S, Fujihara K, Teo WE, Yong T, Ma Z, Ramaseshan R. Electrospun nanofibers: solving global issues. Mater Today 2006;9:40–50.
[38] Luo CJ, Stoyanov SD, Stride E, Pelan E, Edirisinghe M. Electrospinning versus fibre production methods: from specifics to technological convergence. Chem Soc Rev 2012;41:4708–35.

[39] Jong KP, Geus JW. Carbon nanofibers: catalytic synthesis and applications. Catal Rev Sci Eng 2000;42:481–510.
[40] Zhang B, Liu Y, Huang Z, Oh S, Yu Y, Mai Y-W, et al. Urchin-like $Li_4Ti_5O_{12}$–carbon nanofiber composites for high rate performance anodes in Li-ion batteries. J Mater Chem 2012;22:12133.
[41] Arai Y. Pitch based CNF. Nippon Steel Tech Rep 1993;59:65–70.
[42] Dong X-G, Wang C-G, Juan C. Study on the coagulation process of polyacrylonitrile nascent fibers during wet-spinning. Polym Bull 2006;58:1005–12.
[43] Wang Y, Wang C, Bai Y, Bo Z. Effect of the drawing process on the wet spinning of polyacrylonitrile fibers in a system of dimethyl sulfoxide and water. J Appl Polym Sci 2007;104:1026–37.
[44] Lee S-H, Park S-M, Kim Y. Effect of the concentration of sodium acetate (SA) on crosslinking of chitosan fiber by epichlorohydrin (ECH) in a wet spinning system. Carbohydr Polym 2007;70:53–60.
[45] Fujiwara H, Shibayama M, Chen JH, Nomura S. Preparation of high-strength poly(vinyl alcohol) fibers by crosslinking wet spinning. J Appl Polym Sci 1989;37:1403–14.
[46] Szosland L, East GC. The dry spinning of dibutyrylchitin fibers. J Appl Polym Sci 1995;58:2459–66.
[47] Zhang X, Liu T, Sreekumar TV, Kumar S, Hu X, Smith K. Gel spinning of PVA/SWNT composite fiber. Polymer 2004;45:8801–7.
[48] MInus M, Kumar S. The processing, properties, and structure of carbon fibers. JOM 2005;57:52–8.
[49] Shen L, Che Q, Li H, Zhang X. Mesoporous $NiCo_2O_4$ nanowire arrays grown on carbon textiles as binder-free flexible electrodes for energy storage. Adv Funct Mater 2014;24:2630–7.
[50] Mao X, Hatton T, Rutledge G. A review of electrospun carbon fibers as electrode materials for energy storage. Curr Org Chem 2013;17:1390–401.
[51] Persano L, Camposeo A, Tekmen C, Pisignano D. Industrial upscaling of electrospinning and applications of polymer nanofibers: a review. Macromol Mater Eng 2013;298:504–20.
[52] Cooley JF. US patent No. 692631.
[53] Morton JM. US patent No. 0,705,691.
[54] Teo WE, Ramakrishna S. A review on electrospinning design and nanofibre assemblies. Nanotechnology 2006;17:89–106.
[55] Baji A, Mai Y-W, Wong S-C, Abtahi M, Chen P. Electrospinning of polymer nanofibers: effects on oriented morphology, structures and tensile properties. Compos Sci Technol 2010;70:703–18.
[56] Taylor GI. Electrically driven jets. Proc R Soc Lond A 1969;313:453–75.
[57] Hohman MM, Shin M, Rutledge G, Brenner MP. Electrospinning and electrically forced jets. II. Applications. Phys Fluids 2001;13:2221.
[58] Yarin aL, Koombhongse S, Reneker DH. Bending instability in electrospinning of nanofibers. J Appl Phys 2001;89:3018–26.
[59] Huang Z-M, Zhang Y-Z, Kotaki M, Ramakrishna S. A review on polymer nanofibers by electrospinning and their applications in nanocomposites. Compos Sci Technol 2003;63:2223–53.
[60] Rafiei S, Maghsoodloo S, Noroozi B, Mottaghitalab V, Haghi AK. Mathematic modeling in electrospinning process of nanofibers: a detailed review. Cellulose Chem Technol 2013;47:323–38.
[61] Li D, Xia Y. Electrospinning of nanofibers: reinventing the wheel? Adv Mater 2004;16:1151–70.
[62] Li D, McCann JT, Xia Y, Marquez M. Electrospinning: a simple and versatile technique for producing ceramic nanofibers and nanotubes. J Am Ceram Soc 2006;89:1861–9.
[63] Zou L, Gan L, Kang F, Wang M, Shen W, Huang Z. Sn/C non-woven film prepared by electrospinning as anode materials for lithium ion batteries. J Power Sources 2010;195:1216–20.
[64] Kuriger RJ, Alam MK, Anderson DP, Jacobsen RL. Processing and characterization of aligned vapor grown carbon fiber reinforced polypropylene. Compos A: Appl Sci Manuf 2002;33:53–62.
[65] Fu K, Yildiz O, Bhanushali H, Wang Y, Stano K, Xue L, et al. Aligned carbon nanotube-silicon sheets: a novel nano-architecture for flexible lithium ion battery electrodes. Adv Mater 2013;25:5109–14.
[66] Matthews JA, Wnek GE, Simpson DG, Bowlin GL. Electrospinning of collagen nanofibers. Biomacromolecules 2002;3:232–8.
[67] Fennessey SF, Farris RJ. Fabrication of aligned and molecularly oriented electrospun polyacrylonitrile nanofibers and the mechanical behavior of their twisted yarns. Polymer 2004;45:4217–25.
[68] Chew SY, Wen J, Yim EKF, Leong KW. Sustained release of proteins from electrospun biodegradable fibers. Biomacromolecules 2005;6:2017–24.
[69] Search H, Journals C, Contact A, Iopscience M, Address IP. Electrostatic field-assisted alignment of electrospun nanofibers. Nanotechnology 2001;12:384–90.
[70] Zhou Z, Lai C, Zhang L, Qian Y, Hou H, Reneker DH, et al. Development of carbon nanofibers from aligned electrospun polyacrylonitrile nanofiber bundles and characterization of their microstructural, electrical, and mechanical properties. Polymer 2009;50:2999–3006.
[71] Katta P, Alessandro M, Ramsier RD, Chase GG. Continuous electrospinning of aligned polymer nanofibers onto a wire drum collector. Nano Lett 2004;4:2215–8.
[72] Li D, Wang Y, Xia Y. Electrospinning of polymeric and ceramic nanofibers as uniaxially aligned arrays. Nano Lett 2003;3:1167–71.
[73] Jalili R, Morshed M, Ravandi SAH. Fundamental parameters affecting electrospinning of PAN nanofibers as uniaxially aligned fibers. J Appl Polym Sci 2006;101:4350–7.
[74] Sun Z, Zussman E, Yarin AL, Wendorff JH, Greiner A. Compound core–shell polymer nanofibers by co-electrospinning. Adv Mater 2003;15:1929–32.
[75] Li D, Babel A, Jenekhe Sa, Xia Y. Nanofibers of conjugated polymers prepared by electrospinning with a two-capillary spinneret. Adv Mater 2004;16:2062–6.
[76] Zussman E, Yarin aL, Bazilevsky aV, Avrahami R, Feldman M. Electrospun polyacrylonitrile/poly(methyl methacrylate)-derived turbostratic carbon micro-/nanotubes. Adv Mater 2006;18:348–53.
[77] Li D, Xia Y. Direct fabrication of composite and ceramic hollow nanofibers by electrospinning. Nano Lett 2004;4:933–8.
[78] Li D, McCann JT, Xia Y. Use of electrospinning to directly fabricate hollow nanofibers with functionalized inner and outer surfaces. Small 2005;1:83–6.

[79] Yu Y, Gu L, Wang C, Dhanabalan A, van Aken Pa, Maier J. Encapsulation of Sn @ carbon nanoparticles in bamboo-like hollow carbon nanofibers as an anode material in lithium-based batteries. Angew Chem Int Ed 2009;48:6485–9.
[80] Hwang TH, Lee YM, Kong B-S, Seo J-S, Choi JW. Electrospun core–shell fibers for robust silicon nanoparticle-based lithium ion battery anodes. Nano Lett 2012;12:802–7.
[81] Cho T-H, Tanaka M, Onishi H, Kondo Y, Nakamura T, Yamazaki H, et al. Battery performances and thermal stability of polyacrylonitrile nano-fiber-based nonwoven separators for Li-ion battery. J Power Sources 2008;181:155–60.
[82] Rahaman MSa, Ismail AF, Mustafa A. A review of heat treatment on polyacrylonitrile fiber. Polym Degrad Stab 2007;92:1421–32.
[83] Zhu D, Xu C, Nakura N, Matsuo M. Study of carbon films from PAN/VGCF composites by gelation/crystallization from solution. Carbon 2002;40:363–73.
[84] Laffont L, Monthioux M, Serin V, Mathur RB, Guimon C, Guimon MF. An EELS study of the structural and chemical transformation of PAN polymer to solid carbon. Carbon 2004;42:2485–94.
[85] Park SH, Kim C, Choi YO, Yang KS. Preparations of pitch-based CF/ACF webs by electrospinning. Carbon 2003;41:2655–7.
[86] Kim B, Bui N, Yang K, Cruz ME, Ferraris JP. Electrochemical properties of activated polyacrylonitrile/pitch carbon fibers produced using electrospinning. Bull Korean Chem Soc 2009;30:1967–72.
[87] Park SH, Kim C, Yang KS. Preparation of carbonized fiber web from electrospinning of isotropic pitch. Synth Met 2004;143:175–9.
[88] Lai C, Zhou Z, Zhang L, Wang X, Zhou Q, Zhao Y, et al. Free-standing and mechanically flexible mats consisting of electrospun carbon nanofibers made from a natural product of alkali lignin as binder-free electrodes for high-performance supercapacitors. J Power Sources 2014;247:134–41.
[89] Wang S-X, Yang L, Stubbs LP, Li X, He C. Lignin-derived fused electrospun carbon fibrous mats as high performance anode materials for lithium ion batteries. ACS Appl Mater Interfaces 2013;5:12275–82.
[90] Ago M, Okajima K, Jakes JE, Park S, Rojas OJ. Lignin-based electrospun nanofibers reinforced with cellulose nanocrystals. Biomacromolecules 2012;13:918–26.
[91] Ruiz-Rosas R, Bedia J, Lallave M, Loscertales IG, Barrero A, Rodríguez-Mirasol J, et al. The production of submicron diameter carbon fibers by the electrospinning of lignin. Carbon 2010;48:696–705.
[92] Li X-F, Xu Q, Fu Y, Guo Q-X. Preparation and characterization of activated carbon from Kraft lignin via KOH activation. Environ Prog Sustain Energy 2014;33:519–26.
[93] Miao Y-E, Zhu G-N, Hou H, Xia Y-Y, Liu T. Electrospun polyimide nanofiber-based nonwoven separators for lithium-ion batteries. J Power Sources 2013;226:82–6.
[94] Xuyen NT, Ra EJ, Geng H-Z, Kim KK, An KH, Lee YH. Enhancement of conductivity by diameter control of polyimide-based electrospun carbon nanofibers. J Phys Chem B 2007;111:11350–3.
[95] Kim C, Choi Y-O, Lee W-J, Yang K-S. Supercapacitor performances of activated carbon fiber webs prepared by electrospinning of PMDA–ODA poly(amic acid) solutions. Electrochim Acta 2004;50:883–7.
[96] Yan H, Mahanta NK, Wang B, Wang S, Abramson AR, Cakmak M. Structural evolution in graphitization of nanofibers and mats from electrospun polyimide–mesophase pitch blends. Carbon 2014;71:303–18.
[97] Yang KS, Edie DD, Lim DY, Kim YM, Choi YO. Preparation of carbon fiber web from electrostatic spinning of PMDA–ODA poly(amic acid) solution. Carbon 2003;41:2039–46.
[98] Choi SW, Kim JR, Ahn YR, Jo SM, Cairns EJ. Characterization of electrospun PVDF fiber-based polymer electrolytes. Chem Mater 2007;19:104–15.
[99] Kim JR, Choi SW, Jo SM, Lee WS, Kim BC. Electrospun PVDF-based fibrous polymer electrolytes for lithium ion polymer batteries. Electrochim Acta 2004;50:69–75.
[100] Gao K, Hu X, Dai C, Yi T. Crystal structures of electrospun PVDF membranes and its separator application for rechargeable lithium metal cells. Mater Sci Eng B 2006;131:100–5.
[101] Prasanth R, Shubha N, Hng HH, Srinivasan M. Effect of poly(ethylene oxide) on ionic conductivity and electrochemical properties of poly(vinylidenefluoride) based polymer gel electrolytes prepared by electrospinning for lithium ion batteries. J Power Sources 2014;245:283–91.
[102] Zhang F, Ma X, Cao C, Li J, Zhu Y. Poly(vinylidene fluoride)/$SiO_2$ composite membranes prepared by electrospinning and their excellent properties for nonwoven separators for lithium-ion batteries. J Power Sources 2014;251:423–31.
[103] Yang Y, Centrone A, Chen L, Simeon F, Alan Hatton T, Rutledge GC. Highly porous electrospun polyvinylidene fluoride (PVDF)-based carbon fiber. Carbon 2011;49:3395–403.
[104] Uemura K, Gotoh Y. Fabrication of carbon fibers from electrospun poly(vinyl alcohol) nanofibers. Text Res J 2010;81:659–72.
[105] Norharyati W, Salleh W, Ismail AF. Fabrication and characterization of PEI/PVP-based carbon hollow fiber membranes for $CO_2/CH_4$ and $CO_2/N_2$ separation. AIChE J 2012;58:17–20.
[106] Cherian CT, Sundaramurthy J, Kalaivani M, Ragupathy P, Kumar PS, Thavasi V, et al. Electrospun $\alpha$-$Fe_2O_3$ nanorods as a stable, high capacity anode material for Li-ion batteries. J Mater Chem 2012;22:12198.
[107] Chen Q, Zhang T, Qiao X, Li D, Yang J. $Li_3V_2(PO_4)_3$/C nanofibers composite as a high performance cathode material for lithium-ion battery. J Power Sources 2013;234:197–200.
[108] Yu Y, Gu L, Zhu C, van Aken Pa, Maier J. Tin nanoparticles encapsulated in porous multichannel carbon microtubes: preparation by single-nozzle electrospinning and application as anode material for high-performance Li-based batteries. J Am Chem Soc 2009;131:15984–5.
[109] Zhang X, Kumar PS, Aravindan V, Liu HH, Sundaramurthy J, Mhaisalkar SG, et al. Electrospun $TiO_2$–graphene composite nanofibers as a highly durable insertion anode for lithium ion batteries. J Phys Chem C 2012;116:14780–8.
[110] Lewis JA. Binder removal from ceramics. Annu Rev Mater Sci 1997;27:147–73.
[111] Gupta P, Elkins C, Long TE, Wilkes GL. Electrospinning of linear homopolymers of poly(methyl methacrylate): exploring relationships between fiber formation, viscosity, molecular weight and concentration in a good solvent. Polymer 2005;46:4799–810.
[112] Uyar T, Besenbacher F. Electrospinning of uniform polystyrene fibers: the effect of solvent conductivity. Polymer 2008;49:5336–43.

[113] Fong H, Chun I, Reneker DH. Beaded nanofibers formed during electrospinning. Polymer 1999;40:4585–92.
[114] Fang J, Wang H, Niu H, Lin T, Wang X. Evolution of fiber morphology during electrospinning. J Appl Polym Sci 2010;118:2553–61.
[115] Wang C, Hsu C-H, Lin J-H. Scaling laws in electrospinning of polystyrene solutions. Macromolecules 2006;39:7662–72.
[116] Gu SY, Ren J, Vancso GJ. Process optimization and empirical modeling for electrospun polyacrylonitrile (PAN) nanofiber precursor of carbon nanofibers. Eur Polym J 2005;41:2559–68.
[117] Angammana CJ, Member S, Jayaram SH. Analysis of the effects of solution conductivity on electrospinning process and fiber morphology. IEEE Trans Ind Appl 2011;47:1109–17.
[118] Casper CL, Stephens JS, Tassi NG, Chase DB, Rabolt JF. Controlling surface morphology of electrospun polystyrene fibers: effect of humidity and molecular weight in the electrospinning process. Macromolecules 2004;37:573–8.
[119] Fridrikh S, Yu J, Brenner M, Rutledge G. Controlling the fiber diameter during electrospinning. Phys Rev Lett 2003;90:144502.
[120] Thompson CJ, Chase GG, Yarin AL, Reneker DH. Effects of parameters on nanofiber diameter determined from electrospinning model. Polymer 2007;48:6913–22.
[121] Yan X, Gevelber M. Investigation of electrospun fiber diameter distribution and process variations. J Electrostat 2010;68:458–64.
[122] Ital JM, Bahi OP, Mathur RB. Single step carbonization and graphitization of highly stabilized PAN fibers. Carbon 1997;35:1196–7.
[123] Sun F, Wang J, Chen H, Li W, Qiao W, Long D, et al. Immobilization of sulfur on nitrogen-enriched mesoporous carbons for Li–S batteries. ACS Appl Mater Interfaces 2013;5:5630–8.
[124] Li Q, Xu P, Gao W, Ma S, Zhang G, Cao R, et al. Graphene/graphene-tube nanocomposites templated from cage-containing metal-organic frameworks for oxygen reduction in Li–$O_2$ batteries. Adv Mater 2014;26:1378–86.
[125] Ryu M, Jung K, Shin K, Han K, Yoon S. High performance N-doped mesoporous carbon decorated $TiO_2$ nanofibers as anode materials for lithium-ion batteries. J Phys Chem C 2013;117:8092–8.
[126] Yan X, Liu Y, Fan X, Jia X, Yu Y, Yang X. Nitrogen/phosphorus co-doped nonporous carbon nanofibers for high-performance supercapacitors. J Power Sources 2014;248:745–51.
[127] Zhang B, Xu Z, He Y, Abouali S, Akbari Garakani M, Kamali Heidari E, et al. Exceptional rate performance of functionalized carbon nano fiber anodes containing nanopores created by (Fe) sacrificial catalyst. Nano Energy 2014;4:88–96.
[128] Kim B-H, Yang KS. Enhanced electrical capacitance of tetraethyl orthosilicate-derived porous carbon nanofibers produced via electrospinning. J Electroanal Chem 2014;714–715:92–6.
[129] Zhang B, Yu Y, Huang Z, He Y-B, Jang D, Yoon W-S, et al. Exceptional electrochemical performance of freestanding electrospun carbon nanofiber anodes containing ultrafine $SnO_x$ particles. Energy Environ Sci 2012;5:9895.
[130] Yu Y, Yang Q, Teng D, Yang X, Ryu S. Reticular Sn nanoparticle-dispersed PAN-based carbon nanofibers for anode material in rechargeable lithium-ion batteries. Electrochem Commun 2010;12:1187–90.
[131] Chen Y, Lu Z, Zhou L, Mai Y-W, Huang H. Triple-coaxial electrospun amorphous carbon nanotubes with hollow graphitic carbon nanospheres for high-performance Li ion batteries. Energy Environ Sci 2012;5:7898–902.
[132] Ju Y-W, Choi G-R, Jung H-R, Lee W-J. Electrochemical properties of electrospun PAN/MWCNT carbon nanofibers electrodes coated with polypyrrole. Electrochim Acta 2008;53:5796–803.
[133] Li Y, Xu G, Xue L, Zhang S, Yao Y, Lu Y, et al. Enhanced rate capability by employing carbon nanotube-loaded electrospun Si/C composite nanofibers as binder-free anodes. J Electrochem Soc 2013;160:A528–34.
[134] Guo Q, Zhou X, Li X, Chen S, Seema A, Greiner A, et al. Supercapacitors based on hybrid carbon nanofibers containing multiwalled carbon nanotubes. J Mater Chem 2009;19:2810–6.
[135] Zhou Z, Wu X-F, Hou H. Electrospun carbon nanofibers surface-grown with carbon nanotubes and polyaniline for use as high-performance electrode materials of supercapacitors. RSC Adv 2014;4:23622–9.
[136] Chen Y, Li X, Zhou X, Yao H, Huang H, Mai Y-W, et al. Hollow-tunneled graphitic carbon nanofibers through Ni-diffusion-induced graphitization as high-performance anode materials. Energy Environ Sci 2014;7:2689–96.
[137] Tai Z, Yan X, Lang J, Xue Q. Enhancement of capacitance performance of flexible carbon nanofiber paper by adding graphene nanosheets. J Power Sources 2012;199:373–8.
[138] Zhou Z, Wu X-F. Graphene-beaded carbon nanofibers for use in supercapacitor electrodes: synthesis and electrochemical characterization. J Power Sources 2013;222:410–6.
[139] Zhou X, Guo Y-G. A PEO-assisted electrospun silicon–graphene composite as an anode material for lithium-ion batteries. J Mater Chem A 2013;1:9019.
[140] Zhu N, Liu W, Xue M, Xie Z, Zhao D, Zhang M, et al. Graphene as a conductive additive to enhance the high-rate capabilities of electrospun $Li_4Ti_5O_{12}$ for lithium-ion batteries. Electrochim Acta 2010;55:5813–8.
[141] Zhu J, Lei D, Zhang G, Li Q, Lu B, Wang T. Carbon and graphene double protection strategy to improve the $SnO_x$ electrode performance anodes for lithium-ion batteries. Nanoscale 2013;5:5499–505.
[142] Nan D, Wang J-G, Huang Z-H, Wang L, Shen W, Kang F. Highly porous carbon nanofibers from electrospun polyimide/$SiO_2$ hybrids as an improved anode for lithium-ion batteries. Electrochem Commun 2013;34:52–5.
[143] Ji L, Zhang X. Fabrication of porous carbon nanofibers and their application as anode materials for rechargeable lithium-ion batteries. Nanotechnology 2009;20:155705.
[144] Lee B, Son S, Park K, Lee G, Oh KH, Lee S, et al. Effect of pores in hollow carbon nanofibers on their negative electrode properties for a lithium rechargeable battery. ACS Appl Mater Interfaces 2012;4:6702–10.
[145] Tran C, Kalra V. Fabrication of porous carbon nanofibers with adjustable pore sizes as electrodes for supercapacitors. J Power Sources 2013;235:289–96.
[146] Liang C, Li Z, Dai S. Mesoporous carbon materials: synthesis and modification. Angew Chem Int Ed 2008;47:3696–717.
[147] Zou L, Gan L, Lv R, Wang M, Huang Z, Kang F, et al. A film of porous carbon nanofibers that contain Sn/$SnO_x$ nanoparticles in the pores and its electrochemical performance as an anode material for lithium ion batteries. Carbon 2011;49:89–95.
[148] Kim C, Yang KS. Electrochemical properties of carbon nanofiber web as an electrode for supercapacitor prepared by electrospinning. Appl Phys Lett 2003;83:1216.

[149] Chen Y, Li X, Park K, Song J, Hong J, Zhou L, et al. Hollow carbon-nanotube/carbon-nanofiber hybrid anodes for Li-ion batteries. J Am Chem Soc 2013;135:16280–3.
[150] Kim C, Ngoc BTN, Yang KS, Kojima M, Kim Ya, Kim YJ, et al. Self-sustained thin webs consisting of porous carbon nanofibers for supercapacitors via the electrospinning of polyacrylonitrile solutions containing zinc chloride. Adv Mater 2007;19:2341–6.
[151] El-Hendawy AN. An insight into the KOH activation mechanism through the production of microporous activated carbon for the removal of $Pb^{2+}$ cations. Appl Surf Sci 2009;255:3723–30.
[152] Kim B-H, Yang KS, Woo H-G, Oshida K. Supercapacitor performance of porous carbon nanofiber composites prepared by electrospinning polymethylhydrosiloxane (PMHS)/polyacrylonitrile (PAN) blend solutions. Synth Met 2011;161:1211–6.
[153] Nishihara H, Itoi H, Kogure T, Hou P-X, Touhara H, Okino F, et al. Investigation of the ion storage/transfer behavior in an electrical double-layer capacitor by using ordered microporous carbons as model materials. Chemistry 2009;15:5355–63.
[154] Largeot C, Portet C, Chmiola J, Taberna P, Gogotsi Y, Simon P. Relation between the ion size and pore size for an electric double-layer capacitor. J Am Chem Soc 2008:2730–1.
[155] Kim Y, Horie Y, Ozaki S, Matsuzawa Y, Suezaki H, Kim C, et al. Correlation between the pore and solvated ion size on capacitance uptake of PVDC-based carbons. Carbon 2004;42:1491–500.
[156] Pandolfo aG, Hollenkamp AF. Carbon properties and their role in supercapacitors. J Power Sources 2006;157:11–27.
[157] Xu Z-L, Zhang B, Kim J-K. Electrospun carbon nanofiber anodes containing monodispersed Si nanoparticles and graphene oxide with exceptional high rate capacities. Nano Energy 2014;6:27–35.
[158] Zhang F, Yuan C, Zhu J, Wang J, Zhang X, Lou XWD. Flexible films derived from electrospun carbon nanofibers incorporated with $Co_3O_4$ hollow nanoparticles as self-supported electrodes for electrochemical capacitors. Adv Funct Mater 2013;23:3909–15.
[159] Zhu C, Mu X, van Aken Pa, Yu Y, Maier J. Single-layered ultrasmall nanoplates of $MoS_2$ embedded in carbon nanofibers with excellent electrochemical performance for lithium and sodium storage. Angew Chem Int Ed 2014;53:2152–6.
[160] Wang JG, Yang Y, Huang Z-H, Kang F. Coaxial carbon nanofibers/$MnO_2$ nanocomposites as freestanding electrodes for high-performance electrochemical capacitors. Electrochim Acta 2011;56:9240–7.
[161] Fu K, Xue L, Yildiz O, Li S, Lee H, Li Y, et al. Effect of CVD carbon coatings on Si@CNF composite as anode for lithium-ion batteries. Nano Energy 2013;2:976–86.
[162] Zhang B, Xu Z-L, Kim J-K. In situ grown graphitic carbon/$Fe_2O_3$/carbon nanofiber composites for high performance freestanding anodes in Li-ion batteries. RSC Adv 2014;4:12298.
[163] Abouali S, Akbari Garakani M, Zhang B, Luo H, Xu ZL, Huang JQ, et al. $Co_3O_4$/porous electrospun carbon nanofibers as anodes for high performance Li-ion batteries. J Mater Chem A 2014;2:16939–44.
[164] Dunn B, Kamath H, Tarascon J-M. Electrical energy storage for the grid: a battery of choices. Science 2011;334:928–35.
[165] Zhang W-J. A review of the electrochemical performance of alloy anodes for lithium-ion batteries. J Power Sources 2011;196:13–24.
[166] Huang Z-D, Oh S-W, He Y-B, Zhang B, Yang Y, Mai Y-W, et al. Porous C–$LiFePO_4$–C composite microspheres with a hierarchical conductive architecture as a high performance cathode for lithium ion batteries. J Mater Chem 2012;22:19643.
[167] Liu H, Cao Q, Fu LJ, Li C, Wu YP, Wu HQ. Doping effects of zinc on $LiFePO_4$ cathode material for lithium ion batteries. Electrochem Commun 2006;8:1553–7.
[168] Oh SW, Huang Z-D, Zhang B, Yu Y, He Y-B, Kim J-K. Low temperature synthesis of graphene-wrapped $LiFePO_4$ nanorod cathodes by the polyol method. J Mater Chem 2012;22:17215–21.
[169] Kim C, Yang KS, Kojima M, Yoshida K, Kim YJ, Kim Ya, et al. Fabrication of electrospinning-derived carbon nanofiber webs for the anode material of lithium-ion secondary batteries. Adv Funct Mater 2006;16:2393–7.
[170] Park SH, Kim BK, Lee WJ. Electrospun activated carbon nanofibers with hollow core/highly mesoporous shell structure as counter electrodes for dye-sensitized solar cells. J Power Sources 2013;239:122–7.
[171] Ji L, Zhang X. Generation of activated carbon nanofibers from electrospun polyacrylonitrile–zinc chloride composites for use as anodes in lithium-ion batteries. Electrochem Commun 2009;11:684–7.
[172] Yang Z, Choi D, Kerisit S, Rosso KM, Wang D, Zhang J, et al. Nanostructures and lithium electrochemical reactivity of lithium titanites and titanium oxides: a review. J Power Sources 2009;192:588–98.
[173] Zhang B, Du H, Li B, Kang F. Structure and electrochemical properties of Zn-doped $Li_4Ti_5O_{12}$ as anode materials in Li-ion battery. Electrochem Solid-State Lett 2010;13:A36.
[174] Zhang B, Huang ZD, Oh SW, Kim J-K. Improved rate capability of carbon coated $Li_{3.9}Sn_{0.1}Ti_5O_{12}$ porous electrodes for Li-ion batteries. J Power Sources 2011;196:10692–7.
[175] Liu S, Wang Z, Yu C, Wu H Bin, Wang G, Dong Q, et al. A flexible $TiO_2$(B)-based battery electrode with superior power rate and ultralong cycle life. Adv Mater 2013;25:3462–7.
[176] Zhao B, Jiang S, Su C, Cai R, Ran R, Tadé MO, et al. A 3D porous architecture composed of $TiO_2$ nanotubes connected with a carbon nanofiber matrix for fast energy storage. J Mater Chem A 2013;1:12310.
[177] Qing R, Sigmund W. Morphological and crystallite size impact on electrochemical performance of electrospun rutile and rutile/multiwall carbon nanotube nanofibers for lithium ion batteries. Ceram Int 2014;40:5665–9.
[178] Yang X, Teng D, Liu B, Yu Y, Yang X. Nanosized anatase titanium dioxide loaded porous carbon nanofiber webs as anode materials for lithium-ion batteries. Electrochem Commun 2011;13:1098–101.
[179] Li H, Shen L, Zhang X, Nie P, Chen L, Xu K. Electrospun hierarchical $Li_4Ti_{4.95}Nb_{0.05}O_{12}$/carbon composite nanofibers for high rate lithium ion batteries. J Electrochem Soc 2012;159:A426.
[180] Park H, Song T, Han H, Paik U. Electrospun $Li_4Ti_5O_{12}$ nanofibers sheathed with conductive TiN/$TiO_xN_y$ layer as an anode material for high power Li-ion batteries. J Power Sources 2013;244:726–30.
[181] Poizot P, Laruelle S, Grugeon S, Dupont L, Tarascon JM. Nano-sized transition-metal oxides as negative-electrode materials for lithium-ion batteries. Nature 2000;407:496–9.
[182] Wu H Bin, Chen JS, Hng HH, Lou XWD. Nanostructured metal oxide-based materials as advanced anodes for lithium-ion batteries. Nanoscale 2012;4:2526–42.

[183] Wang L, Yu Y, Chen PC, Zhang DW, Chen CH. Electrospinning synthesis of C/$Fe_3O_4$ composite nanofibers and their application for high performance lithium-ion batteries. J Power Sources 2008;183:717–23.
[184] Yang G, Li Y, Ji H, Wang H, Gao P, Wang L, et al. Influence of Mn content on the morphology and improved electrochemical properties of $Mn_3O_4$|MnO@carbon nanofiber as anode material for lithium batteries. J Power Sources 2012;216:353–62.
[185] Ji L, Zhang X. Manganese oxide nanoparticle-loaded porous carbon nanofibers as anode materials for high-performance lithium-ion batteries. Electrochem Commun 2009;11:795–8.
[186] Zhang P, Guo ZP, Huang Y, Jia D, Liu HK. Synthesis of $Co_3O_4$/carbon composite nanowires and their electrochemical properties. J Power Sources 2011;196:6987–91.
[187] Wu Y, Zhu P, Reddy MV, Chowdari BVR, Ramakrishna S. Maghemite nanoparticles on electrospun CNFs template as prospective lithium-ion battery anode. ACS Appl Mater Interfaces 2014;6:1951–8.
[188] Zhang M, Yan F, Tang X, Li Q, Wang T, Cao G. Flexible CoO–graphene–carbon nanofiber mats as binder-free anodes for lithium-ion batteries with superior rate capacity and cyclic stability. J Mater Chem A 2014;2:5890.
[189] Chen Y, Lu Z, Zhou L, Mai Y-W, Huang H. In situ formation of hollow graphitic carbon nanospheres in electrospun amorphous carbon nanofibers for high-performance Li-based batteries. Nanoscale 2012;4:6800–5.
[190] Scotia N. Electrochemical and in situ X-ray diffraction studies of the reaction of lithium with tin oxide composites. J Electrochem Soc 1997;144:2045–52.
[191] Wu H, Zheng G, Liu N, Carney TJ, Yang Y, Cui Y. Engineering empty space between Si nanoparticles for lithium-ion battery anodes. Nano Lett 2012;12:904–9.
[192] Idota Y, Kubota T, Matsufuji A, Maekawa Y, Miyasaka T. Tin-based amorphous oxide: a high-capacity lithium-ion-storage material. Science 1997;276:1395–7.
[193] Jung HR, Lee WJ. Electrochemical characterization of electrospun $SnO_x$-embedded carbon nanofibers anode for lithium ion battery with EXAFS analysis. J Electroanal Chem 2011;662:334–42.
[194] Kim C, Noh M, Choi M, Cho J, Park B. Critical size of a nano $SnO_2$ electrode for Li-secondary battery. Chem Mater 2005:3297–301.
[195] Zhou X, Dai Z, Liu S, Bao J, Guo Y-G. Ultra-uniform $SnO_x$/carbon nanohybrids toward advanced lithium-ion battery anodes. Adv Mater 2014;26:3943–9.
[196] Ji L, Jung K-H, Medford AJ, Zhang X. Electrospun polyacrylonitrile fibers with dispersed Si nanoparticles and their electrochemical behaviors after carbonization. J Mater Chem 2009;19:4992.
[197] Xu Z-L, Zhang B, Zhou ZQ, Abouali S, Akbari Garakani M, Huang J, et al. Carbon nanofibers containing Si nanoparticles and graphene-covered Ni for high performance anodes in Li ion batteries. RSC Adv 2014;4:22359.
[198] Lee Y, Heo Y-U, Song D, Shin DW, Kang YM. Si-carbon composite nanofibers with good scalability and favorable architecture for highly reversible lithium storage and superb kinetics. Electrochim Acta 2014;118:100–5.
[199] Wu H, Chan G, Choi JW, Ryu I, Yao Y, McDowell MT, et al. Stable cycling of double-walled silicon nanotube battery anodes through solid-electrolyte interphase control. Nat Nanotechnol 2012;7:310–5.
[200] Ji L, Zhang X. Fabrication of porous carbon/Si composite nanofibers as high-capacity battery electrodes. Electrochem Commun 2009;11:1146–9.
[201] Xu Z-L, Zhang B, Abouali S, Akbari Garakani M, Huang J, Huang JQ, et al. Nanocavity-engineered Si/multi-functional carbon nanofiber composite anodes with exceptional high-rate capacities. J Mater Chem A 2014;2:17944–51.
[202] Toprakci O, Ji L, Lin Z, Toprakci HaK, Zhang X. Fabrication and electrochemical characteristics of electrospun $LiFePO_4$/carbon composite fibers for lithium-ion batteries. J Power Sources 2011;196:7692–9.
[203] Zhu C, Yu Y, Gu L, Weichert K, Maier J. Electrospinning of highly electroactive carbon-coated single-crystalline $LiFePO_4$ nanowires. Angew Chem Int Ed 2011;50:6278–82.
[204] Toprakci O, Toprakci HaK, Ji L, Xu G, Lin Z, Zhang X. Carbon nanotube-loaded electrospun $LiFePO_4$/carbon composite nanofibers as stable and binder-free cathodes for rechargeable lithium-ion batteries. ACS Appl Mater Interfaces 2012;4:1273–80.
[205] Hosono E, Wang Y, Kida N, Enomoto M, Kojima N, Okubo M, et al. Synthesis of triaxial $LiFePO_4$ nanowire with a VGCF core column and a carbon shell through the electrospinning method. ACS Appl Mater Interfaces 2010;2:212–8.
[206] Shao D, Wang J, Dong X, Yu W, Liu G, Zhang F, et al. Coaxial electrospinning fabrication and electrochemical properties of $LiFePO_4$/C/Ag composite hollow nanofibers. J Mater Sci Mater Electron 2013;24:4718–24.
[207] Kim C, Kang SH, Jeon HJ, Son JT. Electrochemical properties of nanostructured $Li[Fe_{0.9}Mn_{0.1}]PO_4$/C as a cathode material for lithium ion batteries prepared by electrospinning method. J Electroceram 2013;31:204–9.
[208] Zhang S, Li Y, Xu G, Li S, Lu Y, Toprakci O, et al. High-capacity $Li_2Mn_{0.8}Fe_{0.2}SiO_4$/carbon composite nanofiber cathodes for lithium-ion batteries. J Power Sources 2012;213:10–5.
[209] Li L, Yin X, Liu S, Wang Y, Chen L, Wang T. Electrospun porous $SnO_2$ nanotubes as high capacity anode materials for lithium ion batteries. Electrochem Commun 2010;12:1383–6.
[210] Gu Y, Chen D, Jiao X. Synthesis and electrochemical properties of nanostructured $LiCoO_2$ fibers as cathode materials for lithium-ion batteries. J Phys Chem B 2005;109:17901–6.
[211] Jayaraman S, Aravindan V, Suresh Kumar P, Ling WC, Ramakrishna S, Madhavi S. Synthesis of porous $LiMn_2O_4$ hollow nanofibers by electrospinning with extraordinary lithium storage properties. Chem Commun 2013;49:6677–9.
[212] Huang ZD, Zhang B, Liang R, Zheng QB, Oh SW, Lin XY, et al. Effects of reduction process and carbon nanotube content on the supercapacitive performance of flexible graphene oxide papers. Carbon 2012;50:4239–51.
[213] Huang ZD, Zhang B, Oh S-W, Zheng Q-B, Lin X-Y, Yousefi N, et al. Self-assembled reduced graphene oxide/carbon nanotube thin films as electrodes for supercapacitors. J Mater Chem 2012;22:3591.
[214] Kim C, Park S-H, Lee W-J, Yang K-S. Characteristics of supercapacitor electrodes of PBI-based carbon nanofiber web prepared by electrospinning. Electrochim Acta 2004;50:877–81.
[215] Kim B-H, Yang KS. Enhanced electrical capacitance of porous carbon nanofibers derived from polyacrylonitrile and boron trioxide. Electrochim Acta 2013;88:597–603.
[216] Zhi M, Manivannan A, Meng F, Wu N. Highly conductive electrospun carbon nanofiber/$MnO_2$ coaxial nano-cables for high energy and power density supercapacitors. J Power Sources 2012;208:345–53.

[217] Ju YW, Choi GR, Jung H-R, Kim C, Yang K-S, Lee W-J. A hydrous ruthenium oxide-carbon nanofibers composite electrodes prepared by electrospinning. J Electrochem Soc 2007;154:A192.
[218] Huang ZD, Liang R, Zhang B, He Y-B, Kim J-K. Evolution of flexible 3D graphene oxide/carbon nanotube/polyaniline composite papers and their supercapacitive performance. Compos Sci Technol 2013;88:126–33.
[219] Snook Ga, Kao P, Best AS. Conducting-polymer-based supercapacitor devices and electrodes. J Power Sources 2011;196:1–12.
[220] Wang J-G, Yang Y, Huang Z-H, Kang F. Rational synthesis of $MnO_2$/conducting polypyrrole@carbon nanofiber triaxial nano-cables for high-performance supercapacitors. J Mater Chem 2012;22:16943–9.
[221] Slater MD, Kim D, Lee E, Johnson CS. Sodium-ion batteries. Adv Funct Mater 2013;23:947–58.
[222] Stevens DA, Dahn JR. The mechanisms of lithium and sodium insertion in carbon materials. J Electrochem Soc 2001;148:A803.
[223] Chen T, Liu Y, Pan L, Lu T, Yao Y, Sun Z, et al. Electrospun carbon nanofibers as anode materials for sodium ion batteries with excellent cycle performance. J Mater Chem A 2014;2:4117–21.
[224] Li W, Zeng L, Yang Z, Gu L, Wang J, Liu X, et al. Free-standing and binder-free sodium-ion electrodes with ultralong cycle life and high rate performance based on porous carbon nanofibers. Nanoscale 2014;6:693–8.
[225] Zhu Y, Han X, Xu Y, Liu Y, Zheng S, Xu K, et al. Electrospun Sb/C fibers for a stable and fast sodium-ion battery anode. ACS Nano 2013;7:6378–86.
[226] Wu L, Hu X, Qian J, Pei F, Wu F, Mao R, et al. Sb–C nanofibers with long cycle life as an anode material for high-performance sodium-ion batteries. Energy Environ Sci 2014;7:323–8.
[227] Ji L, Gu M, Shao Y, Li X, Engelhard MH, Arey BW, et al. Controlling SEI formation on SnSb-porous carbon nanofibers for improved Na ion storage. Adv Mater 2014;26:2901–8.
[228] Liu J, Tang K, Song K, van Aken Pa, Yu Y, Maier J. Electrospun $Na_3V_2(PO_4)_3$/C nanofibers as stable cathode materials for sodium-ion batteries. Nanoscale 2014;6:5081–6.
[229] Xu J-J, Xu D, Wang Z-L, Wang H-G, Zhang L-L, Zhang X-B. Synthesis of perovskite-based porous $La_{0.75}Sr_{0.25}MnO_3$ nanotubes as a highly efficient electrocatalyst for rechargeable lithium–oxygen batteries. Angew Chem Int Ed Engl 2013;52:3887–90.
[230] Peng Z, Freunberger Sa, Chen Y, Bruce PG. A reversible and higher-rate Li–$O_2$ battery. Science 2012;337:563–6.
[231] Tran C, Yang X-Q, Qu D. Investigation of the gas-diffusion-electrode used as lithium/air cathode in non-aqueous electrolyte and the importance of carbon material porosity. J Power Sources 2010;195:2057–63.
[232] Nanosheet MG. Li–air rechargeable battery based on metal-free graphene nanosheet catalysts. ACS Nano 2011:3020–6.
[233] Huang B-W, Liao X-Z, Wang H, Wang C-N, He Y-S, Ma Z-F. Nanofibrous MnNi/CNF composite catalyst for rechargeable Li/$O_2$ cell. J Electrochem Soc 2013;160:A1112–7.
[234] Jung K-N, Lee J-I, Yoon S, Yeon S-H, Chang W, Shin K-H, et al. Manganese oxide/carbon composite nanofibers: electrospinning preparation and application as a bi-functional cathode for rechargeable lithium–oxygen. J Mater Chem 2012;22:21845–8.
[235] Wu J, Park HW, Yu A, Higgins D, Chen Z. Facile synthesis and evaluation of nanofibrous iron–carbon based non-precious oxygen reduction reaction catalysts for Li–$O_2$ battery applications. J Phys Chem C 2012:2–7.
[236] Li J, Zou M, Chen L, Huang Z, Guan L. An efficient bifunctional catalyst of Fe/$Fe_3C$ carbon nanofibers for rechargeable Li–$O_2$ batteries. J Mater Chem A 2014;2:10634–8.
[237] Ottakam Thotiyl MM, Freunberger Sa, Peng Z, Bruce PG. The carbon electrode in nonaqueous Li–$O_2$ cells. J Am Chem Soc 2013;135:494–500.
[238] Ryu W, Yoon T, Song SH, Jeon S, Park Y, Kim I. Bifunctional composite catalysts using $Co_3O_4$ nanofibers immobilized on nonoxidized graphene nano flakes for high- capacity and long-cycle Li–$O_2$ batteries. Nano Lett 2013;13:4190–7.
[239] Itkis DM, Semenenko Da, Kataev EY, Belova AI, Neudachina VS, Sirotina AP, et al. Reactivity of carbon in lithium–oxygen battery positive electrodes. Nano Lett 2013;13:4697–701.
[240] Ji X, Lee KT, Nazar LF. A highly ordered nanostructured carbon–sulphur cathode for lithium–sulphur batteries. Nat Mater 2009;8:500–6.
[241] Ji L, Rao M, Aloni S, Wang L, Cairns EJ, Zhang Y. Porous carbon nanofiber–sulfur composite electrodes for lithium/sulfur cells. Energy Environ Sci 2011;4:5053–9.
[242] Wu Y, Gao M, Li X, Liu Y, Pan H. Preparation of mesohollow and microporous carbon nanofiber and its application in cathode material for lithium–sulfur batteries. J Alloys Compd 2014;608:220–8.
[243] Rao M, Geng X, Li X, Hu S, Li W. Lithium–sulfur cell with combining carbon nanofibers–sulfur cathode and gel polymer electrolyte. J Power Sources 2012;212:179–85.
[244] Chen Y, Li X, Park K-S, Hong J, Song J, Zhou L, et al. Sulfur encapsulated in porous hollow CNTs@CNFs for high-performance lithium–sulfur batteries. J Mater Chem A 2014;2:10126–30.
[245] Wei Seh Z, Li W, Cha JJ, Zheng G, Yang Y, McDowell MT, et al. Sulphur–$TiO_2$ yolk-shell nanoarchitecture with internal void space for long-cycle lithium–sulphur batteries. Nat Commun 2013;4:1331.
[246] Ji X, Evers S, Black R, Nazar LF. Stabilizing lithium–sulphur cathodes using polysulphide reservoirs. Nat Commun 2011;2:325.
[247] Su Y-S, Fu Y, Cochell T, Manthiram A. A strategic approach to recharging lithium–sulphur batteries for long cycle life. Nat Commun 2013;4:2985.
[248] Huang JQ, Zhang B, Xu ZL, Abouali S, Garakani MA, Huang J, et al. Novel interlayer made from $Fe_3C$/carbon nanofiber webs for high performance lithium–sulfur batteries. J Power Sources 2015;285:43–50.
[249] Forney MW, Ganter MJ, Staub JW, Ridgley RD, Landi BJ. Prelithiation of silicon–carbon nanotube anodes for lithium ion batteries by stabilized lithium metal powder (SLMP). Nano Lett 2013;13:4158–63.
[250] Chmiola J, Yushin G, Gogotsi Y, Portet C, Simon P, Taberna PL. Anomalous increase in carbon capacitance at pore sizes less than 1 nanometer. Science 2006;313:1760–3.
[251] Ma SB, Lee DJ, Roev V, Im D, Doo S-G. Effect of porosity on electrochemical properties of carbon materials as cathode for lithium–oxygen battery. J Power Sources 2013;244:494–8.

[252] U.S. Department of Energy. Annual progress report for the energy storage research and development vehicle technologies program, Washington, DC; 2008.
[253] Zhang B, Huang J, Kim JK. Ultrafine amorphous $SnO_x$ embedded in carbon nanofiber/carbon nanotube composites for Li-ion and Na-ion batteries. Adv Funct Mater 2015;25:5222–8.
[254] Zhou G, Li F, Cheng H-M. Progress in flexible lithium batteries and future prospects. Energy Environ Sci 2014;7:1307–38.